NTNU – Trondheim
Norwegian University of
Science and Technology

Wet Chemical Synthesis of Graphene for Battery Applications

Ida Johansen

Nanotechnology
Submission date: June 2014
Supervisor: Ingeborg Kaus, IMTE
Co-supervisor: Ann-Mari Svensson, IMTE

Norwegian University of Science and Technology
Department of Materials Science and Engineering

Problem Description

Graphene is a two-dimensional carbon structure with unique physical properties and great potential for various applications in electric circuits, solar cells, light emitting diodes, thermoelectric and piezoelectric materials, batteries etc. Graphene may be produced using vacuum based methods to produce thin films, and by wet chemical methods for graphene flakes.

Graphite consists of many layers of graphene, and in this project, graphite will be oxidized into graphene oxide by a wet chemical method similar to that described by Chen et al. [27]. Furthermore, the graphene oxide will undergo thermal reduction for the production of graphene.

For battery applications, it is important to be able to disperse the graphene into a solvent to produce slurry for tape casting. Graphene oxide is much more easily dispersed than graphene, and a main part of this project will be to investigate the dispersibility of produced graphene vs. the degree of reduction.

All the samples, including graphite, graphene oxide and graphene, will be characterized by XRD, SEM and FTIR, along with the dispersibility testing.

Abstract

In this thesis, an improved Hummers method is used to produce graphene oxide, while thermal treatment has been used as the reduction process to form reduced graphene oxide. This modified version of Hummers method differs from the original one by the exclusion of $NaNO_3$. This modification eliminates the evolution of NO_2/N_2O_4 toxic gasses.

Several syntheses are done, where parameters such as particle size and oxidation time are varied. In addition, the thermal reduction process has also been investigated, and different final temperatures, heating rates and atmospheres are carried out in order to find the best procedure. Finally, the dispersibility was tested for graphite, graphene oxide and reduced graphene oxide, as solubility is an essential property when considering the use of graphene in battery applications.

All samples, including graphite, graphene oxide and reduced graphene oxide have also been characterized using X-ray diffraction (XRD), Fourier Transform Infrared Spectroscopy (FTIR) and Scanning Electron Microscopy (SEM).

From the XRD results it is found that both the particle size and oxidation time are crucial in order to produce fully oxidized graphite. This was only obtained by using graphite powder smaller than 50 μm and an oxidation time of 5 days. Furthermore, the thermal reduction is also a critical step in the approach to successfully reduce graphene oxide, and it is found that the heating rate has to be 5 °C/s up to at least 900 °C in Ar/H_2 (5% H_2) gas, and the sample needs to be held at this temperature for 30 minutes. Too slow heating will not create enough pressure inside the sample, which is necessary to overcome the van der Waals forces between the graphene layers.

The FTIR results showed that the oxygen containing functional groups attached to the graphene sheets were ketones, epoxy groups, carboxylic acids and hydroxyls. These groups make the graphene oxide soluble. However, these groups are removed during reduction, and hence the reduced graphene oxide becomes insoluble.

This work clearly show that the various parameters are very important to control in order to obtain the desired product and that the end result is highly affected by the synthesis route.

Sammendrag

I denne masteroppgaven er en forbedret Hummers metode brukt for å produsere grafenoksid, mens varmebehandling har blitt benyttet som reduksjonsprosess for å danne redusert grafenoksid. Denne modifiserte versjonen av Hummers metode skiller seg fra den opprinnelige ved utelukkelsen av $NaNO_3$. Denne endringen eliminerer utviklingen av de giftige gassene NO_2 og N_2O_4.

Flere synteser har blitt gjennomført, der parametere som partikkelstørrelse og oksidasjonstid har vært variert. I tillegg har den termiske reduksjonsprosessen også vært studert, og forskjellige temperaturer, varmerater og atmosfærer har blitt prøvd ut for å finne den beste fremgangsmåten. Til slutt ble løseligheten testet for grafitt, grafenoksid og redusert grafenoksid, ettersom løseligheten er en viktig egenskap når det kommer til bruk av materialet i batteriapplikasjoner.

Alle prøver av grafitt, grafenoksid og redusert grafenoksid har også blitt karakterisert ved hjelp av røntgendiffraksjon (XRD), Fourier transform infrarød spektroskopi (FTIR) og sveipeelektronmikroskopi (SEM).

XRD resultatene viser at partikkelstørrelse og oksidasjontid er avgjørende for å produsere fullstendig oksidert grafitt, og dette er oppnådd ved hjelp av grafittpulver som er mindre enn 50 μm, og en oksidasjonstid på 5 dager. Videre er den termiske reduksjonen også et kritisk trinn i tilnærmingen til vellykket redusert grafenoksid, og det er funnet at oppvarmingshastigheten må være 5 °C/s opp til minst 900 °C i Ar/H_2 gass. I tillegg må prøven holdes ved denne temperaturen i 30 minutter. For treg oppvarming vil ikke skape nok trykk inne i prøven, noe som er nødvendig for å overvinne van der Waals kreftene mellom grafenlagene og for å oppnå single grafenlag.

FTIR resultatene viste at de oksygenholdige funksjonelle gruppene som er knyttet til grafenlagene, er ketoner, epoksider, karboksylsyrer og alkoholer. Disse gruppene gjør grafenoksiden løselige, men de fjernes imidlertid under reduksjonen, og dermed blir den reduserte grafenoksiden uløselig.

Dette arbeidet viser tydelig at de ulike parameterne er meget viktig å kontrollere for å oppnå det ønskede produktet og at sluttresultatet er sterkt påvirket av synteseruten.

Preface

The present work has been conducted at Department for Materials Science and Technology (IMTE) at Norwegian University of Science and Technology (NTNU).

The process of doing a master thesis on its own is both complex and extensive. No less, it is also an interesting process characterized by growth in knowledge and self-confidence.
The reason why I became motivated for investigating the synthesis of graphene, is that graphene has been widely discussed in media recent years. It is predicted that graphene will be a very important material in the future and it has a very wide range of applications. So, to learn more about this promising material and its development is something I find really interesting.

The laboratory work has been a very time consuming process, and some of the syntheses took several weeks to finish. If there had been no limitations in the laboratory equipment it would be possible to do multiple syntheses at the same time.
However, when one realizes that one is capable of submitting a complete master's thesis one grows as a person and experiences acknowledgement upon own abilities.

Ida Johansen
Trondheim, June 2014

Acknowledgement

I wish to thank my supervisor Ingeborg Kaus at IMTE for her assistance during the period I have been working on my project. Our weekly meetings have given me the opportunity to ask questions and discuss problems I have encountered and I really appreciate that.

I would also like to thank my co-supervisor Ann Mari Svensson at IMTE for her advisory contributions.

Last but not least, I am also grateful for the sincere interest from Fride Vullum-Bruer, and that she always was available to answer any questions. Furthermore, I would like to thank Gunn Torill Wikdahl for her help to find the necessary equipment for my laboratory work, Julian Tolchard for his effort in obtaining X-ray diffraction patterns and Martin Ystenes for helping me with Fourier Transform Infrared spectroscopy, all of them at IMTE. In addition, Sidsel Meli Hanetho at SINTEF has been very helpful when I had questions regarding my laboratory work.

Table of Contents

List of abbreviations

AFM	Atomic Force Microscopy
BET	Brunauer, Emmett and Teller
DBU	1,8-diazabibyclo[5.4.0]undecene
DCB	Dichlorbenzene
CVD	Chemical Vapor Deposition
FTIR	Fourier Transform Infrared Spectroscopy
GO	Graphene Oxide
r-GO	Reduced Graphene Oxide
RTP	Rapid Thermal Process
SEI	Solid Electrolyte Interface
SEM	Scanning Electron Microscopy
TEM	Transmission Electron Microscopy
THF	Tetrahydrofuran
XRD	X-ray Diffraction

1 Introduction

Renewable and sustainable energy have attracted much attention recent years. One of many interesting fields is the ongoing research and development regarding Li-ion batteries for mobile applications. Different materials are frequently investigated as electrode material in order to improve the performance, and it is found that graphene is a very promising material.

Graphene is a one-atom-thick two-dimensional crystal of sp^2-bonded carbon atoms making up a lattice of hexagons, and its physical properties are outstanding. It does not only have large specific surface area (2630 m^2g^{-1}), but also high intrinsic mobility (200 000 $cm^2 V^{-1} s^{-1}$), high Young's modulus (~1.0 TPa), high thermal conductivity (~5000 W $m^{-1} K^{-1}$), high electrical conductivity and optical transmittance (~97.7%) [1-4]. In addition, graphene is the building block of graphite, and in the graphite structure the graphene sheets are held together by van der Waals forces. However, each graphene layer has exceptional properties, which are totally different from the properties of graphite as a bulk material. Nevertheless, one big issue is the hydrophobic nature of graphene, which make it impossible to produce a stable slurry for tape casting.

There are several methods for the production of graphene, having their own advantages and disadvantages. The preparation routes strongly affect the electrochemical properties, and the most appropriate production method depends on the application and desired properties.
In the present work, a modified Hummers method will be used for the production of graphene oxide, followed by reduction to graphene. Hummers method is a wet chemical method, based on the oxidation of graphite by the presence of strong acids [5]. The oxygen containing functional groups that are introduced between the graphene layers disrupt the van der Waal forces, which is necessary for successful exfoliation.

Furthermore, the graphene oxide can be reduced to graphene in various ways. Chemical reduction is unique and attractive because of its capability of producing single-layer graphene in large scale and at relatively low costs. On the other hand, chemical reduction often uses hazardous and toxic chemicals [6]. Therefore, in the present work, the focus will be on the thermal reduction of graphene oxide.

Even if pristine graphene has been produced by several approaches, such as vapor deposition, epitaxy/sublimation, and mechanical exfoliation, it is very difficult to obtain pristine graphene using Hummers method [7]. Because of the heteroatomic contamination and/or topographical defects that will be present, it will be more correct to refer to the product as reduced graphene oxide (r-GO) instead of graphene.

However, in the present work, the main focus will be on the production of r-GO by using Hummers method, followed by thermal treatment. Finally, as the dispersibility of r-GO plays a crucial role, investigation of the dispersibility vs. the degree of reduction will also be carried out.

2 Theory and background

This chapter goes through the background theory that is necessary in order to understand the present work. It starts out with describing what graphene and graphene oxide are, and the most important milestones in the history and discovery of these materials will be outlined. Further, the synthesis of GO and the reduction process will be explained, along with the use of graphene in batteries. Finally, the basic theory behind the characterization methods used is described.

2.1 Graphene and graphene oxide

2.1.1 What is graphene?

Graphene is a unique material with excellent properties. In fact, it is practically transparent (in the optical region it absorbs only 2.3 % of the light), substantially stronger than steel, very stretchable, and it does also show excellent thermal conductivity [8].

Graphene is the name given to a two-dimensional sheet of carbon atoms tightly packed into a honeycomb lattice, and is the building block for graphitic materials of all other dimensionalities (figure 2.1) [9]. It can be wrapped up into 0D buckyballs, rolled into 1D nanotubes or stacked together to form 3D graphite.

In graphene there are covalent bonds between the carbon atoms, and when several graphene sheets are stacked into graphite, the sheets are held together by van der Waals forces [10]. In fact, the van der Waals forces have to be overcome in order to make graphene from graphite.

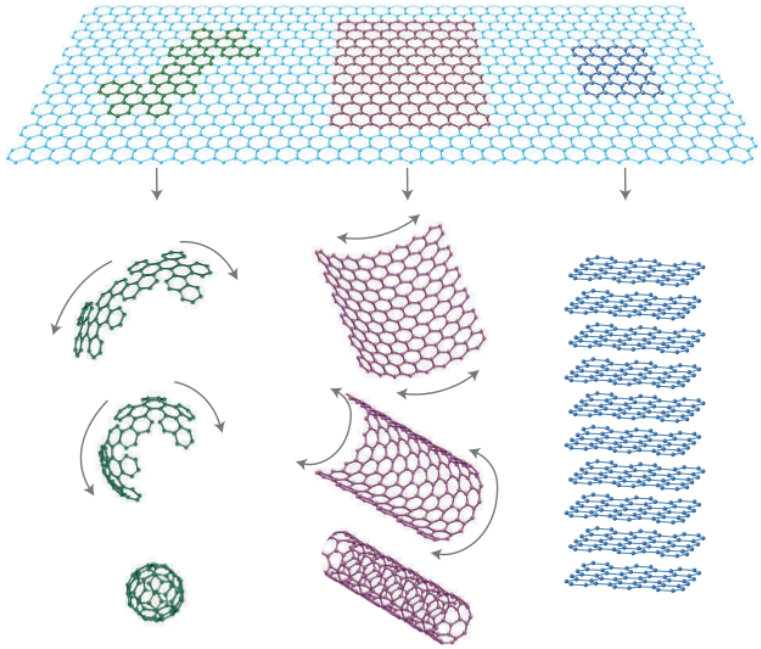

Figure 2.1: Graphene is a 2D building material for carbon materials of all other dimensionalities. It can be wrapped up to 0D buckyballs, rolled into 1D nanotubes and stacked into 3D graphite (from ref. 9).

2.1.2 What is graphene oxide?

First of all, there are some differences between graphite oxide and graphene oxide. The precise chemical formula of graphite oxide has been the subject to considerable debate over the years, and even to this day no unambiguous model exists [11]. When graphite is oxidized, the distance between the graphene sheets is increased, and hence the van der Waals forces are decreased. In other word, graphite oxide is graphite where oxygen containing functional groups are introduced between the graphene layers.

Chemically, graphene oxide is similar, if not identical, to graphite oxide, but structurally it is very different. Rather than retaining a stacked structure, the material is exfoliated into monolayers or a few stacked layers, and graphene oxide contains a range of reactive oxygen functional groups [11]. It is graphene oxide that is the product obtained by Hummers method, and hence it is graphene oxide that undergoes the reduction to graphene, or more precisely GO is reduced to r-GO.

The most well known model of graphene oxide is shown in figure 2.2. This is the Lerf-Klinowski model, and contains epoxy groups (-O-) and hydroxyl groups (-OH). They used steady state nuclear magnetic resonance (NMR) spectroscopy to characterize the material [12]. Another variation of the Lerf-Klinowski model, which is very similar to the one

in figure 2.2 does also exists, but in that model carboxylic acids (-COOH) are included and positioned on the periphery of the basal plane [11].

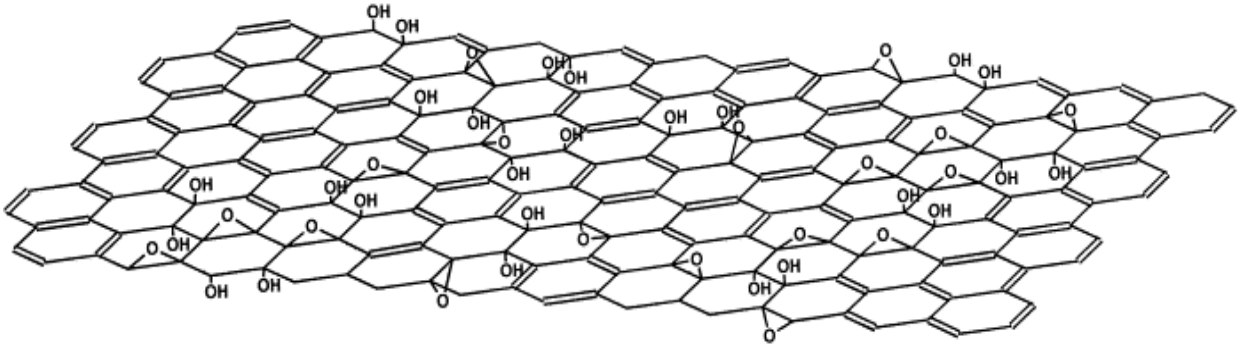

Figure 2.2: The Lerf-Klinowski model of graphene oxide (from ref. 12)

It is also important to notice that the structures and properties of GO can vary due to variations in the degree of oxidation caused by differences in the starting material [11].

2.1.3 A brief history of graphene

There has been an intense surge in interest in graphene during recent years, but as early as 1840 chemical modifications of graphite were described and graphene-like materials derived from graphite oxide were reported in 1962 [7].

First of all, to understand the history of graphene it is also important to mention some other terms, such as graphite oxide (GO), graphene oxide (i.e. exfoliated GO), graphite intercalation compounds (GICs) and reduced graphene oxide (r-GO). The reduced graphene oxide is here referred to as graphene.

In 1840, the first reports of GO were published, and this was done by the German scientist Schafhaeutl [13]. He reported the exfoliation of graphite with sulfuric and nitric acids.

In 1859, the British chemist Brodie did some modifications to Schafhaeutl experiments, in which he used sulfuric and nitric acids, as well as oxidants, such as $KClO_3$ [14]. As a result of this, he did notice the intercalation of the layers of graphite, but also chemical oxidation of the surface. Chemical modification of the surface reduces the interplanar forces that cause lamellar stacking, and therefore these oxidized layers can be readily exfoliated under ultrasonic, thermal, or other energetic conditions. In other words, the formation of GO has been very important in order to prepare graphene (r-GO) [14].

In 1958, Hummers and Offeman developed an alternate oxidation method by reacting graphite with a mixture of potassium permanganate and concentrated sulfuric acid, and today

modified versions of Hummers method are the most common production method of GO. This is also the method that the current work is based on [5].

Boehm et al. [15] did the reduction of dispersions of GO in alkaline suspension in 1962. What they found was that these reductions produced thin, lamellar carbon that contained only small amounts of hydrogen and oxygen, i.e. they made r-GO. They also used electron microscopy to determine the number of layers present in the lamellae, and Boehm concluded, "this observation confirms the assumption that the thinnest of the lamellae really consisted of single carbon layers" [15].

In 1970, Blakely and co-workers found that monolayers of graphite were produced by segregating carbon on the (100) surface of nickel. When exposed to high temperature the carbon dissolved was found to phase separate and form single or multiple layers of carbon on the metal surface [16].

Until 1995, many different terms were used in describing graphene, such as graphite layers, carbon layers or carbon sheets, and International Union of Pure and Applied Chemistry (IUPAC) found it necessary to formalize a definition of graphene: "The term graphene should be used only when the reactions, structural relations or other properties of individual layers are discussed" [17].

In 2004, Andre Geim, Konstantin Novoselov and their collaborators from The University of Manchester (UK), and the Institute of Microelectronics Technology in Chernogolovka (Russia), presented their results on graphene structures [18]. This is an important milestone in the history of graphene. They used a simple but effective mechanical exfoliation method for extracting thin layers of graphite from a graphite crystal with Scotch tape and then transferred these layers to a silicon substrate. By using Atomic Force Microscope, they were able to identify fragments made up of a single layer, in other words; graphene was identified. Even if graphene was produced earlier than 2004, this was the first time someone managed to isolate individual sheets in order to identify and characterize the graphene and to verify its unique two-dimensional properties. For this they were awarded the Nobel Prize in Physics in 2010 [8, 18].

So, as can be understood from this long history, there are many ways to produce graphene and graphene oxide, each with different advantages and disadvantages.

2.1.4 Applications

Despite the fact that graphene was discovered recently, its potential exploitation can be foreseen in many fields, ranging from hydrogen storage devices to batteries. A revolutionary application of graphene might be in electronics, and the material will enable faster and smaller transistors consuming less energy and dissipating heat faster than silicon based devices [19]. Other applications of graphene include fabrication of chemical sensors and transparent conducting films for solar cells and liquid crystal devices [20]. In addition, the high surface-to-mass ratio of graphene makes it suitable for ultracapacitors and batteries [21]. However, there are still many challenges to address before real industrial applications become possible [22], and the present work are done considering the use of graphene in Li-ion batteries.

2.2 Synthesis methods of graphene oxide

2.2.1 The original Hummers method

The production of graphene oxide by using a method called Hummers method was done for the first time in 1859, by Hummers and Offeman [5]. In their work, the GO was accomplished by treating graphite with essentially a water-free mixture of concentrated sulfuric acid (H_2SO_4), sodium nitrate ($NaNO_3$) and potassium permanganate ($KMnO_4$). Well reacted samples of graphene oxide will have a carbon to oxygen ratio lying between 2.1 and 2.9, and they showed that Hummers method resulted in a carbon to oxygen ratio of 2.25, which implies that the graphite was well oxidized and hence a promising production method for graphene oxide [5].

Hummers method is the most important and widely applied method for the synthesis of graphene oxide because of its high efficiency and satisfying reaction safety [23]. The three most important advantages over previous techniques are that the reaction can be completed in a very short time, $KClO_3$ which was used earlier is replaced by $KMnO_4$ in order to improve the reaction safety, and the use of $NaNO_3$ instead of fuming HNO_3 eliminates the formation of acid fog [23]. However, the method still has the following two flaws: (1) the oxidation procedure releases toxic gases such as NO_2 and N_2O_4, and (2) the remaining Na^+ and NO_3^- ions are difficult to remove from the waste water formed from the processes of synthesizing and purifying graphene oxide [23].

2.2.2 A modified Hummers method

In the modified Hummers method used in the present work $NaNO_3$ is excluded from the synthesis. This is done in order to remove the toxic gases released by the original method, NO_2 and N_2O_4. According to Chen et al. [23], this modification does not affect the dispersibility, chemical structure, thickness and lateral dimensions compared to products developed by the conventional method. The main steps of the modified method and the purpose of each step are explained below.

Step 1 – graphite powder + H_2SO_4 + $KMnO_4$

When sulfuric acid reacts with graphite, a graphite intercalation compound is obtained. This intercalation can only be accomplished in the presence of an oxidant, here $KMnO_4$ is used, and graphite bisulfate is produced. This is a compound in which every single-layer graphene sheet is sandwiched by the layers of bisulfate ions [24]. Depending on the nature of the oxidant and the concentration of the acid, graphite bisulfate of various composition $C_{24s}{}^{+}HSO_4{}^{-} \cdot 2H_2SO_4$ can be obtained (*s* is the stage number equal to the number of graphite grids between two closest layers of intercalate) [24]. The intercalation results in larger distances between the graphene sheets, and thus weakens interlayer interactions [12].
N. E. Sorokina et al. [24] studied the reaction of graphite with sulfuric acid in the presence of $KMnO_4$ at a widely varied $KMnO_4$:graphite ratio, and they found that the reaction of graphite with sulfuric acid in the presence of $KMnO_4$ occurred by scheme 1, where *s* is the stage number.

$$5C_{24s} + KMnO_4 + 17H_2SO_4 \rightarrow 5C_{24}^{s}HSO_4^{-} \cdot 2H_2SO_4 + MnSO_4 + KHSO_4 + 4H_2O$$

Scheme 1: The formation of graphite bisulfate by the reaction of graphite with sulfuric acid in the presence of $KMnO_4$, where s is the stage number (from ref. 24).

Besides to accomplish the intercalation of graphite with sulfuric acid, the addition of $KMnO_4$ provides the oxidation of the graphite. The two reactions, the formation of graphite bisulfate and the oxidation, take place simultaneously. Potassium permanganate is one of the strongest oxidants, especially in acidic media, and the complete intercalation ensures the effective penetration of $KMnO_4$ into graphene layers for oxidation of graphite [11].
The active species is, in fact, diamanganese heptoxide (Scheme 2). The bimetallic heptoxide is far more reactive than its nonmetallic tetraoxide counterpart. After this step, the starting material, graphite powder has become graphite oxide [25].

$$KMnO_4 + 3H_2SO_4 \rightarrow K^+ + MnO_3^+ + H_3O^+ + 3HSO_4^-$$

$$MnO_3^+ + MnO_4^- \rightarrow Mn_2O_7$$

Scheme 2: Formation of dimanganese heptoxide (Mn_2O_7) from $KMnO_4$ in the presence of strong acid (from ref. 25)

Step 2 – addition of H_2O_2

When hydrogen peroxide is added, the residual permanganate and manganese dioxide is reduced to colorless soluble manganese sulfate, and the color should turn from dark brown to yellow [5].

Step 3 – wash with 1:10 HCl

When the mixture is washed with 1:10 HCl the metal ions are removed [23].

Step 4 – wash with much water until pH is 7

This washing step is done in order to increase the pH. pH affects the hydrophilicity of the graphene oxide, and hence the desired behavior can be obtained at a pH of 7 [26]. At low pH the carboxyl groups are protonated such that the graphene sheets become less hydrophilic and form aggregates. At high pH the deprotonated carboxyl groups are very hydrophilic such that individual sheets prefer to dissolve in bulk water like regular salts [26].

Step 5 – dispersion into water by ultrasonication

The use of ultrasonication to disperse the paste into water will result in the graphite oxide being exfoliated [23].

Step 6 – centrifugation

After the dispersion by ultrasonication, the suspension is centrifuged in order to remove any unexfoliated graphite oxide, and to make the graphene oxide sediment [27].

Step 7 – drying the graphene oxide on an alumina plate

As a result of this step, the water is removed and sheets of graphene oxide can be scraped off.

2.3 Graphene oxide reduction

To prepare reduced graphene oxide, many chemical and thermal reduction approaches have been proposed. The chemical reduction route is fulfilled by using a wide range of reducing agents, while the thermal reduction methods generally rely on heating the graphene oxide in various atmospheres, as for example Ar or Ar/H_2, or with different heating sources like microwave, flash light, laser and plasma [28].
In general, chemical and thermal reduction approaches have their own advantages and disadvantages. With chemical methods, graphene oxide can be reduced in aqueous phase and the resulting reduced graphene oxide could contain various organic functional groups or nanostructures, which may be used to tune the properties of the reduced graphene oxide [28]. However, the most commonly used reducing agent, hydrazine, is highly toxic and explosive, and it should be avoided in an actual process, especially in large-scale processes [29].
On the other hand, by using thermal reduction, the degree of reduction can be controlled by adjusting the heating temperature, duration and gaseous environment [28]. In the following sections, only the thermal reduction mechanism will be outlined, as this is the approach used in the present work.

2.3.1 Thermal reduction mechanism

By directly heating GO in a furnace it is possible to create thermodynamically stable carbon oxide species. Exfoliation of the stacked structure occurs mainly through the extrusion of carbon dioxide generated by heating graphene oxide to 1050 °C [11]. In addition, carbon monoxide, water and other small molecule hydrocarbons are also possible byproducts [11]. While the decomposition of functional groups of graphene oxide yielding CO_2 is exothermic, the vaporization of water is endothermic and delays the heating process [30].
The high temperature gas creates enormous pressure within the stacked layers. Mc. Allister et al. [31] applied Lifshitz's formulation of van der Waals forces to calculate the binding energy between two adjacent layers. The pressure required to exfoliate GO was found by equation 2.1:

$$P = \frac{\partial G}{\partial l} = \frac{A_{Ham}}{6\pi l^3} \tag{2.1}$$

where G is the interaction free energy per unit area between two semi-infinite slabs, A_{Ham} is the Hamaker coefficient, and l is the interlayer distance [31]. Mc. Allister et al. predicted that a pressure of only 2.5 MPa is necessary to separate two stacked graphene oxide platelets [31]. The release of carbon dioxide inevitably leaves behind vacancies and topological defects on the graphene sheets, and such defects do have a negative impact on the electronic properties of the product by decreasing the ballistic transport path length and introducing scattering sites [30, 31].

2.3.2 Thermal reduction in various atmospheres

GO could be thermally reduced in various atmospheres, as for example Ar and Ar/H_2. GO thermally reduced in Ar prevents foreign adsorbates or contaminants. After the addition of H_2 interestingly and beneficially, the outcome of the reduction differs [28]. Both experimental and theoretical results provide evidence that the reduction level is higher for GO reduced in mixed Ar and H_2 than in pure Ar [32]. D. Yang et al. [32] found that by heating in pure Ar, the initial C/O ratio of 2.8 in GO increased to 11.4 when the reduction temperature was set to 1000 °C. When the atmosphere was changed to Ar/H_2, the same initial C/O ratio was increased to 12.4 at the same temperature, 1000 °C.

A possibly reason for why the Ar/H_2 mix is better than pure Ar, is that the thermally dissociated hydrogen atoms from hydrogen molecules could transform the epoxies into hydroxyls, which further develop into water molecules [33]. This transformation is significant as the outlet of oxygen in the form of CO or CO_2 through epoxies is related to the loss of carbon and implantation of oxygen. However, oxygen released via H_2O does not introduce any oxygen into the carbon backbone, and the exterior hydrogen atoms serve to transform these epoxies into hydroxyls [28].

2.3.4 How the particle size of graphite affects the oxidation

In order to obtain a successful exfoliation, it is necessary to first increase the *c*-axis spacing to 0.7 nm and completely eliminate the 0.34 nm graphite interlayer spacing. [31] The reaction time required to achieve the appropriate level of oxidation for the elimination of the 0.34 nm graphite peak depends on the starting flake size, as can be seen from figure 2.3 [31]. The XRD patterns show that when the flakes of the starting material have a diameter of 400 μm, the oxidation time should be 120 hours to fully eliminate the graphite peak. This time decreases significantly when reducing the starting flake size to 45 μm. The reason for this is

that smaller flakes allow for faster, more reliable oxidation reactions. In addition, the final graphene oxide flake size does not depend on the initial size of the graphite flakes [31].

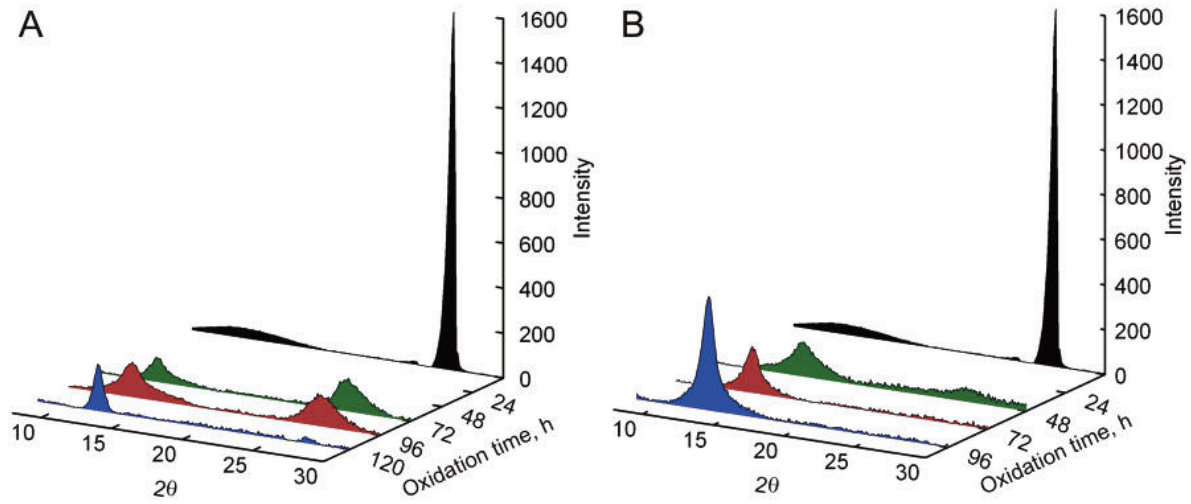

Figure 2.3: a) XRD patterns of 400 μm diameter graphite flakes oxidized for various lengths of time. The black pattern is obtained after 0 hours, the green after 72 hours, the red after 96 hours and the blue is after 120 hours of oxidation. b) XRD patterns of 45 μm diameter graphite flakes oxidized for various lengths of time. The black pattern is obtained after 0 hours, the green after 48 hours, the red after 72 hours and the blue is after 96 hours of oxidation. Note the disappearance of the native graphite peak after relatively short oxidation times. (From ref. 31)

2.4 Dispersibility of graphene

The dispersibility of r-GO is of great importance when using the material for battery applications. High degree of solubility is necessary in order to make a stable slurry that can be used for tape casting.

Before GO undergo thermal reduction, several oxygen containing functional groups are attached to the graphene sheets, and to date it has been found that the greater the polarity of the surface, the greater the dispersibility. Therefore, GO and r-GO show very different behavior when considering solubility [11]. However, the maximum dispersibility of GO does also depend on the solvent [11]. The oxygen functionalities render the GO layers hydrophilic and water molecules can readily intercalate into the interlayer galleries. GO can therefore also be thought of as a graphite-type intercalation compound with both covalently bound oxygen and non-covalently bound water molecules between the carbon layers [34]. Figure 2.4 shows an example of how the water can form hydrogen bonds to GO sheets.

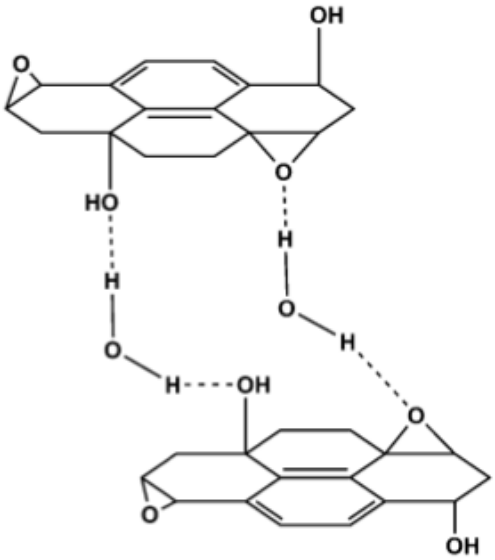

Figure 2.4: Proposed hydrogen bonding network formed between oxygen functionality on GO and water (from ref. 11).

So, as the oxygen groups are removed during thermal reduction, the r-GO has a hydrophobic nature [34]. There are many ways to functionalize r-GO in order to obtain better solubility, but these methods usually have a negative impact on the unique properties of r-GO, as for example the electrical conductivity.

2.4.1 Increasing dispersibility via functionalization

Although the research of functionalization on graphene is still in infancy, some interesting covalent and non-covalent chemistries have been devised for controlled functionalization of the basal plane and/or edge of graphene sheets to obtain desired properties [35]. Figure 2.5 shows the functionalization possibilities for a graphene sheet.

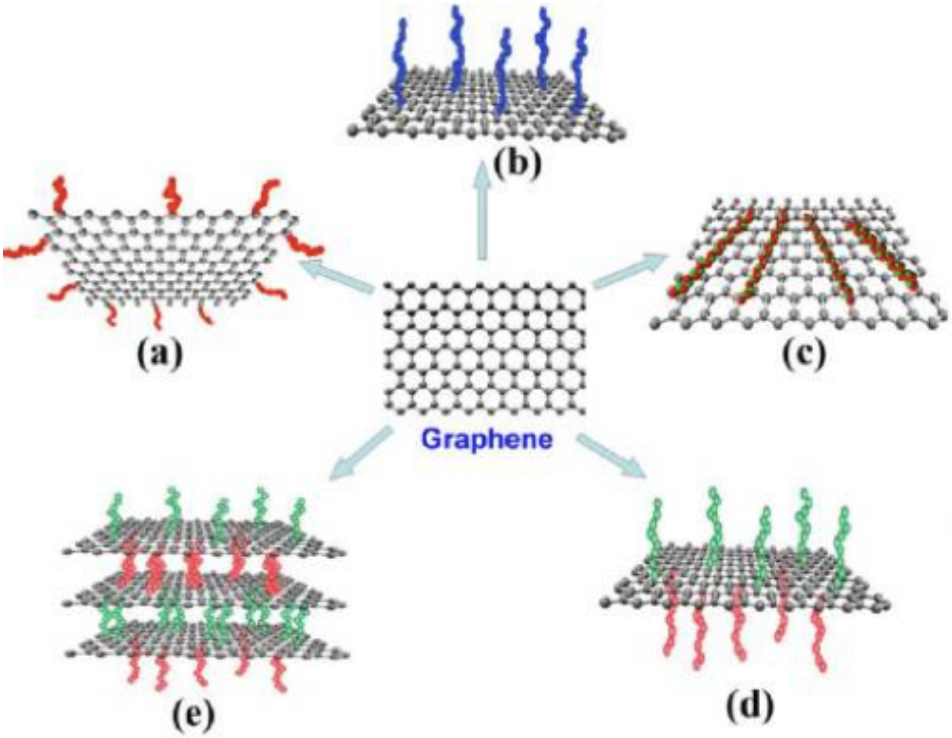

Figure 2.5: Functionalization possibilities for graphene: a) edge-functionalization, b) basal-plane-functionalization, c) non-covalent adsorption on the basal plane, d) asymmetrical functionalization of the basal plane, and e) self-assembling of functionalized graphene sheets (adapted from ref.35)

The edge sites of graphene with dangling bonds are more reactive than the basal plane with highly delocalized π electrons over the sp^2-hybridized carbon atoms [35]. Hence, the dangling bonds at the graphene edge can be used for covalent attachment of various chemical moieties to impart, for example, the solubility [35]. Covalent modification on the basal plane can, on the other hand, cause significant distortions of the π- π conjugation and result in undesirable physiochemical properties. However, the basal plane can undergo non-covalent functionalization, as for example adsorption, and then the basal plane will remain unchanged [35].

The problem with these modifications is that functionalization of pristine graphene sheets is very difficult, if not impossible, because of the poor dispersibility [35].

In spite of that, M. Naebe and co-workers [36] recently produced functionalized graphene directly from graphene sheets via Bingel reaction. They made a suspension of thermally reduced graphene oxide in dry dichlorbenzene (DCB) by sonication. From here, a mixture of 1,8-diazabibyclo[5.4.0]undecene (DBU) and diethylbromomalonate were added, and the resulting mixture was filtered and washed with DCB followed by ethanol. Further, the product was dispersed in a mixture of NaOH, methanol and tetrahydrofuran (THF). After

washing with HCl and several times with distilled water, the functionalized graphene was obtained after drying. The synthesis method is shown in figure 2.6.

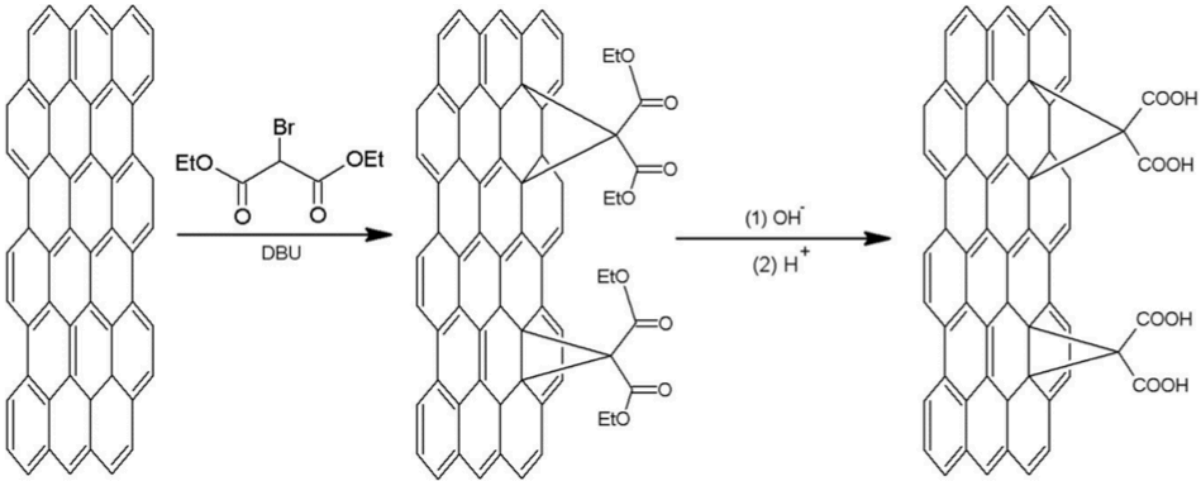

Figure 2.6: Synthesis of functionalized graphene via Bingel reaction (from ref. 36).

So, the end product after bingel reaction is carboxylic acids attached to the graphene sheets. These groups can contribute to improve the dispersibility as they make the surface negatively charged when dispersed in water and therefore electrostatic repulsion can be induced among the flakes and make them more hydrophilic [37, 38]. However, this modification can make significant changes in the properties of graphene, as for example decreasing the electrical conductivity.

Even if this method functionalized the graphene sheets directly from graphene, the GO sheets with the reactive oxygen containing functional groups is one of the most popular starting materials for functionalization of graphene [35].

2.5 Energy storage

Sustainable energy production, storage and consumption are major challenges that our world currently faces. The key achievement is not only to construct renewable and sustainable energy but also, perhaps even more importantly, to store energy efficiently and deliver it on demand, often for mobile applications, such as transportation systems and portable electronic devices. There are three major ways to store energy; chemically, electrochemically and electrically [39]. The main application for the graphene produced in the present work is for use in lithium ion batteries, i.e. to store energy in an electrochemically way [39].

As can be seen from figure 2.5, the Li-ion battery has high energy density, both when considering per unit of weight (W h kg^{-1}) and per unit of volume (W h l^{-3}), i.e. the Li-ion battery has high volumetric and gravimetric capacity [40]. Among the various existing technologies (fig. 2.7), Li-based batteries, because of their high energy density and design flexibility, currently outperform other systems, accounting for 63 % of worldwide sales values in portable batteries [40]. In spite of the good performance already obtained with Li-ion batteries, they are still investigated in order to achieve even better results. Especially the electrode materials are of interest, and the present work has been done considering the use in Li-ion batteries as electrode material.

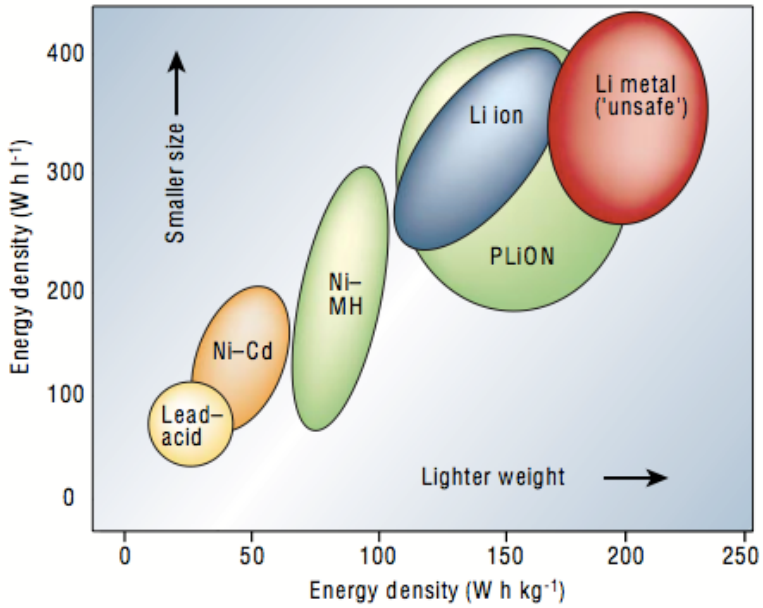

Figure 2.7: Comparison of the different battery technologies in terms of volumetric and gravimetric energy density. Li-based batteries are accounting for 63 % of worldwide sales values in portable batteries. (From ref. 40)

2.5.1 Graphene in lithium ion batteries

Graphene has recently emerged as a promising material for energy storage and battery applications. The superior properties of graphene, such as low weight, chemically inert, low price, outstanding electrical and thermal conductivity and large surface area are hugely favorable for energy storage applications [39].

There are several ways to produce graphene, and information as to how the graphene was prepared is crucial because the properties of graphene strongly depend on the method of fabrication [39].

Figure 2.8 shows a typical Li-ion battery, with graphite as anode material and $LiCoO_2$ as cathode material. The main principle of such a battery is that Li^+-ions migrate from the cathode towards the anode during charging, and the opposite way during discharging causing the electrons to flow in an outer circuit [41].

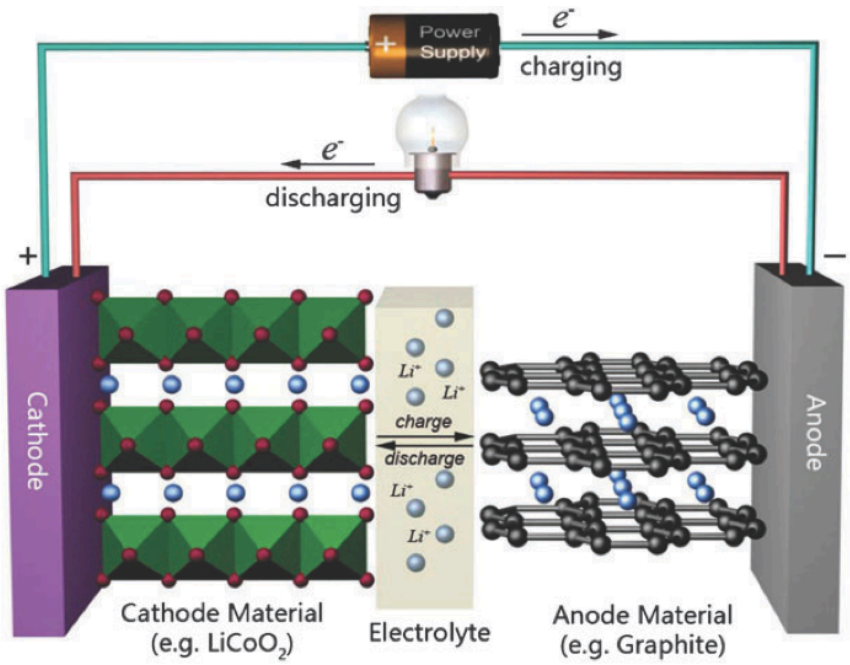

Figure 2.8: A typical Li-ion battery showing the charge/discharge intercalation mechanism (from ref. 41)

The structure of graphite is such that Li^+-ions can be stored in the centers, and the reason why graphene has been investigated as a better electrode material than graphite is that even more Li^+-ions can be stored, and hence give rise to higher gravimetric capacity [41]. The maximum specific lithium insertion capacity for graphite is 372 mAh/g, corresponding to the formation of LiC_6 [42]. During the intercalation process lithium transfers its 2s electrons to the carbon host and is situated between the carbon sheets [42]. Owing to its large surface-to-volume ratio and highly conductive nature, graphene may have properties that make it suitable for reversible lithium storage in lithium-ion batteries [42]. This is because lithium ions could be bound not only on both sides of graphene sheets, but also on the edges and covalent sites of the graphene nanoplatelets. Therefore it is expected that graphene could overtake its 3D counterpart (graphite) for enhanced lithium storage in lithium-ion batteries [42].
G. Wang et al. [42], made graphene sheets for anode material, and their cycling results are shown in figure 2.4. The cyclability of graphene nanosheet electrode was examined under

long-term cycling over 100 cycles, which demonstrated a good cyclic performance and reversibility (fig. 2.9). As can be seen from the figure, after 100 cycles, the graphene anode still maintained a specific capacity of 460 mAh/g, which represents a much enhanced performance than that of graphite anodes.

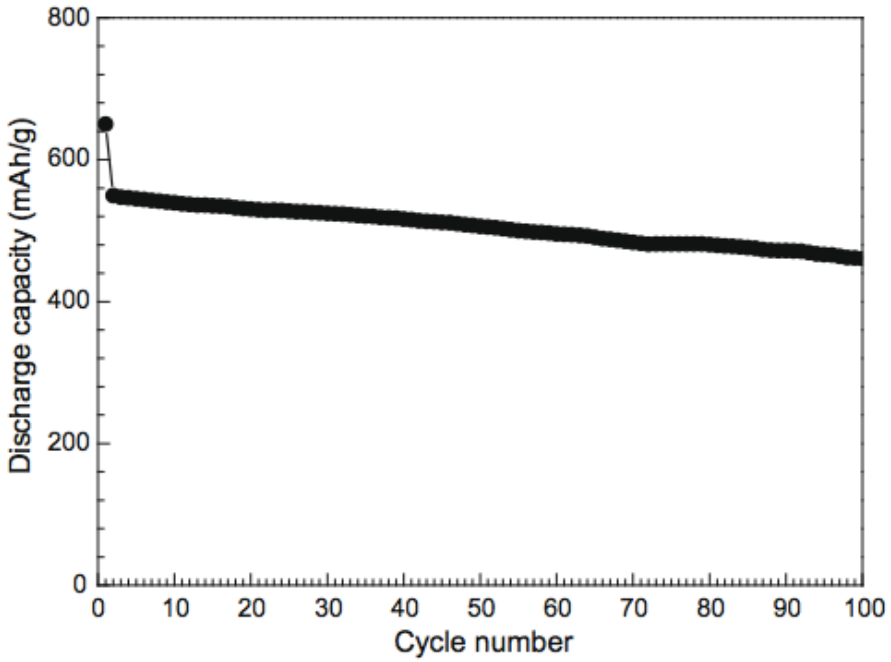

Figure 2.9: Discharge capacity (lithium storage) of graphene nanosheet electrode versus cycle number. (From ref. 42)

However, even if these results seems promising, it has also been shown that pure graphene cannot be used as anode material in Li-ion batteries due to its large irreversible capacity loss [43]. This means that a too big part of the Li-ions will be stored in the graphene structure, or in the thin film produced by the electrolyte at the electrode during the first cycle, and not let out [44]. Because graphene has very large surface area, this will increase the amount of this solid electrolyte interphase (SEI), resulting in larger irreversible capacity losses.
In other words, even if higher specific capacity is obtained by using graphene as electrode, graphene does also show large irreversible capacity loss, which is undesired.
In spite of that, graphene can be used as a part of a composite with other active materials [43]. Transition metal oxides, silicon and tin have been explored as active anode materials to replace graphite because of their high theoretical capacities. However, these materials have large volume changes during cycling that lead to the failure of the batteries. To resolve this

problem, additives have been added to these materials to mitigate this volume change. In recent years, graphene has been employed as an encapsulating agent for these materials [43].

2.6 Characterization methods

Different characterization methods have been used in order to investigate the materials. Laser diffraction is used to measure particle size and XRD is applied to find the crystal structure. In addition, SEM shows the morphology of the materials, and FTIR tells which atomic bonds that are present in the samples.

2.6.1 Particle size distribution by laser diffraction

Laser diffraction is a method used for measuring particle size distributions. This is done by measuring the angular variation in intensity of light scattered as a laser beam passes through a dispersed particulate sample. Large particles scatter light at small angles relative to the laser beam and small particles scatter light at large angles, as shown in figure 2.10 [45]. The optics in the instrument are arranged so that particles of the same size scatter light to the same part of the detector array.

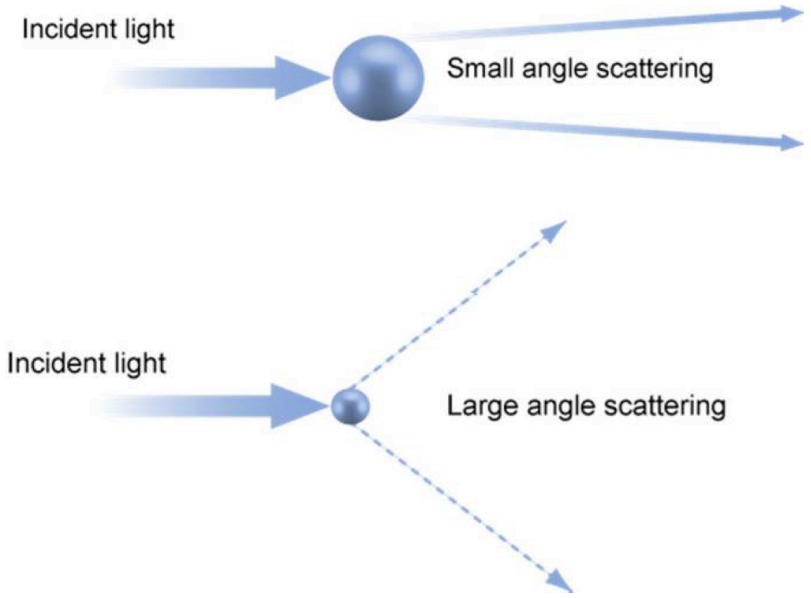

Figure 2.10: Large particles scatter light at small angles and small particles scatter light at large angles.

The angular scattering intensity data is then analyzed to calculate the size of the particles responsible for creating the scattering pattern, using the Mie theory of light scattering. The particle size is reported as a volume equivalent sphere diameter [45].
This method is assuming a volume equivalent sphere model and requires knowledge of the optical properties (refractive index and imaginary component) of both the sample being measured and the dispersant. These are easy to find from the in-built databases.
A schematic figure of the instrument is shown in figure 2.11.

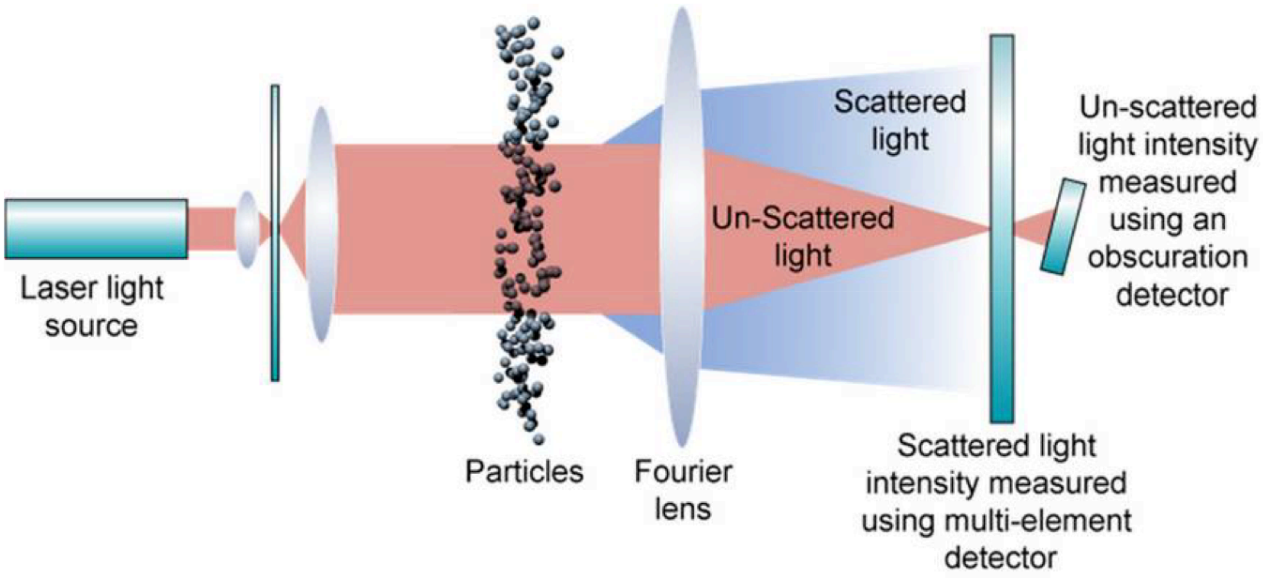

Figure 2.11: A basic laser diffraction system.

2.6.2 X-ray diffraction (XRD)

(The description of the principle of XRD given below is based on the book "Materials Science and Engineering: An Introduction" of Callister and Rethwisch, ref. 46)
X-rays are a form of electromagnetic radiation, and have large energies and short wavelengths. In fact, the wavelengths are in the order of the atomic spacings for solids. When the x-rays impinges on a solid material, a portion of the beam will be scattered in all directions by the electrons associated with each atom or ion that lies within the beam's path. When using XRD for characterization, usually a monochromatic and in-phase x-ray beam with wavelength λ is sent towards a specimen, making an angle θ with the specimen, see figure 2.12. Two parallel planes of atoms A-A' and B-B', which have the same h, k and l Miller indices and are separated by the interplanar spacing d_{hkl}, are represented in the figure. The phase relationship between the diffracted and the incident beam is dependent on the difference in path length the beams travel. When the path length difference is an integral

number of the wavelength, the diffracted beams will still be in phase. They are said to constructively interfere with one another, and this is the manifestation of diffraction. On the other hand, when the difference in path length is some integral number of half wavelengths, the scattered waves will be out of phase, they destructively interfere.
So, the condition that needs to be fulfilled in order to get diffraction, is:

$$n\lambda = \overrightarrow{SQ} + \overrightarrow{QT} \tag{2.2}$$

$$n\lambda = d_{hkl}sin\theta + d_{hkl}sin\theta \tag{2.3}$$

$$n\lambda = 2d_{hkl}sin\theta \tag{2.4}$$

Equation 2.4 is known as Bragg's law, and from this it is possible to calculate the graphene distance layer.

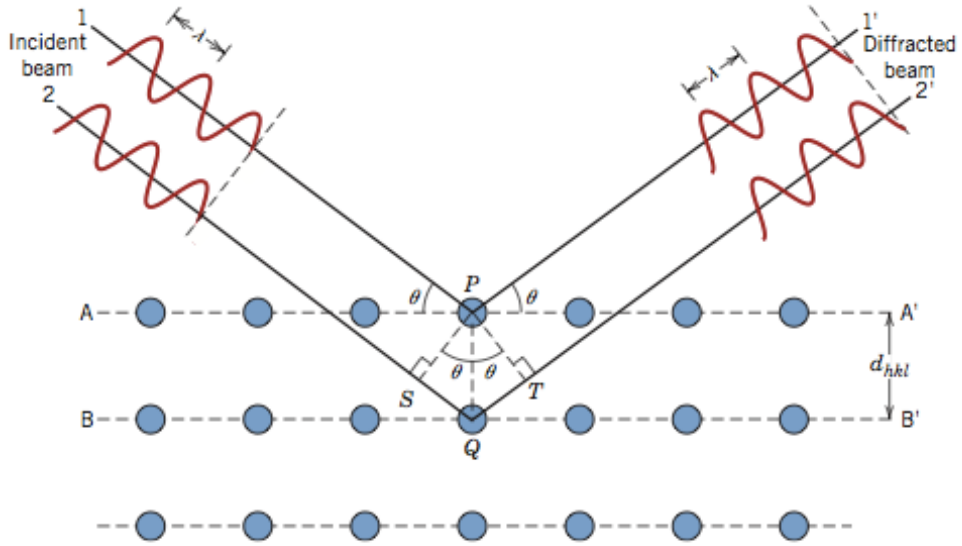

Figure 2.12: Diffraction of x-rays by planes of atoms (from ref. 46).

Figure 2.13 shows a schematic of the diffractometer. The diffractometer is an apparatus used to determine the angles at which diffraction occurs for powdered specimens. A specimen *S* in the form of a flat plate is supported so that rotations about the axis labeled *O* (perpendicular to the paper) are possible. The monochromatic x-ray is generated at point *T*, and the intensities of the diffracted beams are detected with a counter, *C*. The counter is mounted on a movable

carriage, and its angular position in terms of 2θ is marked on a graduated scale. Carriage and specimen are mechanically coupled such that a rotation of the specimen through θ is accompanied by a 2θ rotation of the counter. Because of this coupling, the angle of the incident and reflected beam is the same.

After a certain time of exposure, a diffraction pattern is obtained. In the diffraction pattern, the intensities are along the y-axis, and the diffraction angle, 2θ, is along the x-axis. The unit cell size and geometry may be resolved from the angular positions of the diffraction peaks, whereas the intensities can give information about the arrangement of atoms within the unit cell. Every crystalline material gives a unique powder x-ray diffraction pattern, it is a fingerprint, and the most common way to identify a compound is by comparing the obtained diffraction pattern with database containing diffraction patterns of known materials.

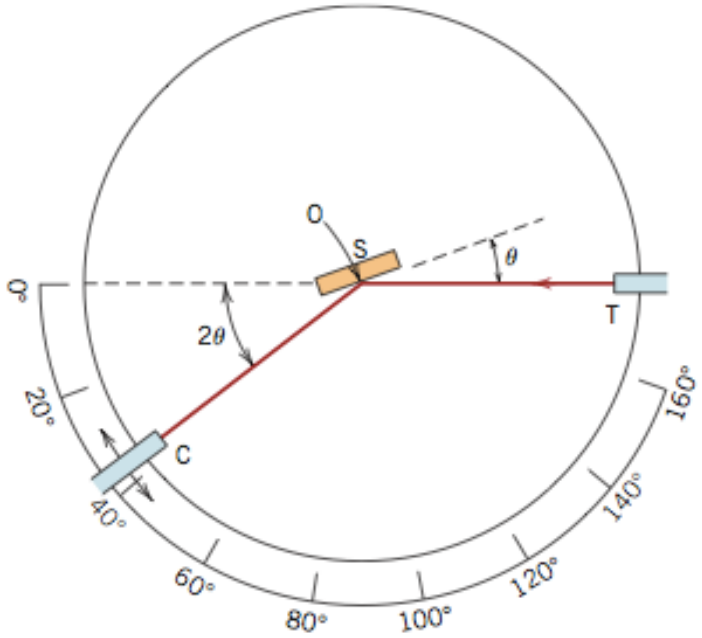

Figure 2.13: Schematic diagram of a x-ray diffractometer; T = x-ray source, S = specimen, C = detector and O = the axis around which the specimen and the detector rotate (from ref. 46).

The XRD patterns of graphite, graphene oxide and graphene are shown in figure 2.14. Graphite powder exhibits a characteristic peak (002) at 26.58°, and after oxidation this peak disappears and a new one is observed at 11.36°, corresponding to the (001) diffraction peak of graphene oxide. In addition, no peaks are seen for graphene [47].

In addition to Bragg's law, there is another equation that is important when considering XRD patterns, and this is called the "Scherrer's equation":

$$t = \frac{0.9\lambda}{B_{1/2} cos\theta_B} \tag{2.5}$$

where t is the crystallite size, λ is the X-ray wavelength, $B_{1/2}$ is the width at half the maximum intensity and θ_B is the Bragg angle [48]. So, as t decreases, $B_{1/2}$ increases. From this equation, it is possible to calculate the crystallite size, which can be an important parameter

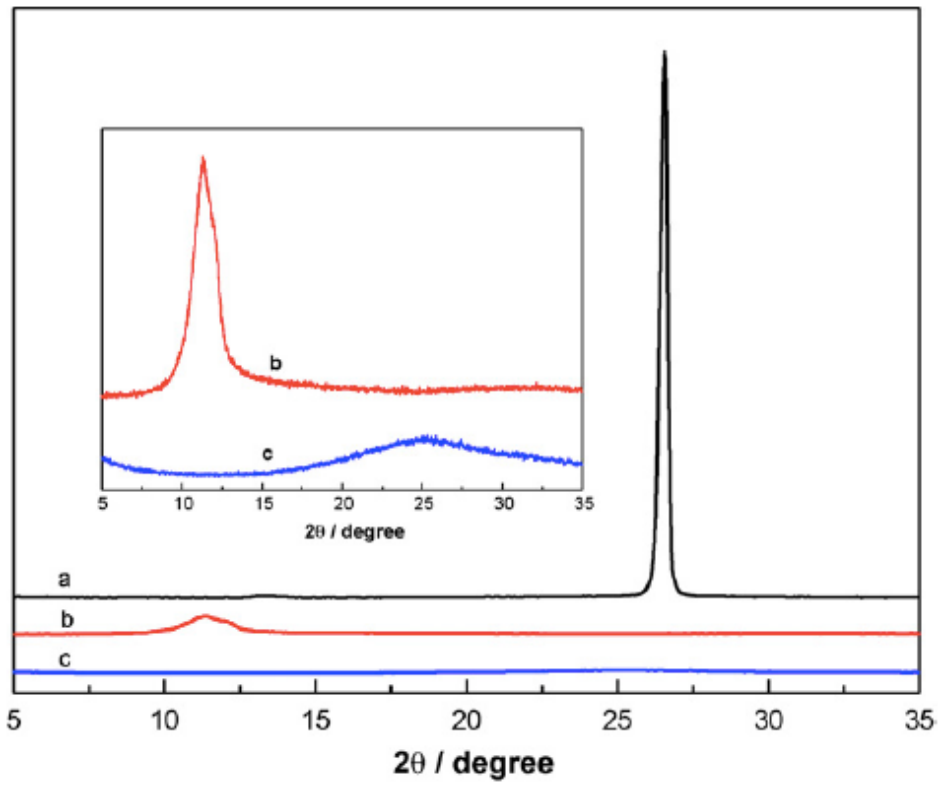

Figure 2.14: XRD patterns of a) graphite powder, b) graphite oxide and c) graphene sheets. (From ref. 47)

2.6.3 Scanning Electron Microscopy (SEM)

(The description of the principle of SEM given below is based on the books "Materials Science and Engineering: An Introduction" by Callister and Rethwish, ref. 46, and "Semiconductor Manufacturing Technology" by Quirk and Serda, ref. 49)

The upper limit to the magnification possible with an optical microscope is approximately 2000 times. Consequently, some structural elements are too fine or small to permit observation using optical microscopy. When this is the case, the scanning electron

microscope, which is capable of much higher magnification, may be employed. The first commercial SEMs were produced in the 1960s, and the SEM can achieve magnifications up to 300000 times, which is significantly higher than optical microscopes. The resolution, that is the smallest feature detectable, for SEMs is in the order of 40 to 50 Å.

Compared to an optical microscope, a SEM uses an electron beam instead of photons to make an image. According to quantum mechanics, a high-velocity electron will become wave-like, having a wavelength that is inversely proportional to its velocity. The SEM has an electron gun, focusing lenses for shaping the electrons into a beam and a final electrostatic-magnetic focusing system that makes the electrons strike the sample within a small, 2 to 6 nm spot. When the electrons are accelerated across large voltages, they can be made to have very short wavelengths, for instance 1.22 Å for 100 eV electrons. Because of the short wavelengths, it is possible to obtain very high magnifications and hence small patterns can be viewed.

Once the incident electron beam hits the sample investigated, backscattered, along with other electrons, X-rays and photons are emitted or transmitted due to interaction between the beam and the sample surface. The secondary electrons are collected and an electronic image that represents the surface of the sample is created. Backscattered electrons are also collected and offer superior compositional contrast between different materials.

The surface of the sample you want to analyze has to be electrically conductive, i.e. a very thin metallic surface coating must be applied to nonconductive materials.

A schematic of a SEM is shown in figure 2.15, and SEM images of the morphology of graphite, graphene oxide and reduced graphene oxide are shown in figure 2.16a, b and c, respectively.

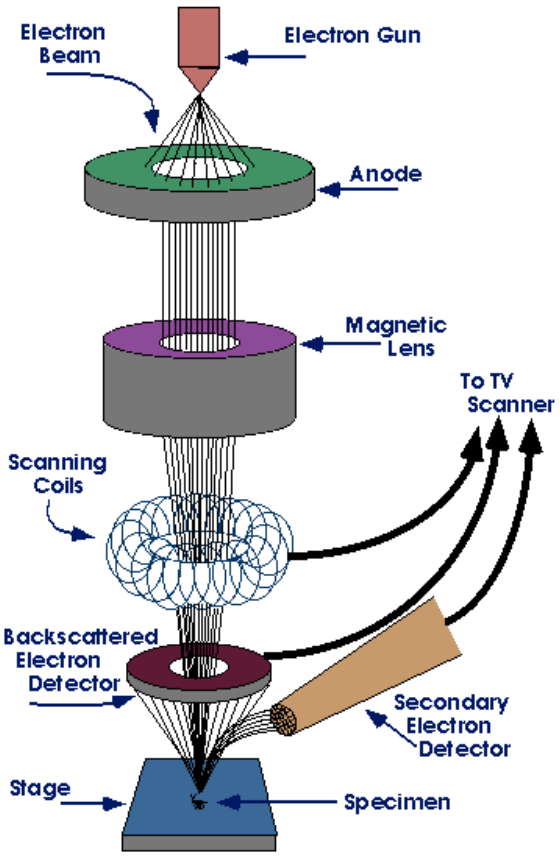

Figure 2.15: A schematic of a SEM (from ref. 50).

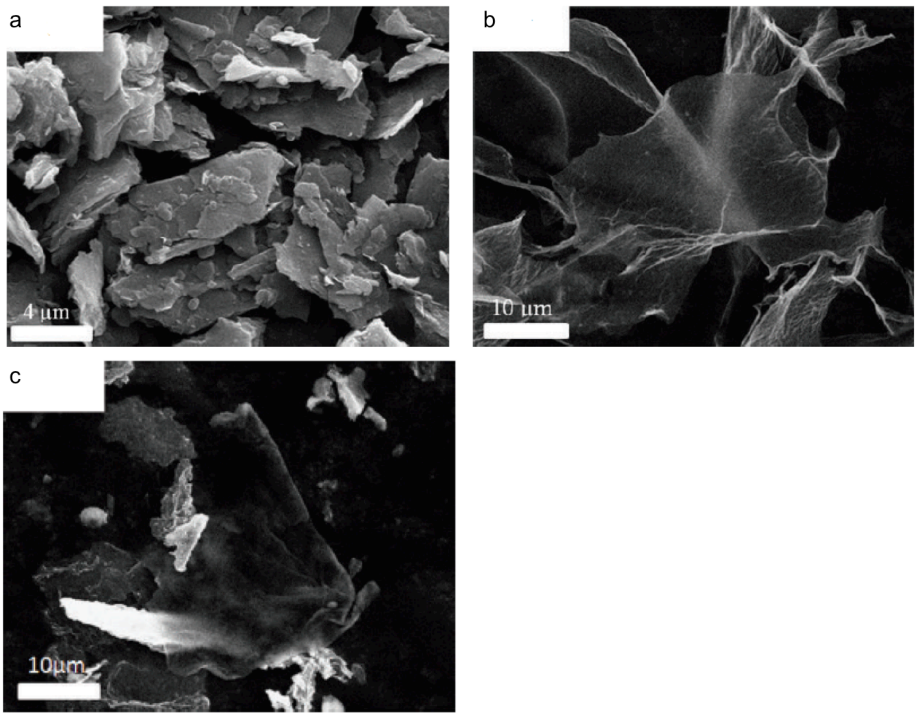

Figure 2.16: SEM images of a) graphite particles, b) graphene oxide and c) reduced graphene oxide (from ref. 51)**.**

2.6.4 Fourier Transform Infrared Spectroscopy (FTIR Spectroscopy)

Infrared spectroscopy (IR) is a characterization technique using infrared radiation to characterize the surface of a material [52]. Materials exposed to the infrared radiation absorb different energies, dependent on the atomic bonds present in the material.

The infrared light is obtained from lasers, and these laser beams are electromagnetic radiation which have characteristic wavelengths. Usually, the wavelengths are represented using wavenumber, the reciprocal of the wavelength. This quantity also related to the frequency of the light wave and speed of light:

$$\tilde{v} = \frac{1}{\lambda}\,[cm^{-1}] = \frac{v}{c}\,[cm^{-1}] \tag{2.6}$$

where $\tilde{v}$ is the wavenumber, λ is the wavelength, v is the frequency of the light and c is the speed of the light [52].

As with other types of energy absorption, molecules are excited to a higher energy state when they absorb infrared radiation. The absorption of infrared radiation is like other absorption processes, a quantized process, which means that a molecule only absorbs selected frequencies (energies) of IR radiation [53]. The energy absorbed serves to increase the amplitude of the vibrational motions of the bonds in the molecule. However, only bonds that have a dipole moment that changes as a function of time are capable of absorbing IR radiation [53].

Since every type of bond has a different natural frequency of vibration, and since two of the same type of bond in different compounds is in two slightly different environments, no two molecules of different structure have exactly the same infrared absorption pattern, i.e. the infrared spectrum is a fingerprint [53].

The instrument that determines the absorption spectrum for a compound is called a spectrometer, and one type of such a spectrometer is called a Fourier Transform Infrared Spectrometer (FTIR) [53]. In this instrument, the design of the optical pathway produces a pattern called an interferogram. The interferogram is a complex signal, but its wave-like pattern contains all the frequencies that make up the infrared spectrum. An interferogram is essentially a plot of intensity versus time, but by using Fourier transform on the interferogram one can obtain a spectrum that is a plot of intensity versus frequency [53]. A typical setup of a FTIR is shown in figure 2.17.

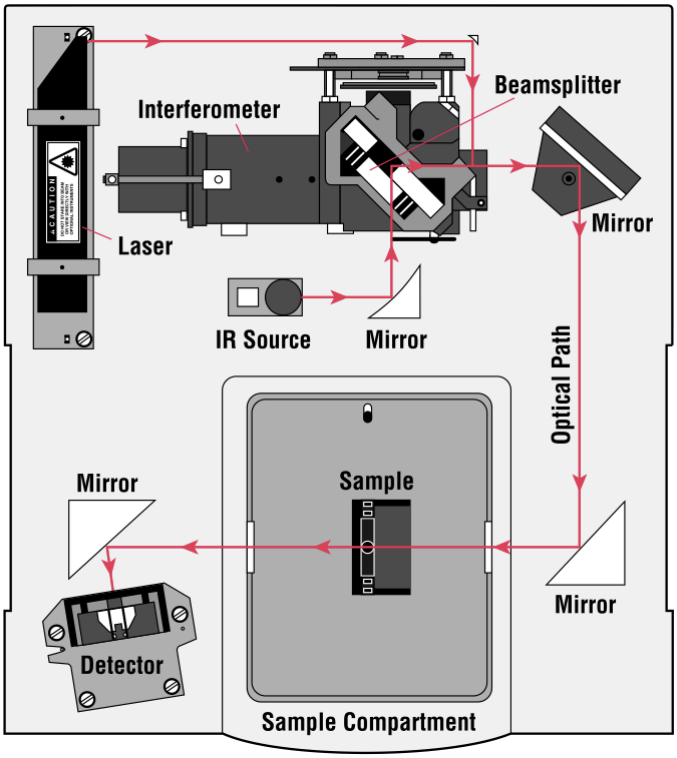

Figure 2.17: A typical FTIR setup (from ref. 54).

Bond properties and absorption trends

When analyzing FTIR spectra, it is important to know how bond strength and the masses of the bonded atoms affect the infrared absorption frequency. Further, a simple physical model will be used in this understanding.

A diatomic molecule can be considered as two vibrating masses connected by a spring. The bond distance changes continually, but an equilibrium or average bond distance can be defined. When the bond vibrates, the energy of vibration is continually and periodically changing from kinetic to potential energy and back again. It is like a harmonic oscillator, and the total amount of energy is proportional to the frequency of the vibration:

$$E_{osc} = h\nu_{osc} \tag{2.7}$$

where E_{osc} is the energy, h is Plank's constant and ν_{osc} is the frequency [53]. The frequency for a harmonic oscillator is determined by the force constant (K) of the spring and the masses m_1 and m_2 of the two boned atoms. The natural frequency of vibration of a bond is given by:

$$\bar{v} = \frac{\pi}{2}\sqrt{\frac{K}{\mu}} \tag{2.8}$$

where μ, the reduced mass, is given by:

$$\mu = \frac{m_1 m_2}{m_1 + m_2} \tag{2.9}$$

As an approximation, the force constant for triple bonds are three times those of single bonds, whereas the force constant for double bonds are twice those of single bonds [53].
Note that stronger bonds have a lager *K*, and vibrate at higher frequencies than weaker bonds. In addition, bonds between atoms of higher masses vibrate at lower frequencies than bonds between lighter atoms. Also bending motions occur at lower energy than the typical stretching motions because of the lower value for the bending force constant *K* [53].
In this project FTIR is used to find which functional groups that are present in the graphene oxide, and which groups that have disappeared after the thermal reduction to reduced graphene oxide. The instrument used is measuring transmittance instead of absorbance. Figure 2.16 is showing the approximate regions where common types of bond absorb, which is a good idea to memorize.

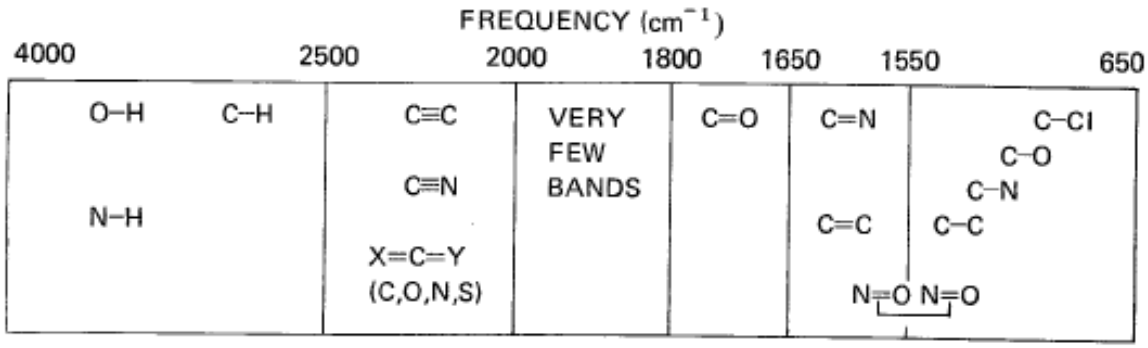

Figure 2.18. The approximate regions where various common types of bonds absorb (stretching vibrations only). (Adapted from ref. 53).

3 Experimental

This chapter describes the procedures used for the syntheses, both the wet chemical synthesis to GO, and the thermal reduction in order to obtain r-GO. Different heating routes are investigated, and all of them will be presented. All the samples are characterized using several techniques, and the sample preparation along with the necessary parameters will also be described in detail.

3.1 Synthesis of graphene oxide

GO was prepared by the oxidation of natural graphite powder according to Hummers method with a modification of removing $NaNO_3$ from the reaction formula. The procedure used is based on Chen et al. [27], and the parameters varied in the different syntheses are the oxidation time and the particle size of the graphite powder.

Graphite powder (3.00 g) was added to concentrated (95-98 %) H_2SO_4 (70 mL). Under vigorous agitation in an ice-bath, $KMnO_4$ (9.00 g) was added slowly so that the temperature of the mixture did not exceed 20 °C, the temperature was controlled continuously using a regular thermometer. The suspension was then stirred for 2 hours at 35 °C, and 150 mL deionized water was added in the end.

Further, the suspension was left for 3, 5 and 10 days for synthesis 1, 2 and 3, respectively. This time is known as the oxidation time, and in the present work this time is varied in order to find the most appropriate oxidation time. When the suspension was oxidized, the next step was to add 500 mL deionized water and 30% H_2O_2 (7.5 mL), and this caused violent effervescence and an increase in temperature. During this step, the solution should change color from dark brown to yellow. The mixture was then washed with 750 mL 1:10 HCl:water by filter paper and funnel, in order to remove metal ions. The resulting solid was dried in air at 60 °C for 6.5 hours, until agglomeration was observed, and then dispersed into 500 mL deionized water in static state for 3 hours and slightly stirred with a glass bar. Purification was done by washing the suspension with large amounts of deionized water. The pH increased from 1 to 5 during these washing processes, and the setup is shown in figure 3.1.

Figure 3.1: The setup used for washing processes.

Further, the paste collected from the filter paper was dispersed into 300 mL deionized water by ultrasonication for 20 min to exfoliate the graphite oxide to graphene oxide. The resulting brown dispersion of graphene oxide was then centrifuged at 4000 rpm for 30 min to remove any unexfoliated graphite oxide. After the centrifugation the graphene oxide was placed in the bottom of the containers, and decanting was done without problems. Furthermore, dried GO was obtained by dehydration on an alumina plate in air. The dehydration step started out at 30 °C for 2 minutes, then 40 °C for 2 minutes, 50 °C for 2 minutes, and finally 60 °C for 1 hour. Flakes of GO were obtained by scraping off the solid from the alumina plate.
Synthesis 4 was done in the same way, but here the graphite powder was sieved so that the particle size was less than 50 μm. The oxidation time was 5 days.
These four syntheses will be referred to as GO1, GO2, GO3 and GO4, respectively.

3.2 Thermal reduction of graphene oxide

Different heating routes are investigated in order to find the best procedure. First, a method using very slow heating rate was performed, followed by medium heating rate and finally a rapid heating rate was investigated.

3.2.1 Slow thermal reduction

In order to reduce the GO, the samples were placed in an alumina boat and inserted into a tube furnace. Figure 3.2 shows an example of GO flakes in the alumina boat before inserting it into the furnace.

Figure 3.2: GO placed in an alumina boat before inserting it into the tube furnace.

The samples were flushed with Ar gas and heated to 150 ˚C with a heating rate of 60˚C/h. From here the GO was heated at a rate of 300 ˚C/h until the temperature reached its maximum. Different maximum temperatures are investigated in order to optimize the reduction process. 300, 400, 700 and 900 ˚C are the maximum temperatures tested, and the samples were held at tis point for 30 min, and finally cooled down to room temperature at a rate of 200 ˚C/h.

This method was also performed using Ar/H_2-gas (5% H_2), and then the temperature was increased to 1000 ˚C. The heating rates were not changed.

The different heating routes are given in figure 3.3.

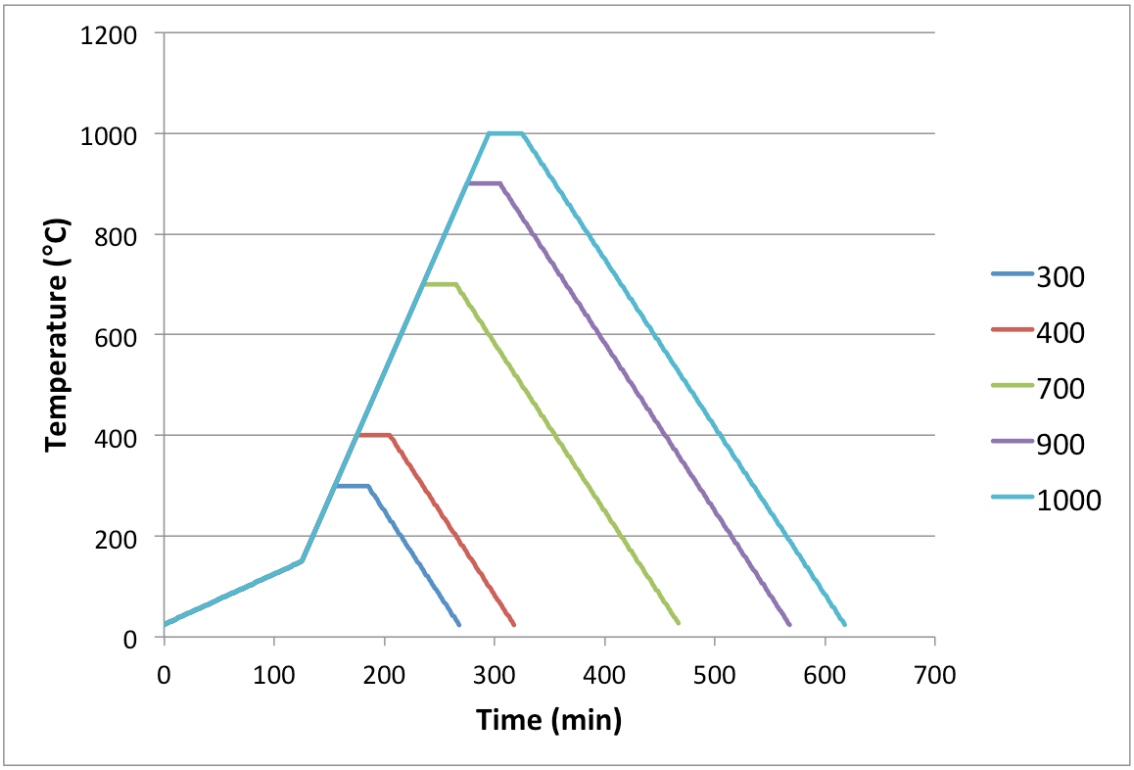

Figure 3.3: The heating routes used for reduction of GO1, GO2, GO3 and GO4.

3.2.2 Medium thermal reduction

After the slow heating rate was investigated, the heating rate was increased. In this case, GO4 was reduced using a chemical vapor deposition instrument (CVD), called CVD TA100 produced by Graphene Square.

The graphene oxide flakes were placed in an alumina container, and put into a quartz tube. Everything was mounted such that the sample was placed in the middle of the furnace, as shown in figure 3.4.

The gas introduced into the chamber was Ar and 5% H_2, and the gas flow was controlled to be 100 sccm (standard cubic centimeters per minute) for Ar and 5 sccm for H_2. The heating rate was set to 25 ˚C/min, and the temperature was held constant at 1000 ˚C for 30 minutes. The cooling rate could not be controlled using this instrument. It took approximately 50 minutes to cool down to 500 ˚C, and from this point the cooling rate was seen to be a bit faster. Figure 3.5 shows an illustration of the heating process.

However, when using this method, it is important that the GO flakes are large enough, see Appendix A.

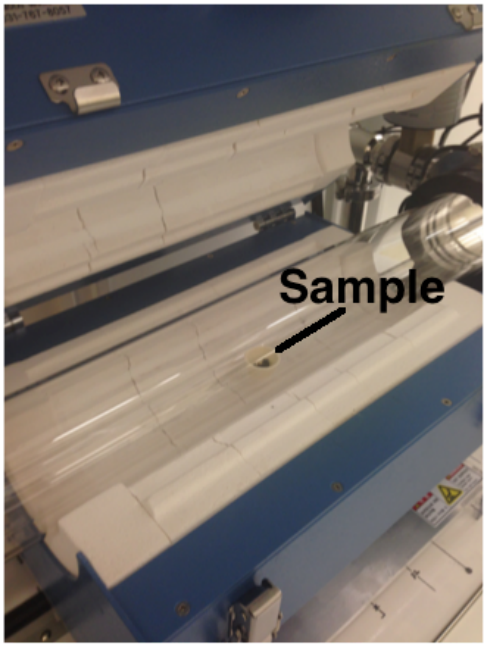

Figure 3.4: The setup of the CVD. The GO flakes are placed in an alumina container inside a quartz tube, in the middle of the furnace.

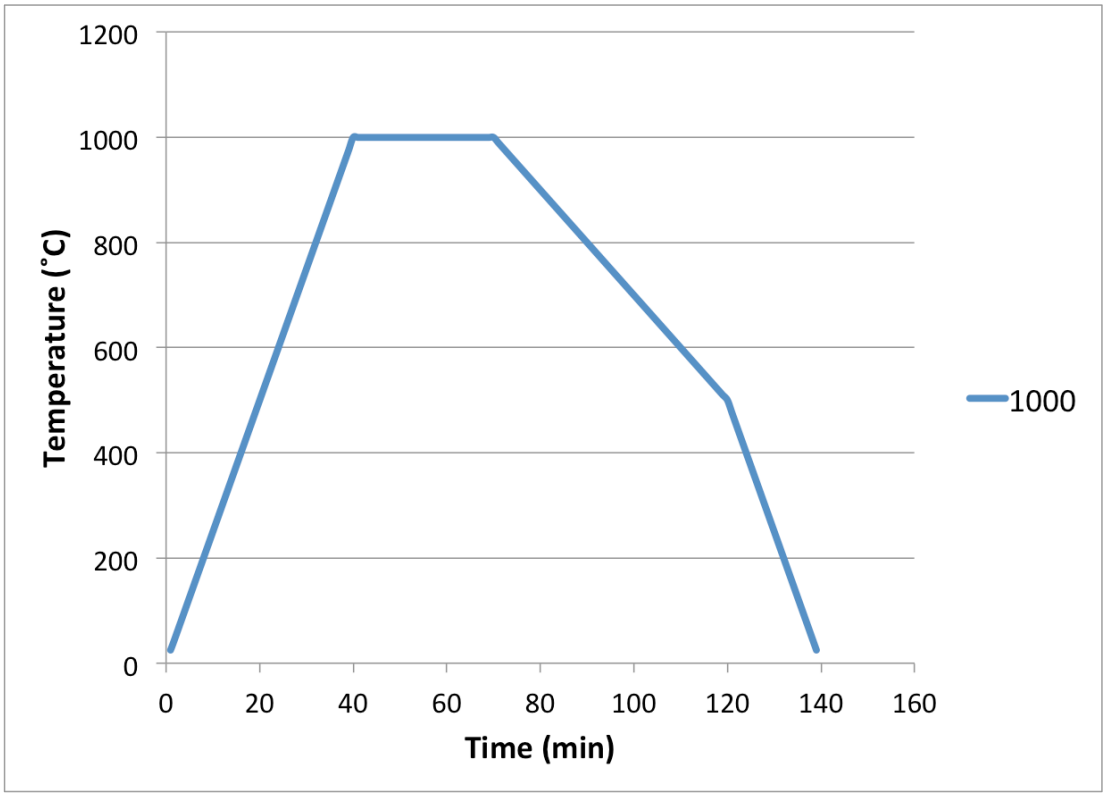

Figure 3.5: The heating process used for reduction of GO4 using CVD.

3.2.2 Rapid thermal reduction

After trying both slow and medium heating rates, a rapid thermal process was applied in order to reduce GO4. By doing this, one can see if the heating rate has an impact on the end result. The instrument used is Jipelec Jetfirst 200 mm RTP oven, and some flakes of GO4 were placed onto a SiC susceptor and covered with a Si wafer on top to prevent the flakes from moving around, as shown in figure 3.6.

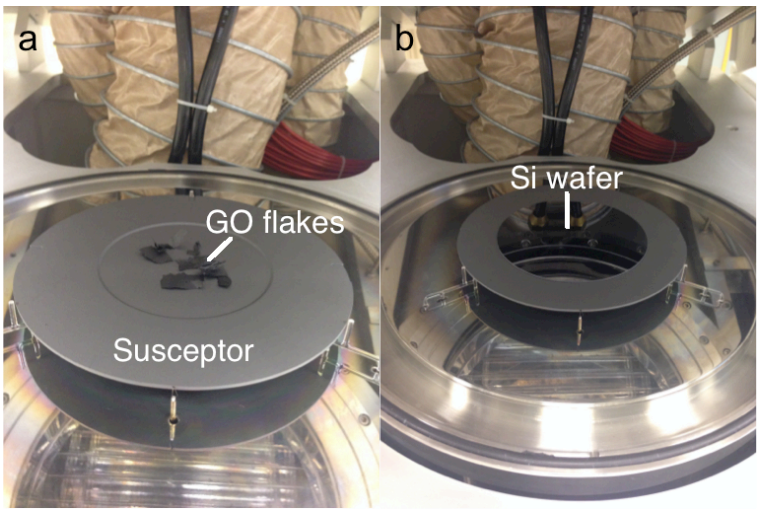

Figure 3.6: a) GO flakes placed on a SiC susceptor, and b) GO flakes covered with a Si wafer to ensure that they do not move around during heating.

The heating rate was set to 5 ˚C/s, which is remarkably faster than the slow and medium processes outlined above. When the temperature reached its maximum, 700, 900 or 1000 ˚C, it was held at this temperature for 30 min. Further, the cooling rate was the same as the heating rate. In addition, the samples were flushed with Ar/H_2 (5% H_2), and the gas flow was controlled to be 500 sccm. Figure 3.7 shows the heating routes used in the RTP.

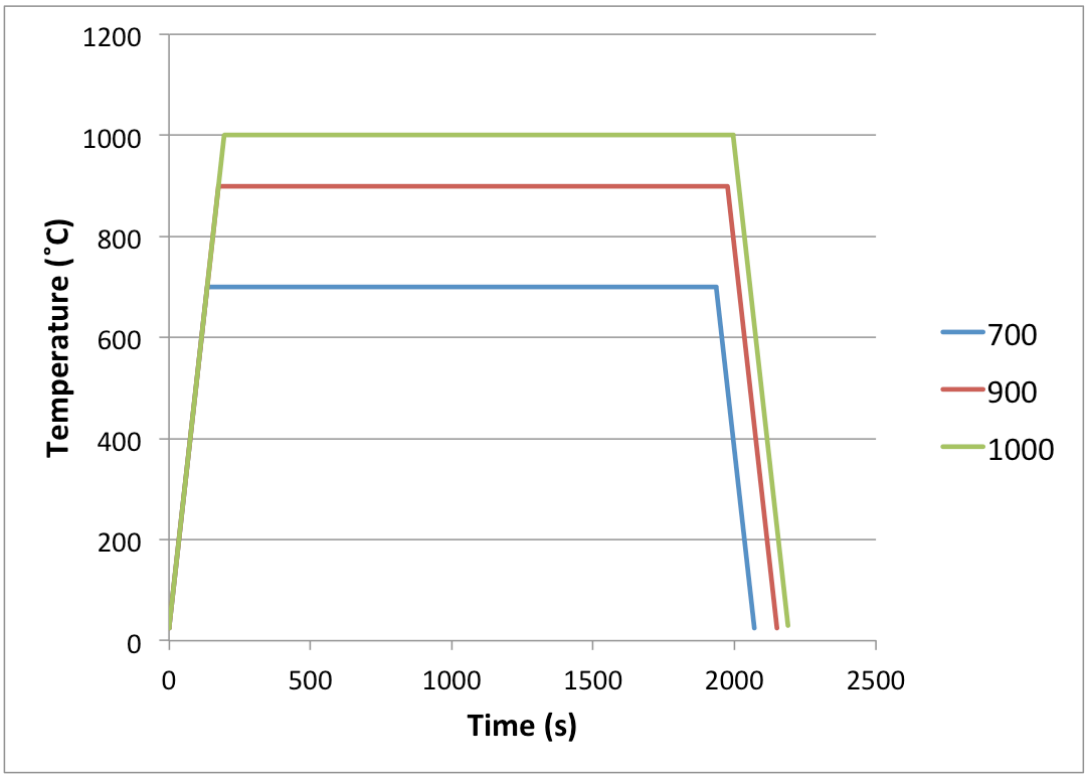

Figure 3.7: The heating routes used for reduction of GO4 and GO5.

3.3 Characterization

3.3.1 Laser diffraction

The starting material, graphite, was analyzed in order to find the particle size. The particle size affects the oxidation time, and the larger the particles are the longer oxidation time is required to obtain fully oxidized graphite [31]. In fact, when the diameter is 400 μm the oxidation time has to be longer than 120 hours. On the other hand, if the diameter of the graphite particles is decreased to 45 μm, an oxidation time of approximately 48 hours is needed [31].

In order to do the laser diffraction, some graphite powder was added to deionized water in a beaker, and placed into the instrument; Malvern Mastersizer 2000. The optical properties of the dispersant, deionized water, were found in the built-in database, and the refractive index of the graphite powder was set to the same as carbon, 2.42. Both a red and a blue laser were applied, with wavelengths of 632.8 and 466 nm, respectively.

3.3.2 XRD

The crystal structure of graphite powder, the GO samples and the r-GO were characterized by XRD using a Bruker D8 DaVinci X-ray Diffractometer. For all samples, the 2θ range measured was from 5° to 75°, the detector step size was 0.045°, time per step was 0.55 s and the slit size was set to 6.000 mm. The diffractometer applied Cu Kα radiation with wavelength of 1.54060 Å.

For sample preparation, s small amount of the carbon sample was grounded into powder, using an agate mortar and some droplets of ethanol, just enough to cover the powder. Finally the mixture was put into a sample holder. It is important that the top of the sample is flat, and that it is leveled with the top of the sample holder.

In some of the XRD experiments, approximately 40wt% Si powder was mixed together with the carbon sample in order to make a standard so that the exact peak positions could be found. Figure 3.8 shows how the flakes of GO and Si powder looked before and after they were grounded into powder and mounted on the sample holder.

Computer programs called *BRUKER DIFFRAC.EVA* and *DIFFRAC^{PLUS} TOPAS V 4.2* was used to analyze the results from the scans.

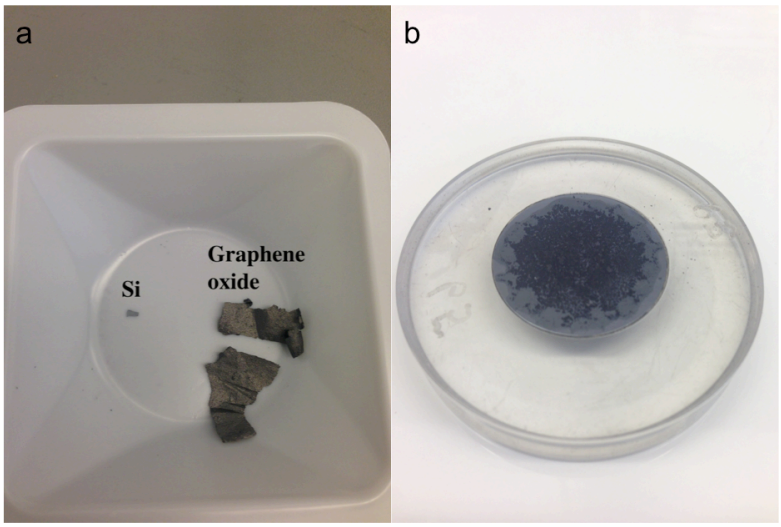

Figure 3.8: a) Si was used in the XRD in order to have a reference, b) Graphene oxide and Si powder placed on the Si holder.

3.3.3 FTIR Spectroscopy

In order to examine the oxygen containing functional groups, all the samples were characterized by FTIR transmission spectra (4000 – 550 cm^{-1}), using a Thermo Nicolet Nexus instrument with ATR (attenuated total reflectance) module.

The samples were analyzed directly, by placing small flakes of the samples between the metal tip and the diamond part of the instrument, as shown in figure 3.9. No sample pretreatment was done.
The results were analyzed using a software called *OMNIC*.

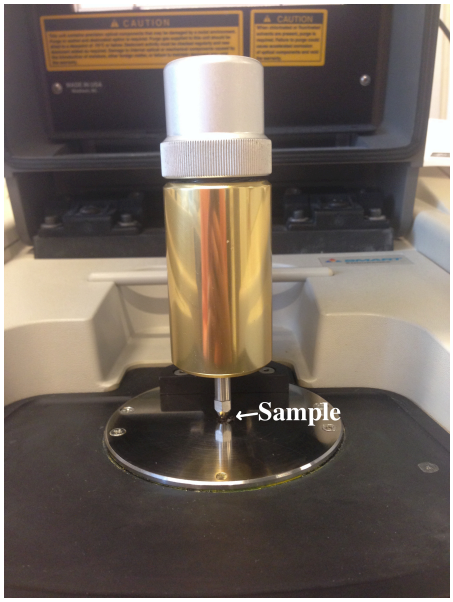

Figure 3.9: The FTIR instrument.

3.3.4 SEM

The surfaces of all samples, including graphite, GO and r-GO, were analyzed by scanning electron microscope using a Hitachi TM3000 Table Top SEM in NTNU NanoLab. The instrument was set to use the backscattered electrons to form images of the surfaces.
Some flakes of the samples were mounted to the sample holder by a piece of carbon tape, and the accelerating voltage was set to 5 kV while the working distance (the distance between the sample and the final lens) was 10.4 mm. How the sample was placed on the sample holder is shown in figure 3.10.

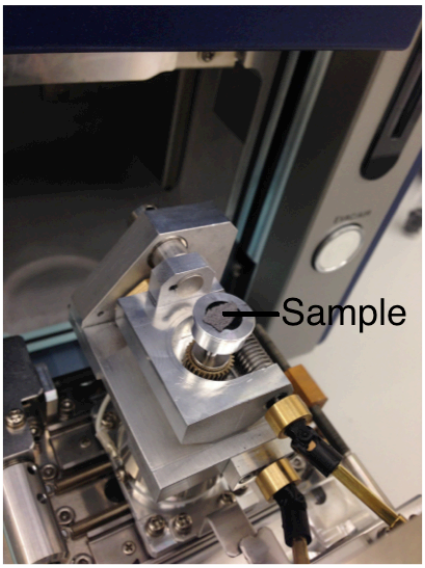

Figure 3.10: The sample placed onto a carbon tape on the sample holder in a SEM.

3.4 Dispersibility testing

In the present work, the purpose of making r-GO is for use in battery applications. Hence, the r-GO has to be easily dispersed in order to make a stable slurry for tape casting.
This dispersibility test was done to graphite, the most successful r-GOs, and also to some GOs. The goal of this work is to see how the dispersibility changes with the degree of reduction.
First, the flakes were grounded into powder. Then small amounts (only a few mg) of the samples were added to 5 mL of the solvent. For graphite and GO, the solvent used was deionized water, but for r-GO 0.05% calgon was used instead. Calgon is seen as a better solvent for carbon samples, as it reduces the surface tension of water.
The dispersibility was evaluated at three times; just after adding the sample to the solvent, just after 15 minutes of ultrasonication, and 24 hours after the ultrasonication was done. The degree of dispersibility was evaluated according to figure 3.11, where 1 and 5 correspond to poor and good dispersibility, respectively.

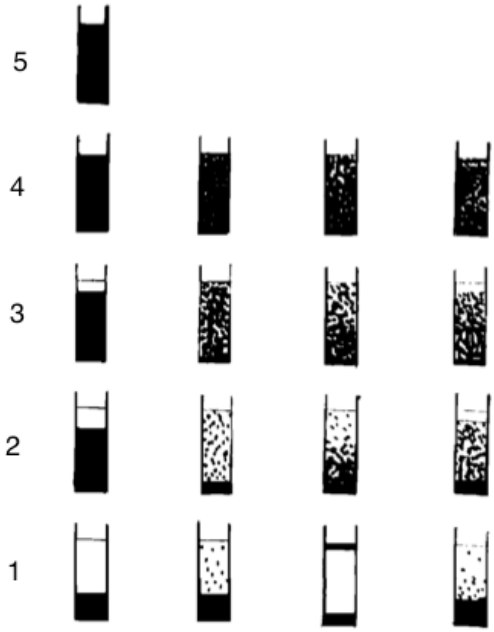

Figure 3.11: Criteria for evaluation of dispersion state (adapted from ref. 55).

4 Results

4.1 Observations during the syntheses

In this section, pictures taken during the syntheses will be presented. This is done in order to see if there are any visual differences between the syntheses produced with graphite powder with an average particle size of ~200 μm, and the synthesis with particles smaller than 50 μm. Figure 4.1 shows the color change for GO1, GO2 and GO3 (the syntheses with an average particle size of ~200 μm) when hydrogen peroxide was added to the solution. Figure 4.2 shows the color change obtained for GO4 (particle size less than 50 μm). Note that the color turned more bright yellow for the synthesis of GO4.

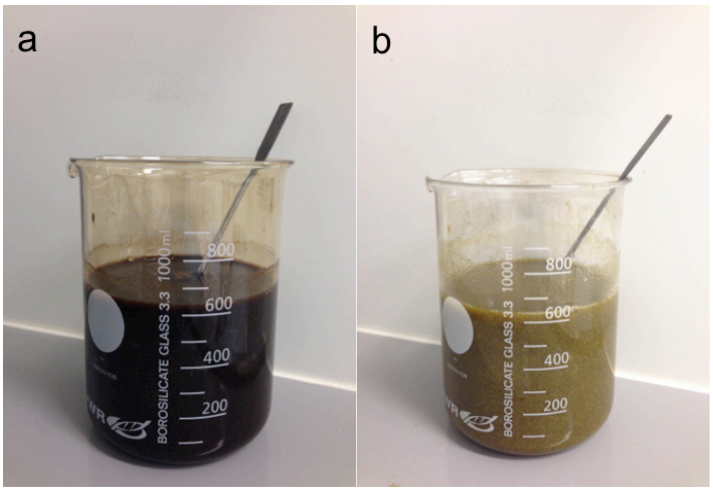

Figure 4.1: How synthesis 1, 2 and 3 looked a) before and b) after the addition of H_2O_2. Note that the solution did not turn bright yellow.

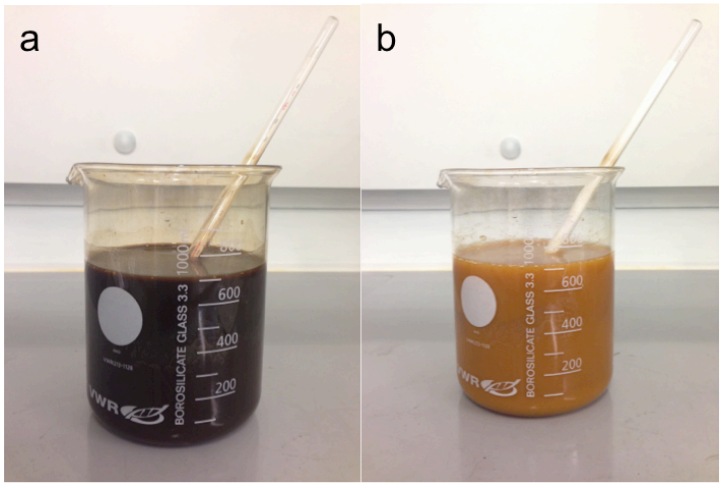

Figure 4.2: a) Synthesis 4 before b) and after the addition of H_2O_2.

Figure 4.3a shows how the syntheses of GO1-3 looked after washing with 1:10 HCl:water in order to remove metal ions, while 4.3b shows the paste after it was dried at 60 °C for 6.5 hours, i.e. until it started to agglomerate. Figure 4.4 shows the same steps for the synthesis of GO4. From these pictures one can easily see that the color change caused by the addition of hydrogen peroxide was maintained for the synthesis of GO4.

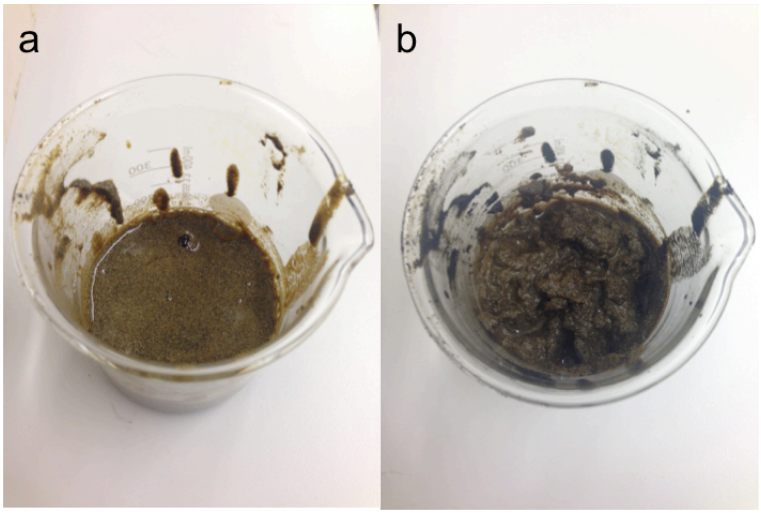

Figure 4.3: How synthesis 1, 2 and 3 looked a) after washing with HCl, and b) after agglomeration at 60 °C for 6.5 hours.

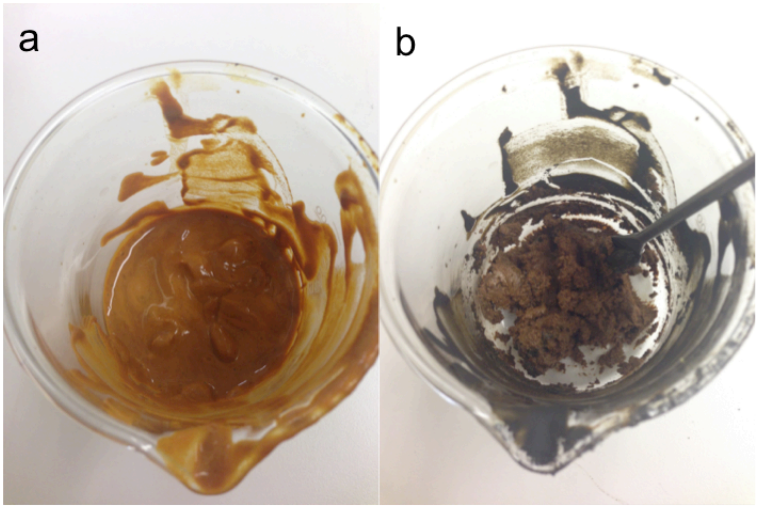

Figure 4.4: Synthesis 4 a) after washing with HCl, and b) after agglomeration at 60 °C for 6.5 hours.

After the agglomeration, the pastes was washed with much deionized water, until the pH reached 5. Then the paste was dispersed into 300 ml deionized water by ultrasonication for 20 minutes. What the different suspensions looked like at this time is shown in figure 4.5a and 4.6a for GO1-3 and GO4, respectively. Moreover, figure 4.5b and 4.6b show that the GO has precipitated during centrifugation at 4000 rpm for 30 minutes. There were still some difference in the color between the syntheses.

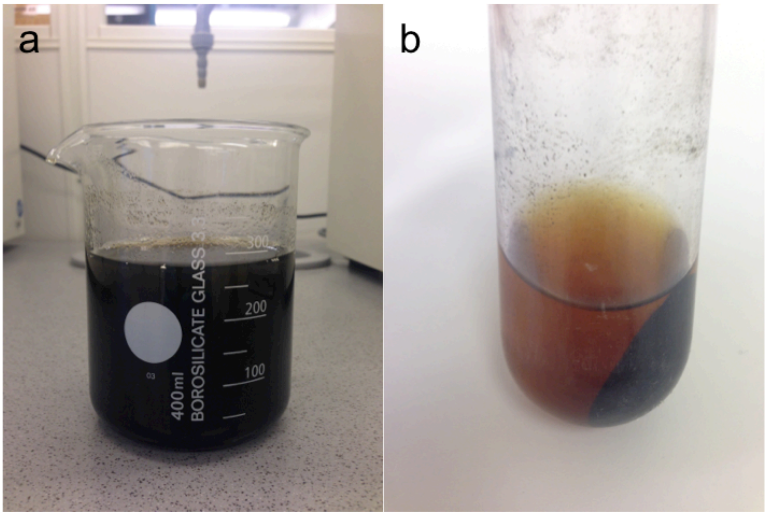

Figure 4.5: How synthesis 1, 2 and 3 looked a) after ultrasonication, and b) after centrifugation.

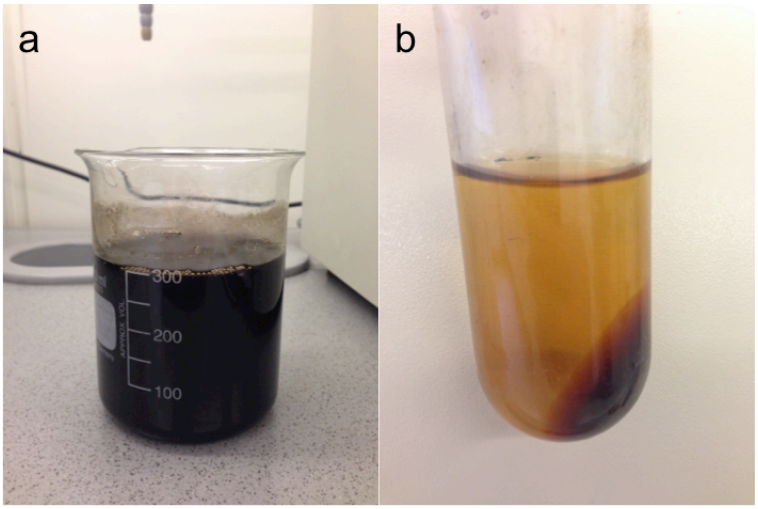

Figure 4.6: Synthesis 4 a) after ultrasonication, and b) after centrifugation.

The last step in the syntheses of GO was to dry the obtained GO on an alumina plate, and figure 4.9 and 4.10 show the alumina plates coated with GO before and after drying for GO1-3 and GO4, respectively. At this step all the synthesis showed the same behavior.

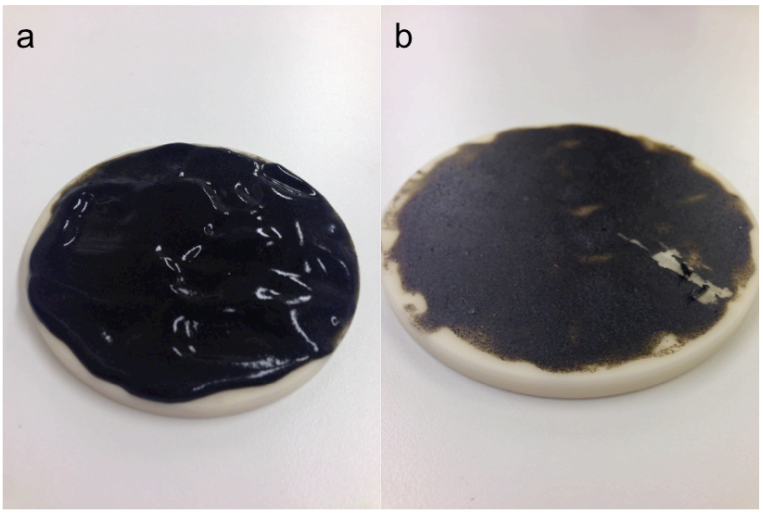

Figure 4.7: How synthesis 1, 2 and 3 looked a) before and b) after drying the graphene oxide on an alumina plate.

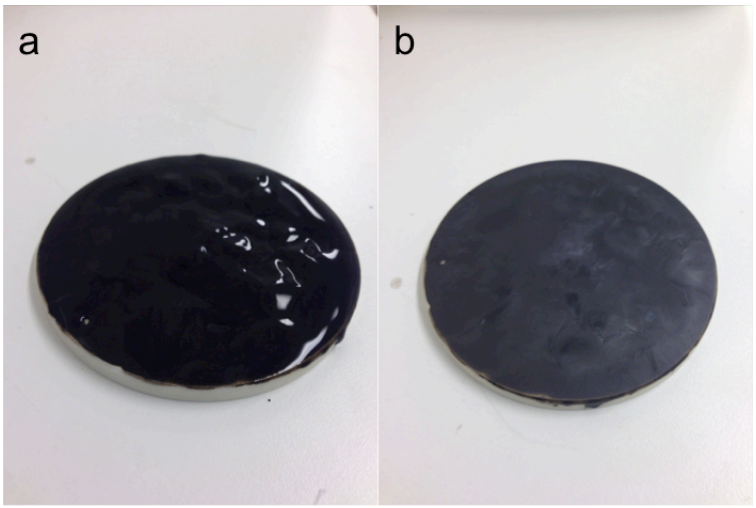

Figure 4.8: Synthesis 4 a) before and b) after drying the graphene oxide on an alumina plate.

4.2 Particle size distribution

The particle size distribution of the graphite powder used in GO1, GO2 and GO3 was investigated using laser diffraction, and the result is given in figure 4.9. As can be seen, the distribution is very broad, and both particles as small as 13 μm and as large as 630 μm were detected. The average diameter was measured to be ~200 μm.

In addition, the particle size was also examined in SEM, and figure 4.10a shows the particles of the graphite powder used in GO1, GO2 and GO3, while figure 4.10b shows the graphite powder used in GO4. Note the difference in particle size in these two figures. The graphite powder used for GO4 was sieved so that all particles were smaller than 50 μm.

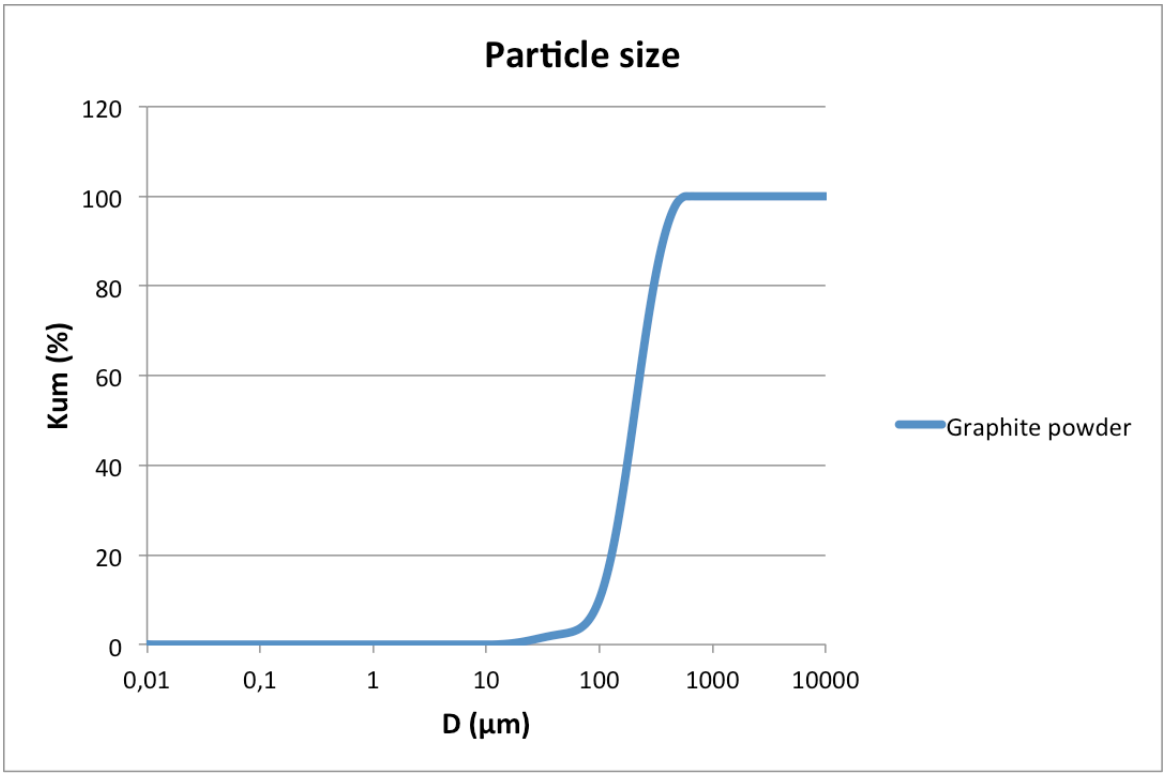

Figure 4.9: Particle size distribution of graphite powder used for GO1, GO2 and GO3.

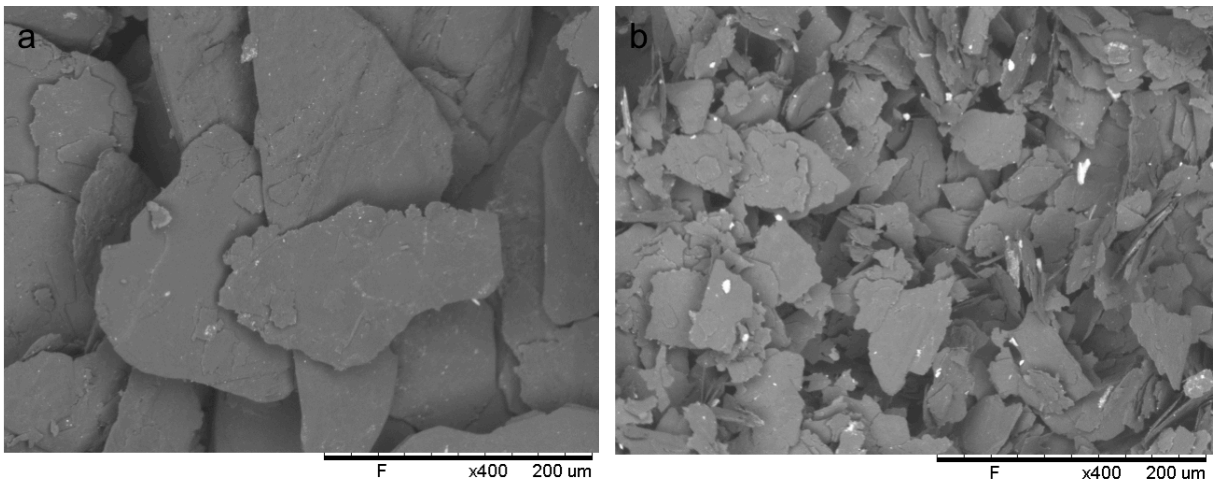

Figure 4.10: SEM images of graphite powder used in the syntheses of a) GO1, GO2 and GO3, and b) GO4. Note the difference in particle size.

4.3. XRD

XRD was used in order to investigate the crystal structure of graphite, GO and r-GO, and how they were affected by different parameters such as particle size, oxidation time, heating rate, reduction temperatures and atmospheres. The results are given in the following sections.

4.3.1 Graphite

Figure 4.11 shows the XRD pattern obtained for graphite powder, which shows two characteristic diffraction peaks. The one located at a 2θ value of 26.58° is the 002 peak, and the much less intense peak at 54.65° is the 004 peak. By applying Bragg's law, the resulting *d*-spacing is 3.35.

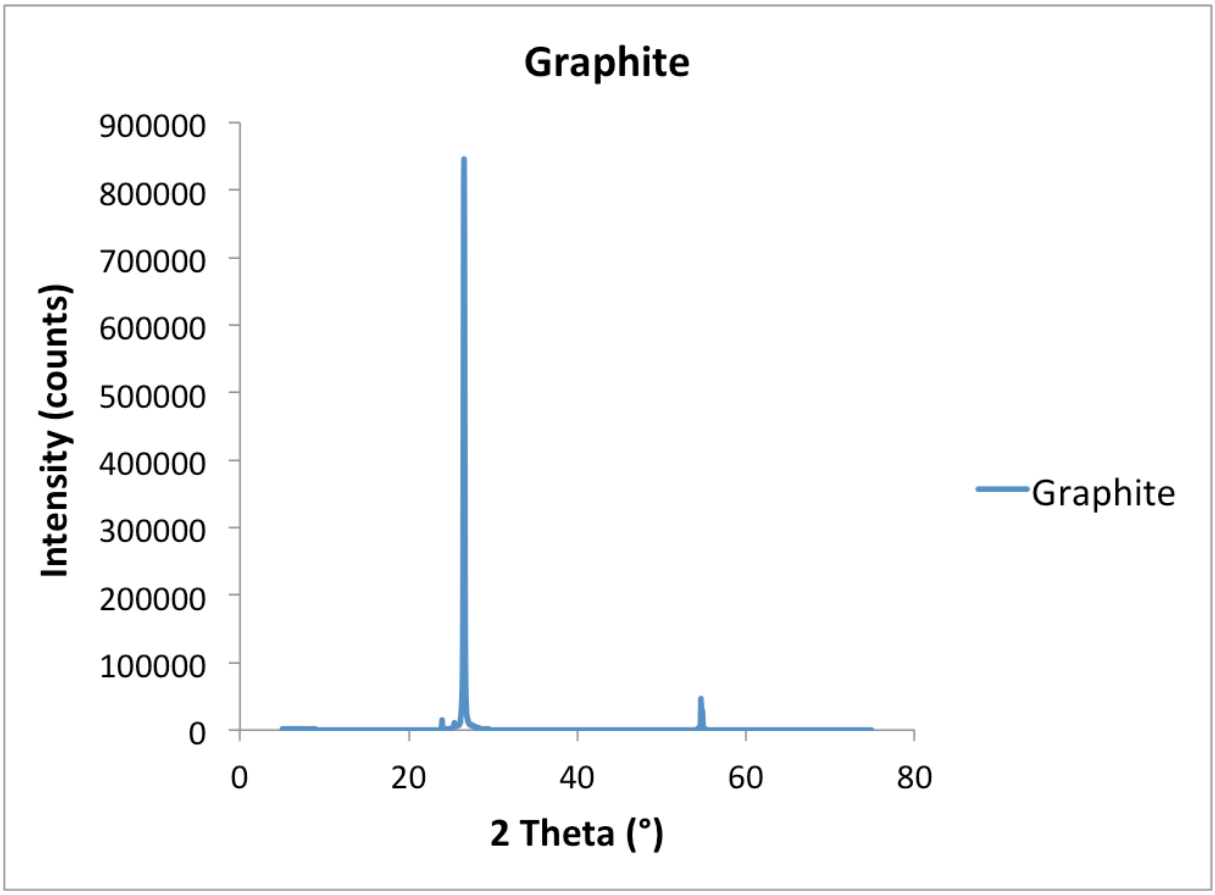

Figure 4.11: XRD pattern of the starting material, graphite powder.

4.3.2 GO

Figure 4.12 shows the XRD patterns of GO1, GO2 and GO3, which were oxidized for 3, 5 and 10 days respectively. From the figure, it can be seen that GO1, GO2 and GO3 do all have diffraction peaks at 26.58° and 54.65°, in addition to a peak at approximately 11-12°, which corresponds to the 002 peak of GO.

Figure 4.13 shows the XRD pattern of GO4, which was oxidized for 5 days. For GO4, Si powder was mixed in during sample preparation in order to have a standard so that exact peak position could be found. However, it turned out that the error was so small that the use of Si was not necessary. From the figure, it can be seen that GO4 does only show one diffraction peak, and this is localized at 12.65° (GO4 was verified to be reproducible, see Appendix A).

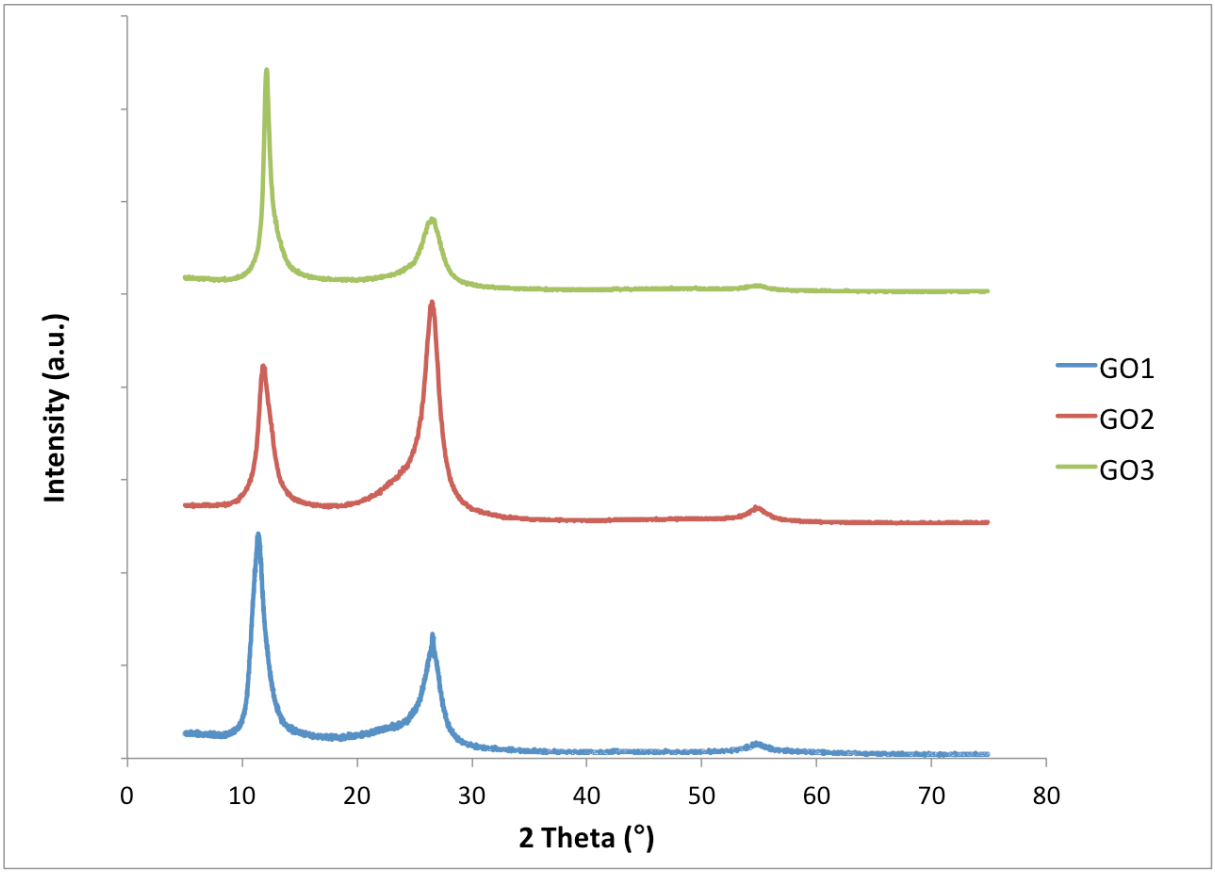

Figure 4.12: The diffraction patterns of GO1, GO2 and GO3. GO1 was oxidized for 3 days, GO2 for 5 days and GO3 for 10 days.

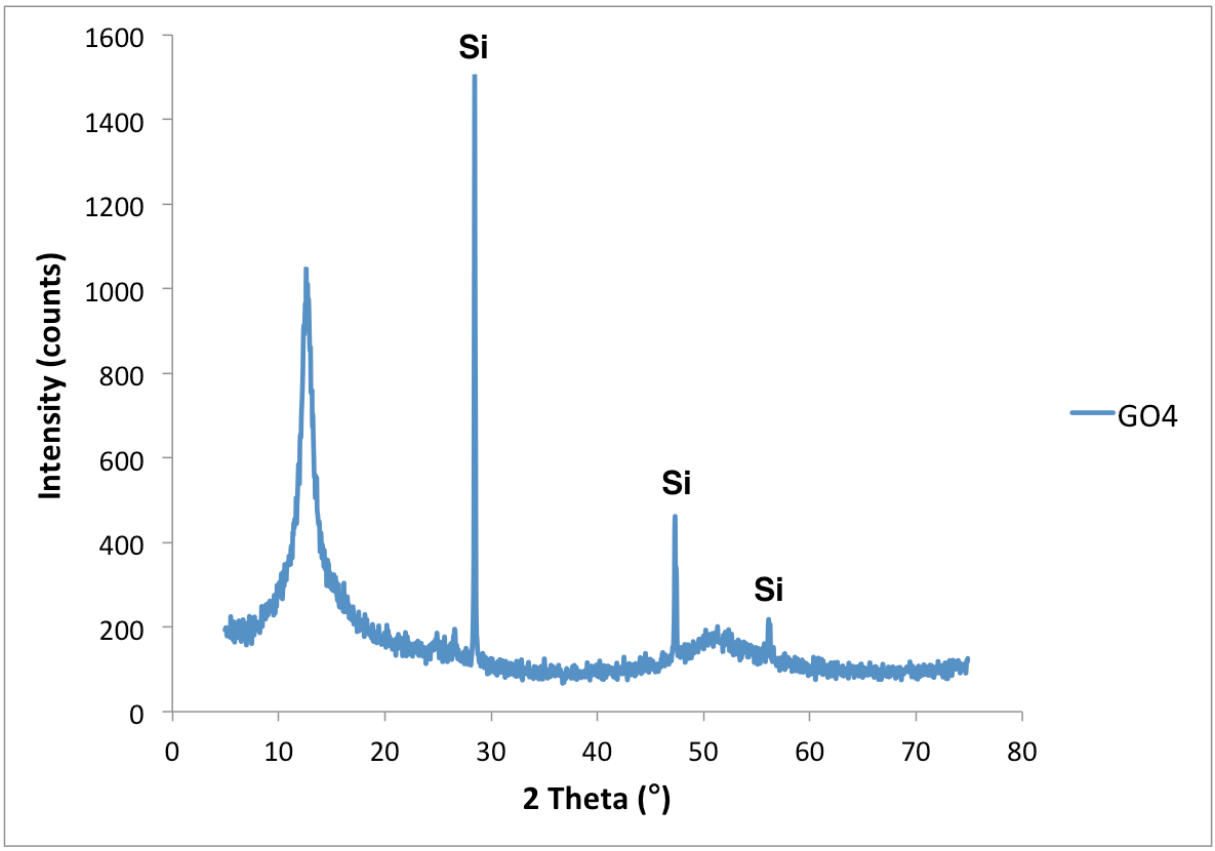

Figure 4.13: The diffraction pattern of GO4 mixed with a Si standard. GO4 was oxidized for 5 days.

4.3.3 r-GO produced by slow reduction in Ar

Figure 4.14 shows the XRD patterns of GO1 and r-GO1 obtained by slow reduction at 700 and 900 ºC in Ar. Table 4.1 presents the 2θ values and the corresponding *d*-spacings. Further, figure 4.15 shows the XRD patterns of GO2 and r-GO2 obtained by slow reduction at 300, 400, 700 and 900 ºC in Ar while table 4.2 presents the 2θ values and the corresponding *d*-spacings. In addition, figure 4.16 shows the XRD patterns of GO3 and r-GO3 obtained by slow reduction at 300, 400, 700 and 900 ºC in Ar. Table 4.3 presents the 2θ values and the corresponding *d*-spacings.

Note the decrease in *d*-spacings after the reduction.

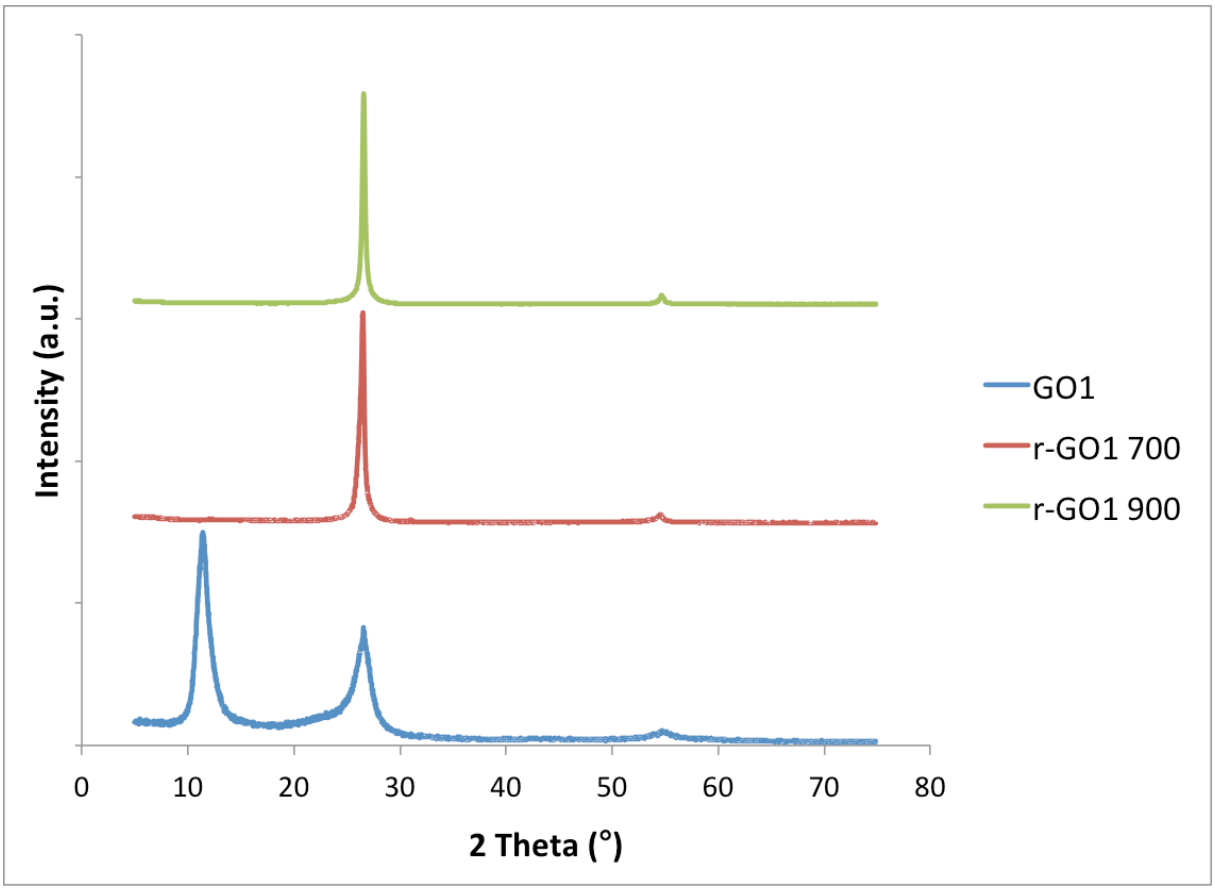

Figure 4.14: The XRD patterns of GO1 and r-GO1 reduced at different temperatures in Ar-gas.

Table 4.1: The 2θ values and the corresponding *d*-spacings for GO1 and r-GO1.

Samples	**2θ (°)**	**d_{002}, layer distance (Å)**
GO1	11.36	7.79
r-GO1 700	26.50	3.36
r-GO1 900	26.58	3.35

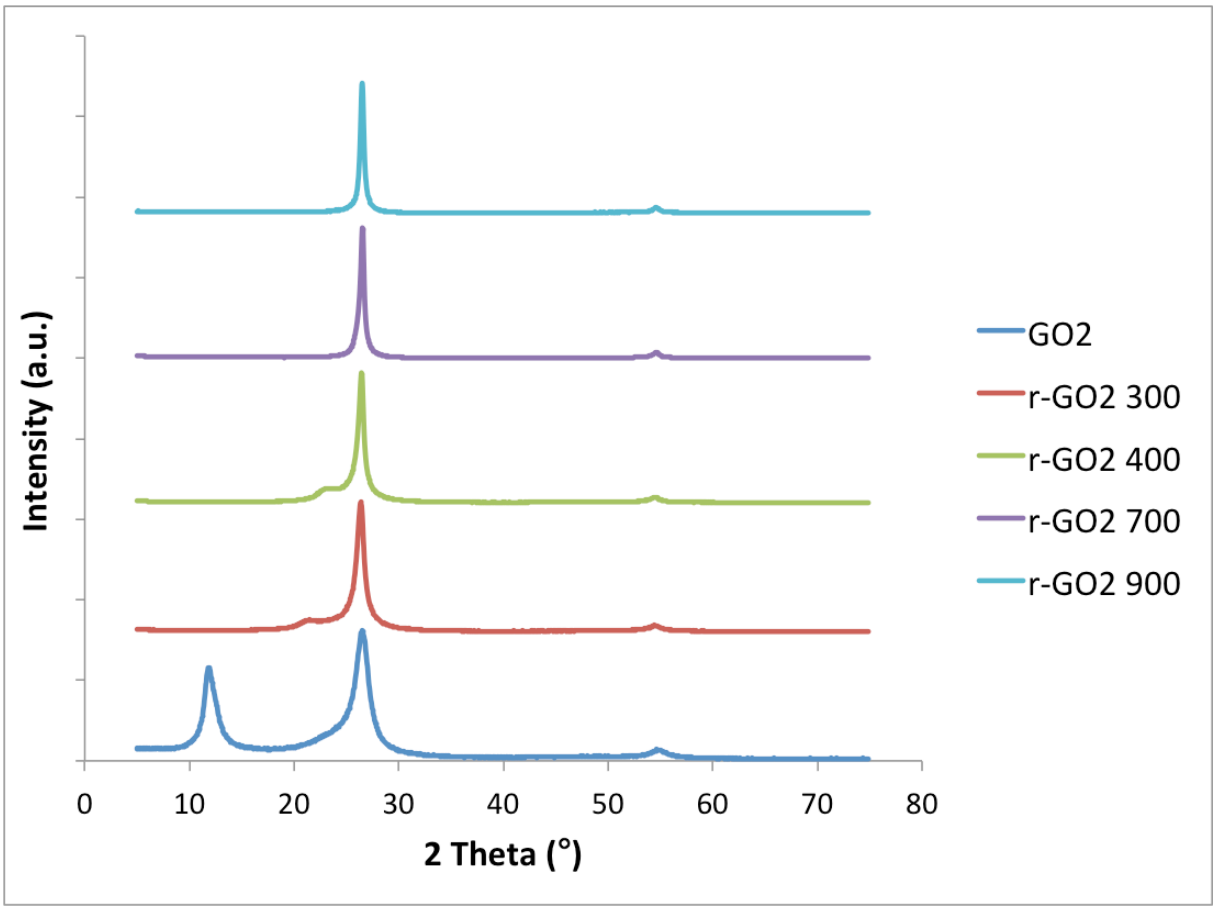

Figure 4.15: The XRD patterns of GO2 and r-GO2 reduced at different temperatures in Ar-gas.

Table 4.2: The 2θ values and the corresponding *d*-spacings for GO2 and r-GO2.

Samples	**2θ (°)**	**d_{002}, layer distance (Å)**
GO2	11.82	7.48
r-GO2 300	26.39	3.37
r-GO2 400	26.43	3.37
r-GO2 700	26.53	3.36
r-GO2 900	26.53	3.36

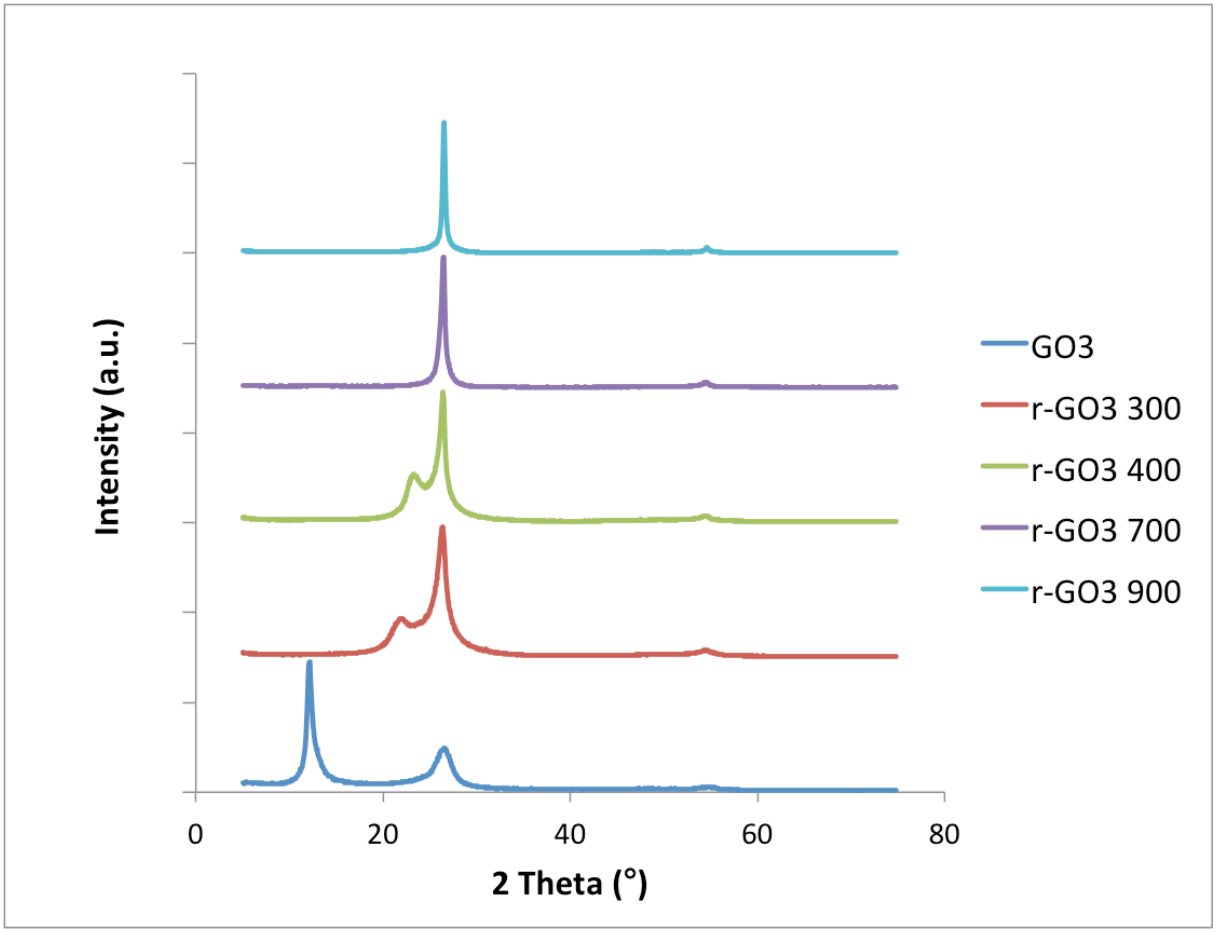

Figure 4.16: The XRD patterns of GO3 and r-GO3 reduced at different temperatures in Ar-gas.

Table 4.3: The 2θ values and the corresponding *d*-spacings for GO3 and r-GO3.

Samples	**2θ (°)**	**d_{002}, layer distance (Å)**
GO3	12.14	7.28
r-GO3 300	26.35	3.38
r-GO3 400	26.39	3.37
r-GO3 700	26.43	3.37
r-GO3 900	26.52	3.36

4.3.4 r-GO produced by slow reduction in Ar/H_2

Figure 4.17 show the XRD patterns obtained of r-GO3 and r-GO4 reduced by slow reduction at 1000 °C in Ar/H_2. In addition, table 4.4 shows the 2θ values and the corresponding *d*-spacings.

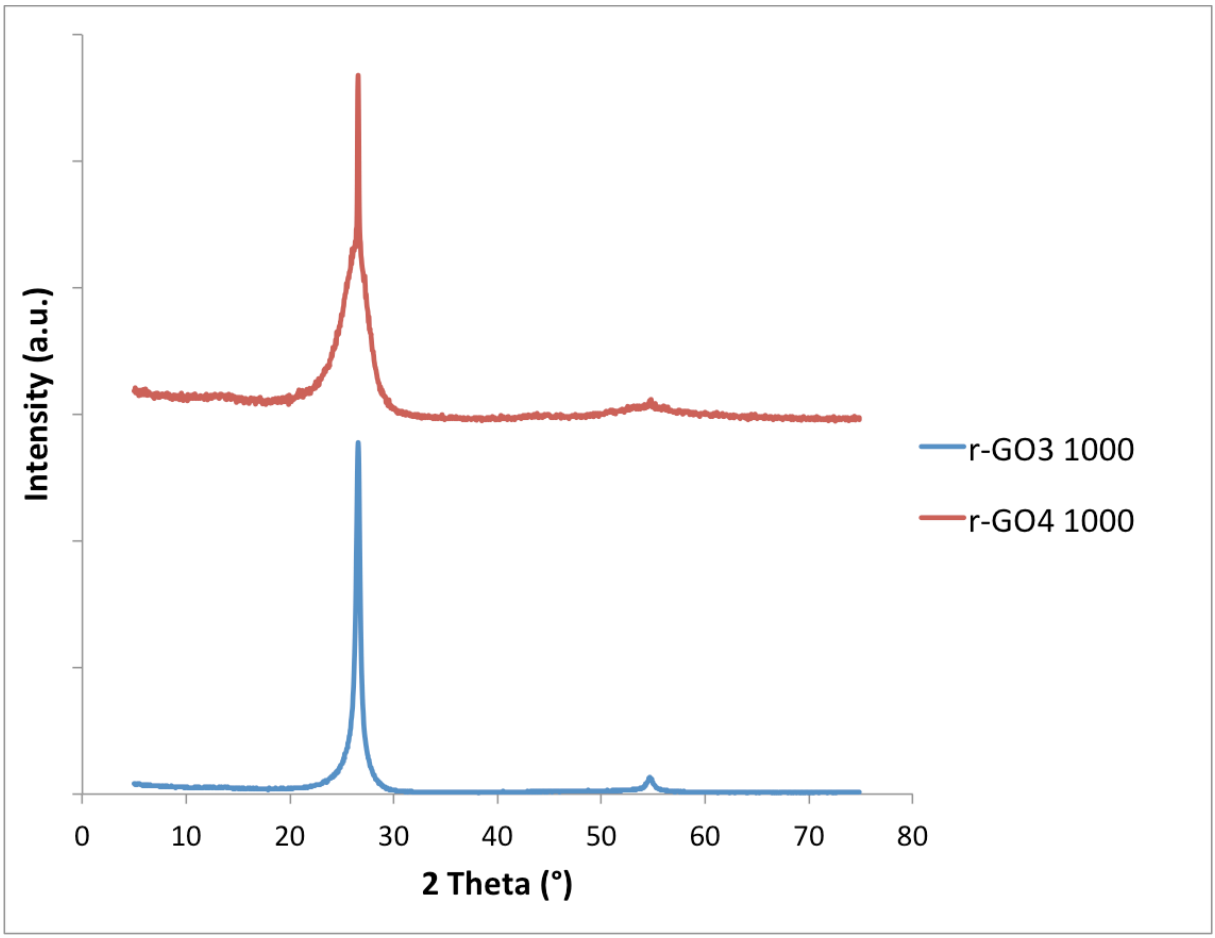

Figure 4.17: XRD patterns of r-GO3 and r-GO5 reduced by slow reduction to 1000 °C in Ar/H_2-gas.

Table 4.4: The 2θ values and the corresponding *d*-spacings for r-GO3 and r-GO4.

Samples	**2θ (°)**	**d_{002}, layer distance (Å)**
r-GO3 1000	26.57	3.35
r-GO4 1000	26.57	3.35

4.3.5 r-GO produced by medium reduction in Ar/H_2

GO4 was also reduced by using medium heating rate (25 ˚C/min) in Ar/H_2, and the XRD pattern of GO4 and r-GO4 reduced at 1000 °C is shown in figure 4.18. Table 4.5 shows the 2θ values and the corresponding *d*-spacings, and as can be seen the *d*-spacing decreases during reduction.

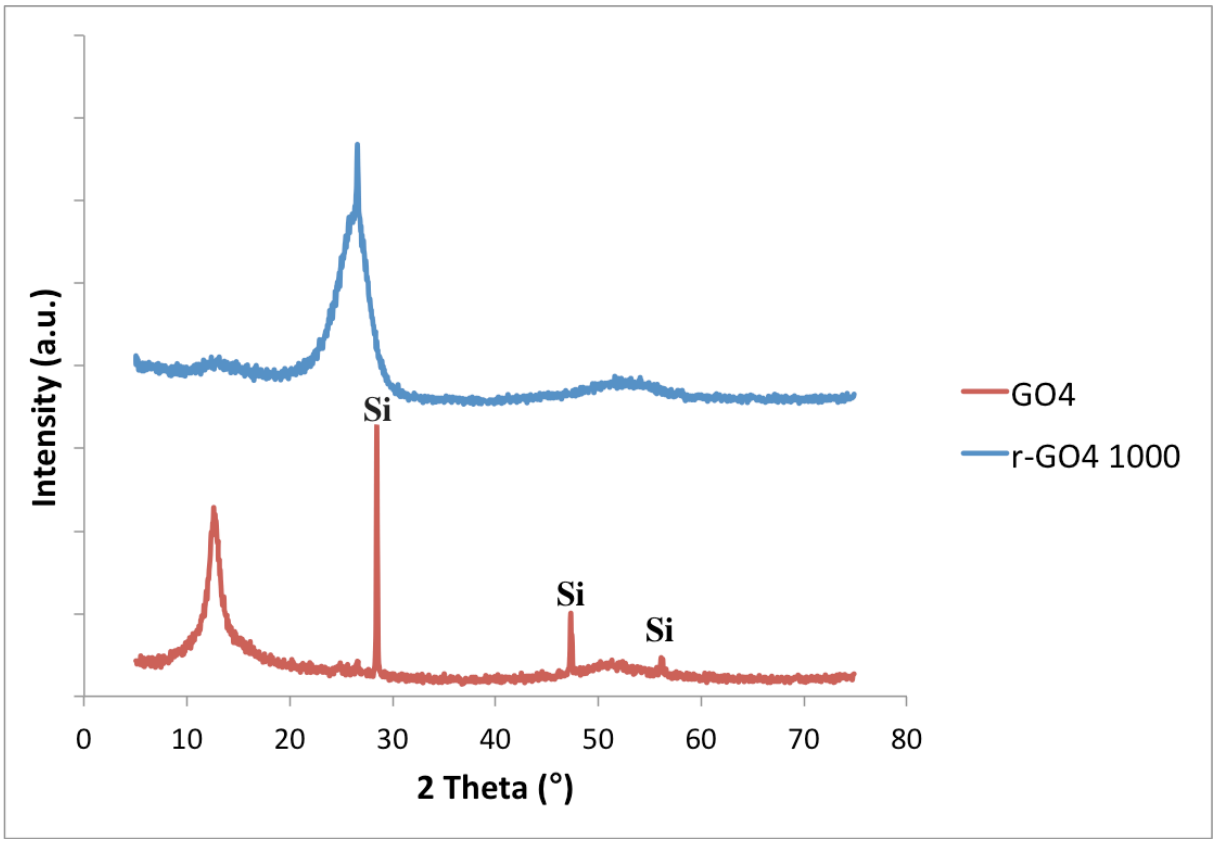

Figure 4.18: The XRD patterns of GO4 and r-GO4 reduced at 25 °C/min up to 1000 °C in Ar/H_2-gas.

Table 4.5: The 2θ values and the corresponding *d*-spacings for GO4 and r-GO4.

Samples	**2θ (°)**	**d_{002}, layer distance (Å)**
GO4	12.65	6.99
r-GO4 1000	26.57	3.38

4.3.6 r-GO produced by rapid reduction in Ar/H_2

Figure 4.19 shows the XRD patterns obtained of r-GO4 reduced by rapid heating (5 °C/s) to different temperatures in Ar/H_2. Also here, Si was mixed in as a standard. Table 4.6 shows the 2θ values and the corresponding *d*-spacings, and as can be seen the *d*-spacing decreases during reduction. Note the disappearance of diffractions peak at 900 and 1000 °C, only the diffraction peaks of Si are present.

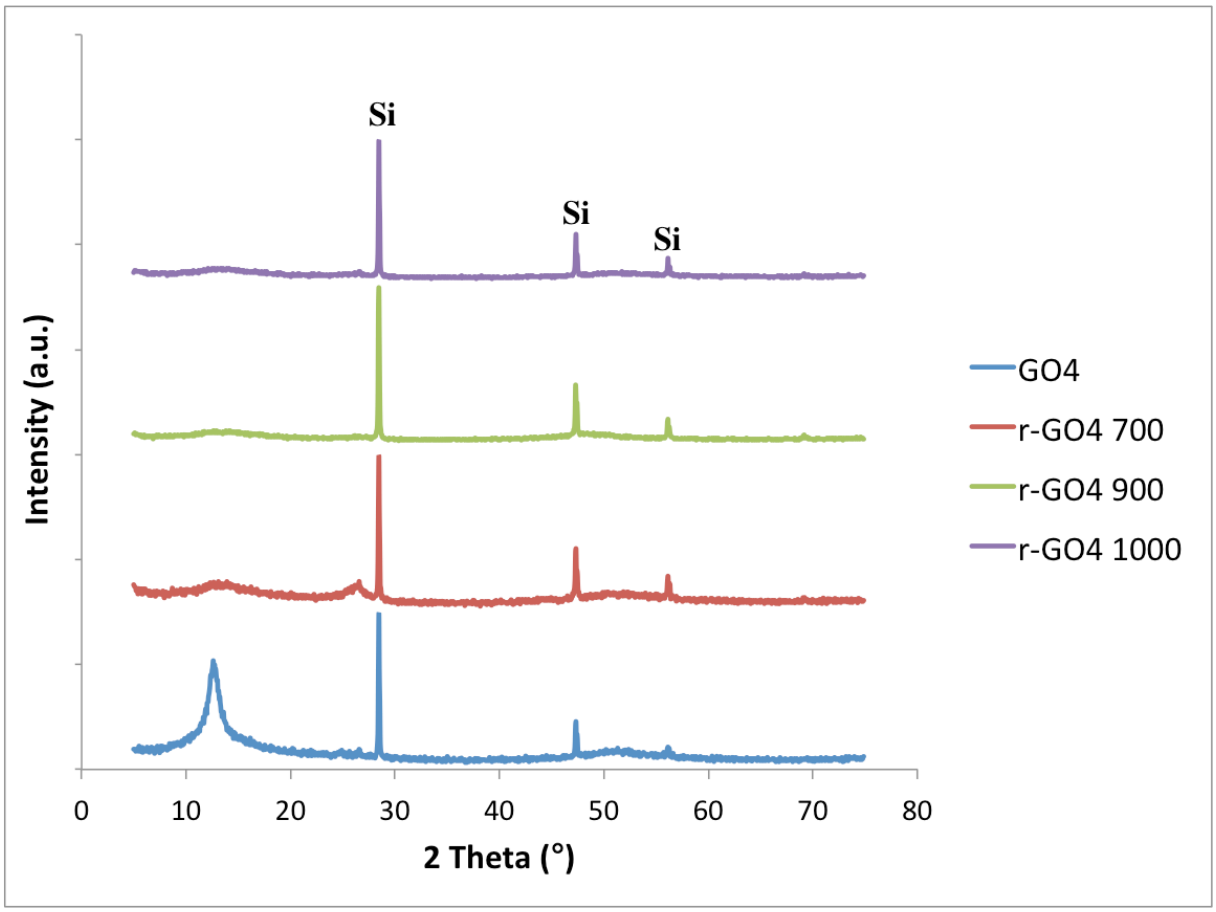

Figure 4.19: The XRD patterns of GO4 and r-GO4 reduced at 5 °C/s in Ar/H2-gas up to different temperatures.

Table 4.6: The 2θ values and the corresponding *d*-spacings for GO4 and r-GO4.

Samples	**2θ (°)**	**d_{002}, layer distance (Å)**
GO4	12.65	6.99
r-GO4 700	26.61	3.35
r-GO4 900	-	-
r-GO4 1000	-	-

4.4 FTIR

FTIR spectroscopy was used in order to examine the oxygen-containing functional groups in the graphene oxide, and also to determine which groups that were left and which that had disappeared after the reduction. The obtained spectrums are given in the following sections, and each absorption band corresponds to a frequency that has been absorbed by a molecule in the material.

4.4.1 Graphite

Figure 4.20 shows the FTIR spectrum of graphite. The absorption bands and the corresponding functional groups are marked on the figure. The circled area is an unknown band.

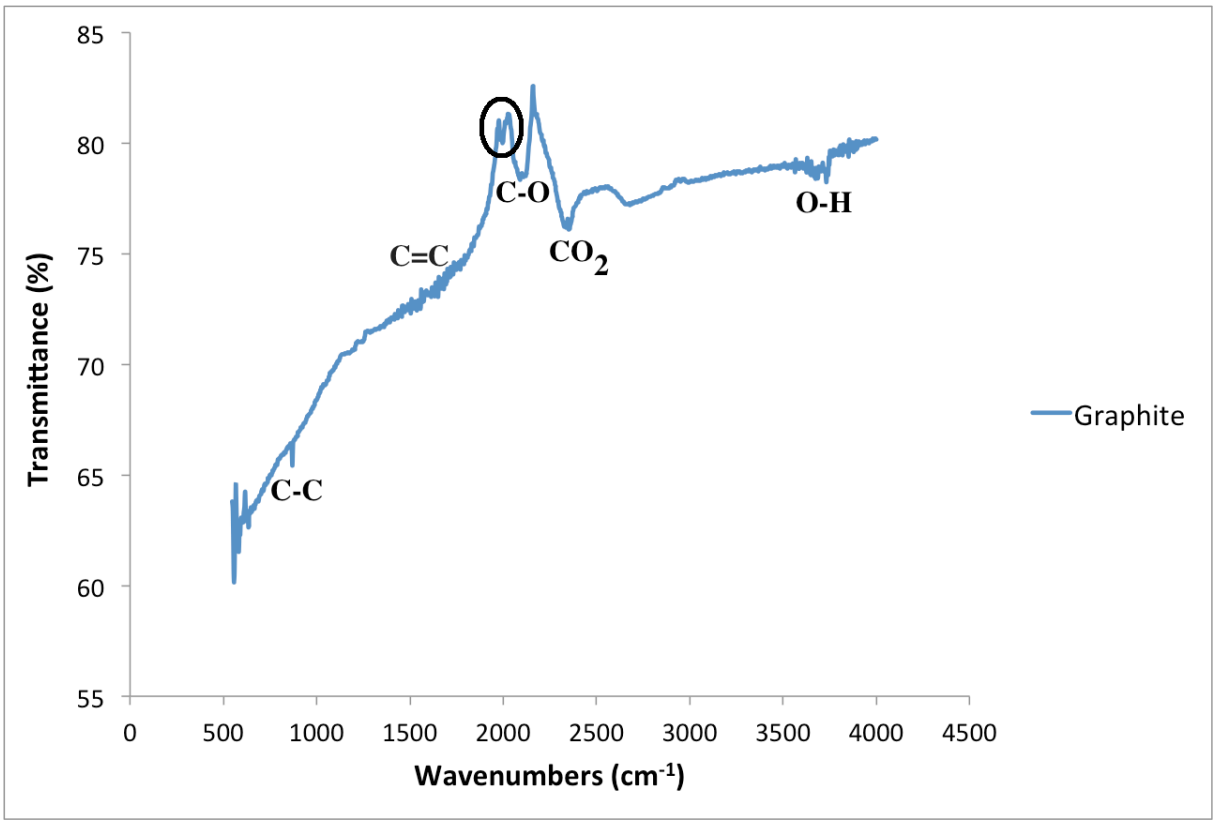

Figure 4.20: The FTIR spectrum of graphite.

4.4.2 GO

Figure 4.21 shows the FTIR spectra of all the GOs obtained. As can be seen from the figure, all the samples have absorption bands at the same frequencies, but the strength of the bands does vary from sample to sample.

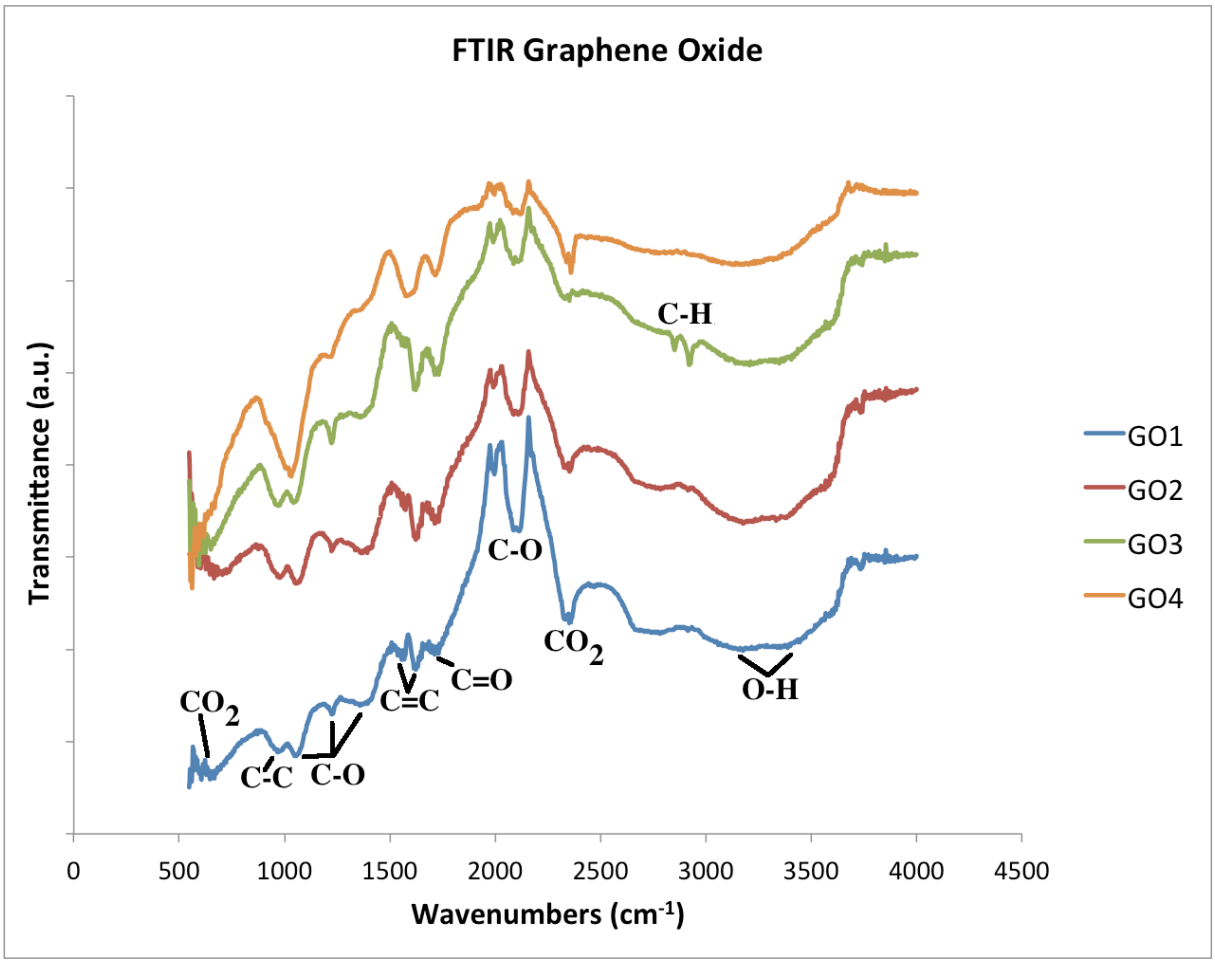

Figure 4.21: FTIR spectra of GO1, GO2, GO3 and GO4.

4.4.4 r-GO produced by slow reduction in Ar

Figure 4.22 shows the FTIR spectra of GO1 and r-GO1 obtained by slow reduction in Ar at 700 and 900 ºC. Further, figure 4.23 shows the FTIR spectra of GO2 and r-GO2 obtained by slow reduction in Ar at 300, 400, 700 and 900 ºC. Finally, figure 4.24 shows the FTIR spectra of GO3 and r-GO2 obtained by slow reduction in Ar at 300, 400, 700 and 900 ºC.

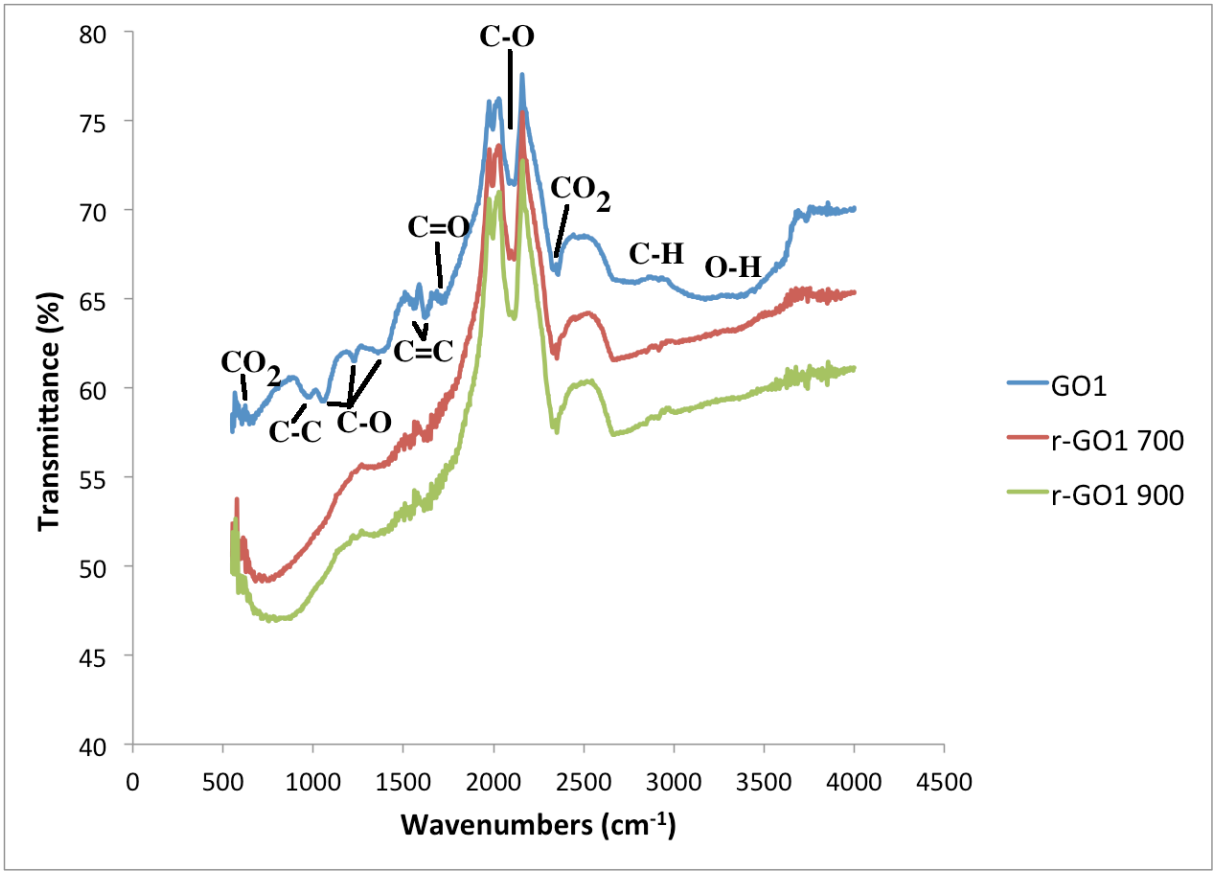

Figure 4.22: FTIR spectra of GO1 and r-GO1 reduced by slow reduction to 700 and 900 °C in Ar-gas.

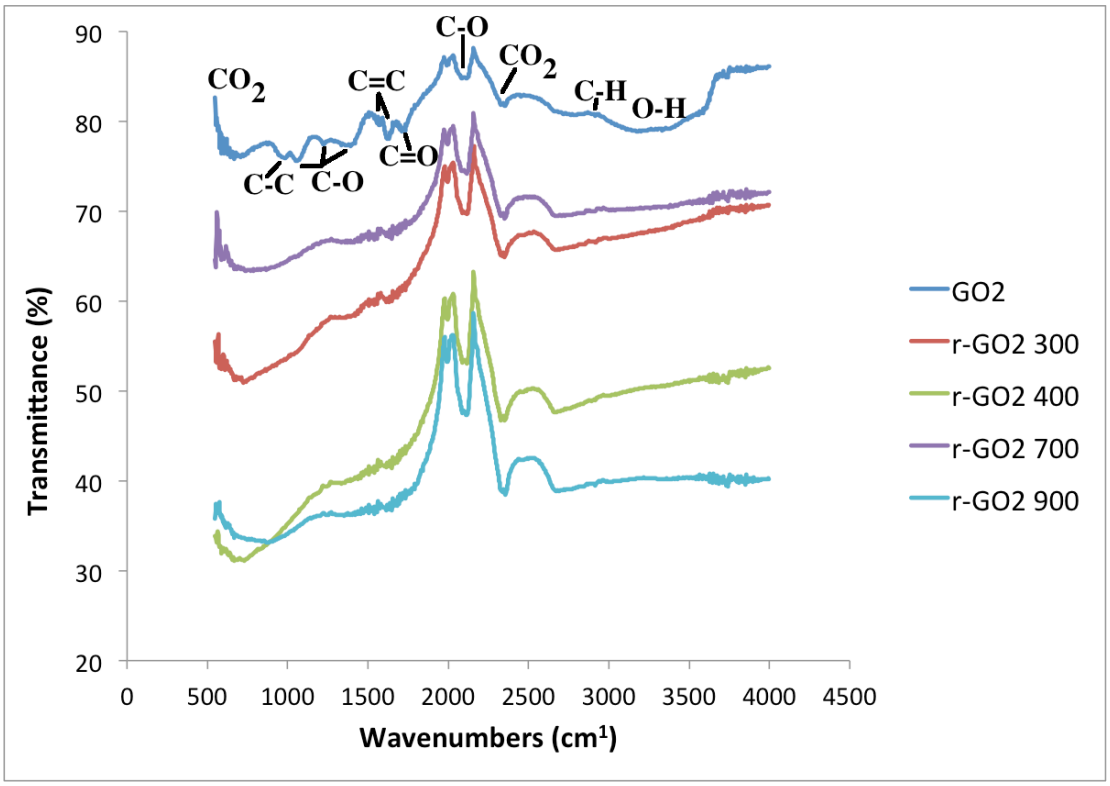

Figure 4.23: FTIR spectra of GO2, and r-GO2 reduced by slow reduction to 300, 400, 700 and 900 °C in Ar-gas.

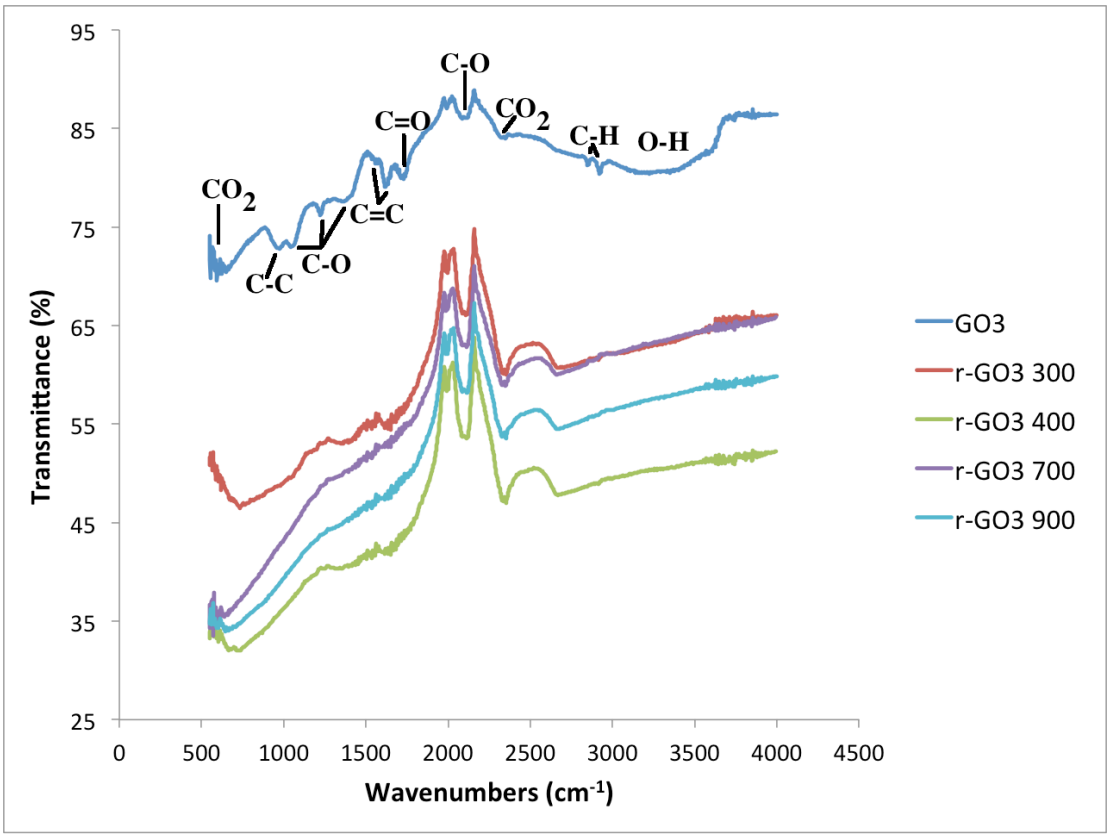

Figure 4.24: FTIR spectra of GO3, and r-GO3 reduced by slow reduction to 300, 400, 700 and 900 °C in Ar-gas.

4.4.5 r-GO produced by slow reduction in Ar/H_2

Figure 4.25 shows the FTIR spectra of r-GO3 and r-GO4 reduced by slow heating rate in Ar/H_2 at 1000 °C.

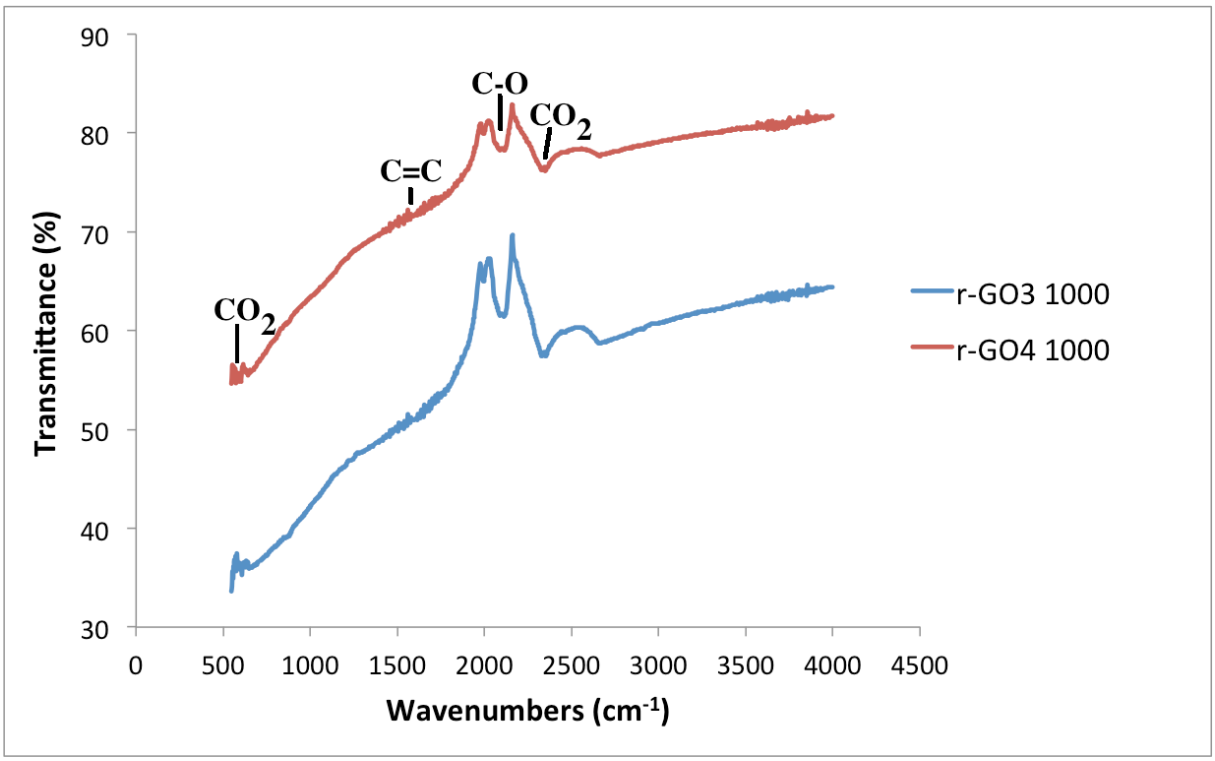

Figure 4.25: FTIR spectra of r-GO3 and r-GO4 reduced by slow reduction to 1000 °C in Ar/H_2-gas.

4.4.6 r-GO produced by medium reduction in Ar/H_2

Figure 4.26 shows the FTIR spectra of GO4 and r-GO4 reduced at 1000 °C by medium heating rate (25 °C/min) in Ar/H_2.

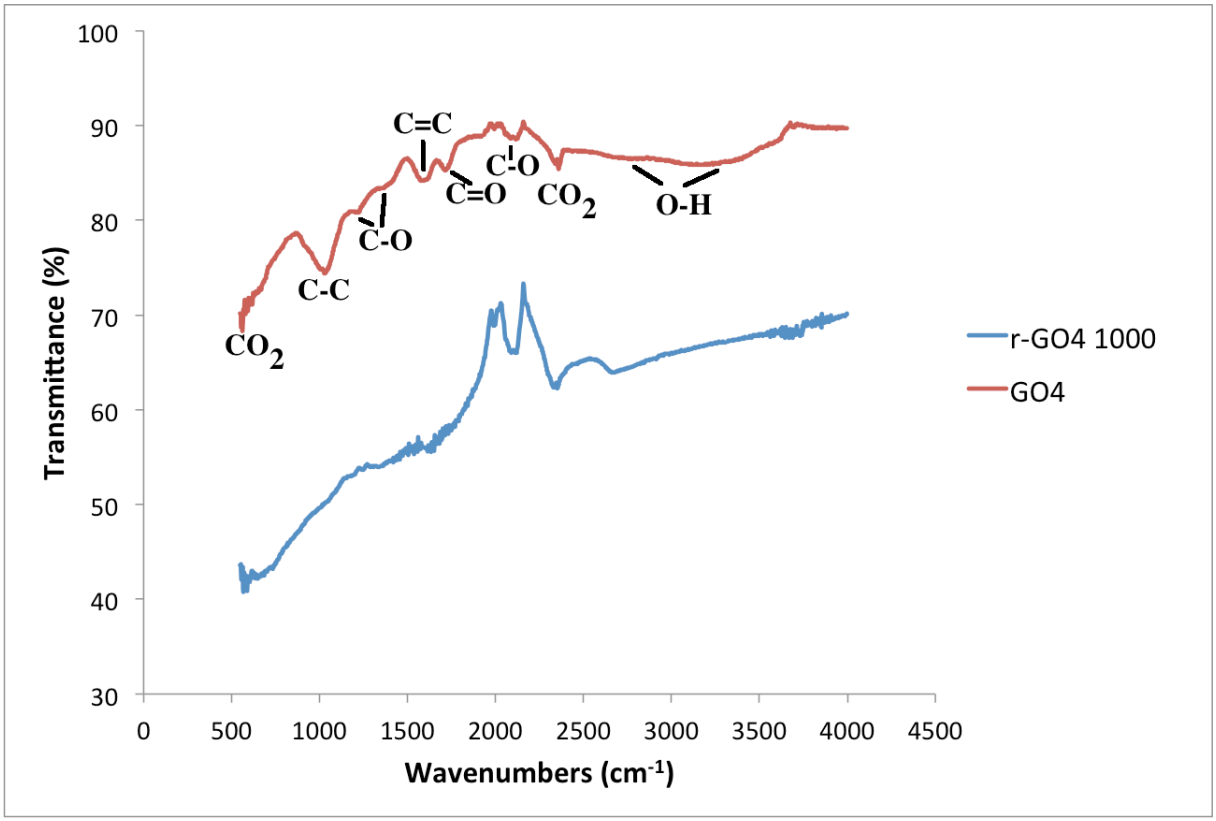

Figure 4.26: The FTIR spectra of GO4 and r-GO4 reduced by medium reduction to 1000 °C in Ar/H_2-gas.

4.4.5 r-GO produced by rapid reduction in Ar/H_2

Figure 4.27 shows the FTIR spectra of GO4 and r-GO4 obtained reduced by rapid reduction (5 °C/s) at 700, 900 and 1000 °C in Ar/H_2.

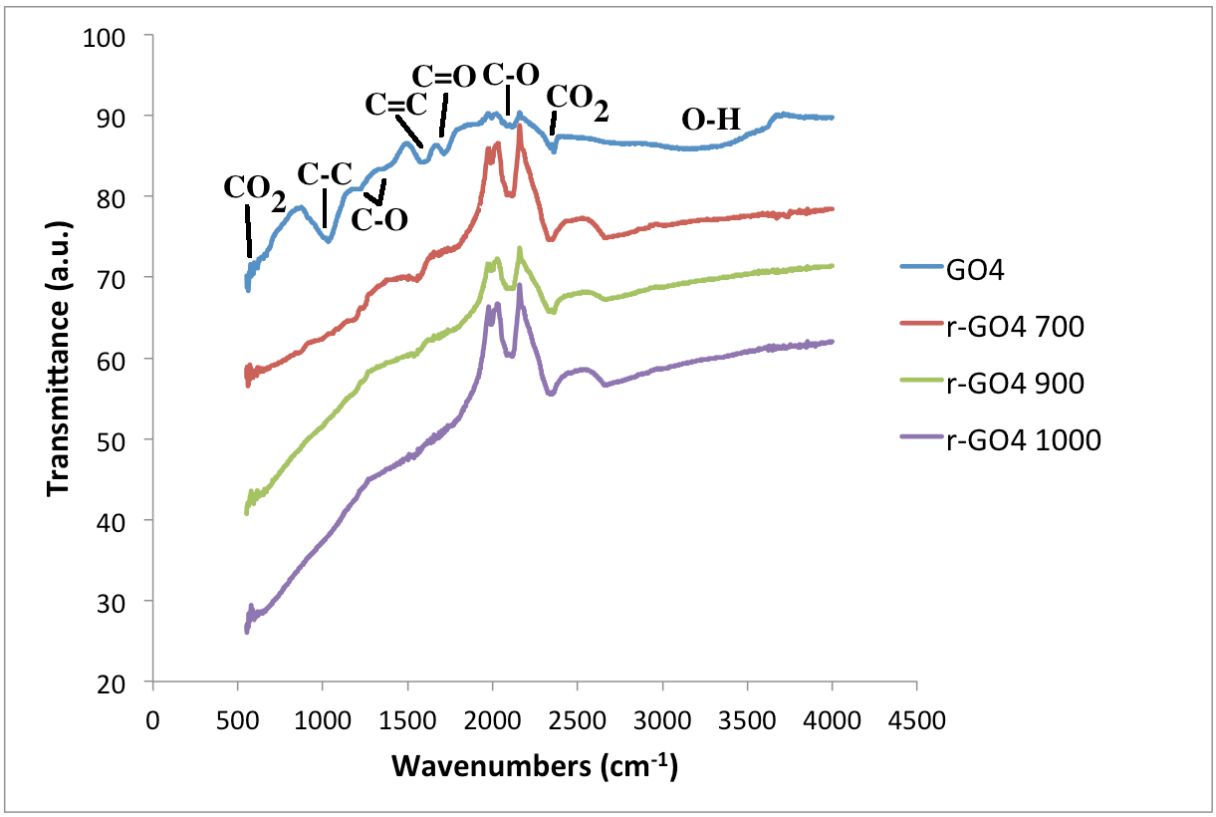

Figure 4.27: FTIR spectra of GO4, and r-GO4 reduced by rapid reduction to 700, 900 and 1000 °C in Ar/H_2-gas.

4.5 SEM

All the samples were investigated using SEM, but as some of them showed the same tendencies, only a selection of the samples are shown in this section. Figure 4.28 shows SEM images of GO2 and r-GO2 reduced by slow reduction at 300, 400, 700 and 900 °C in Ar-gas, and for each image the same scale bar is used. In addition, figure 4.29 shows SEM images of GO4 and r-GO4 reduced by rapid reduction at 700, 900 and 1000 °C in Ar/H_2. Note that the r-GO flakes become smaller when fast reduction is used at high temperatures.

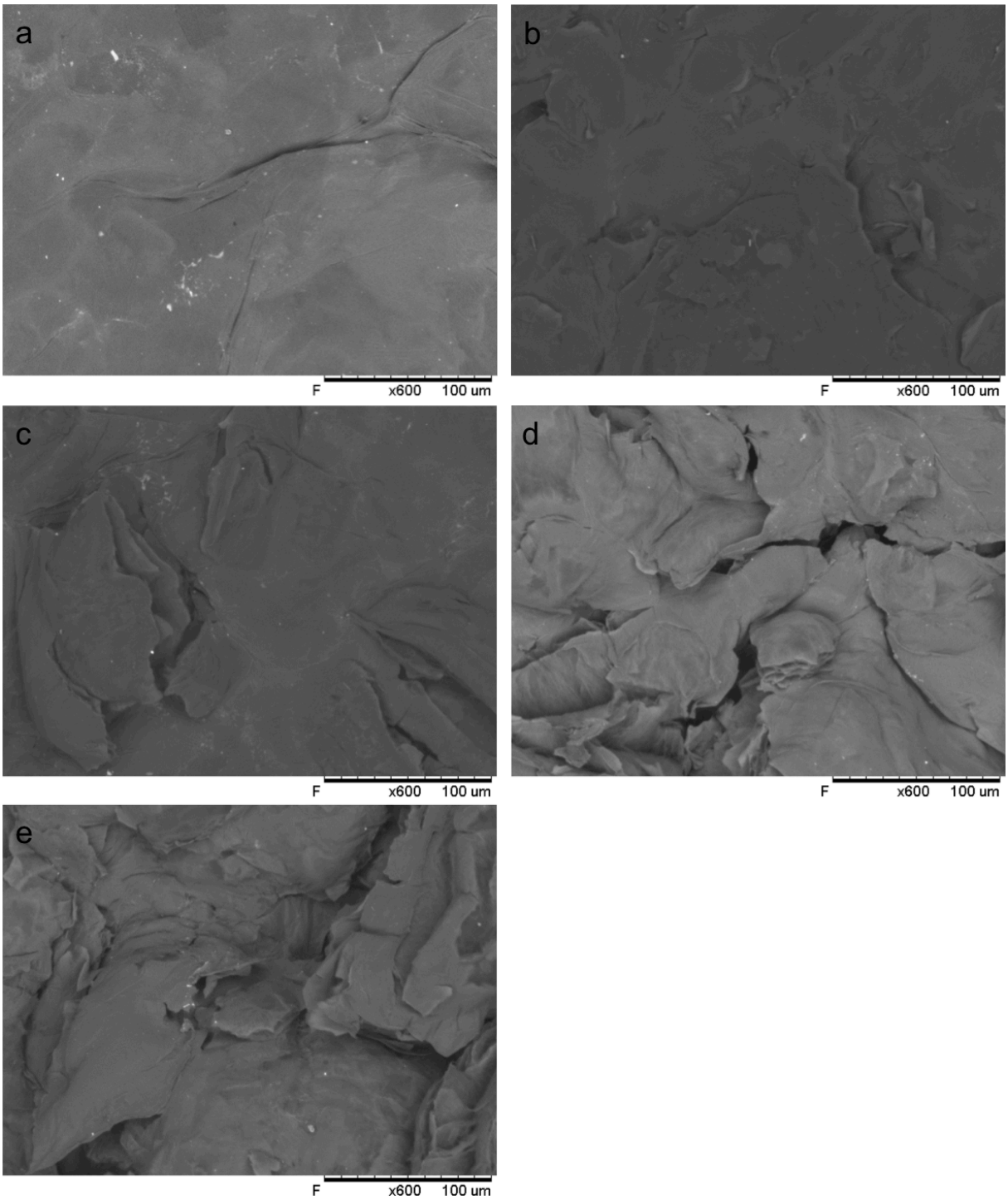

Figure 4.28: SEM images of a) GO2, b) r-GO2 300 °C, c) r-GO2 400 °C, d) r-GO2 700 °C and e) r-GO2 900 °C reduced by slow reduction in Ar/H_2-gas.

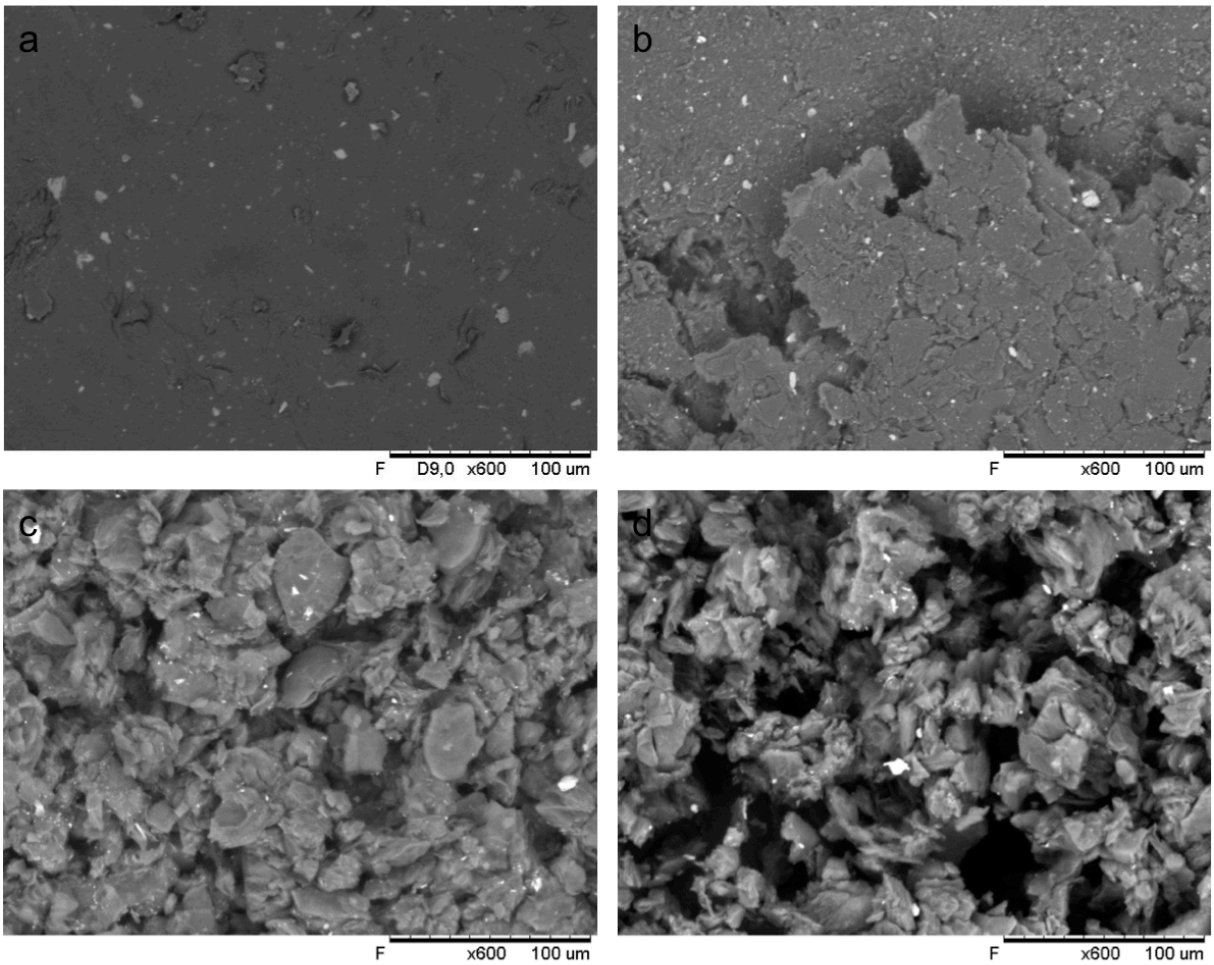

Figure 4.29: SEM images of a) GO4, b) r-GO4 700 °C, c) r-GO4 900 °C and d) r-GO4 1000 °C reduced by rapid reduction in Ar/H_2. Note that the flake sizes of r-GO get smaller with higher temperature.

4.6 Dispersibility

For the dispersibility testing, graphite and some GO and r-GO samples are investigated. The graphite and GOs were dispersed in 5 mL of deionized water, while the reduced ones were dispersed in 0.05 % calgon, which is seen as a better solvent for carbon material because the calgon reduces the surface tension of water. Table 4.2, 4.3 and 4.4 placed in the end of this chapter show a summary of the dispersibility, evaluated according to figure 3.11 where 1 means poor dispersibility and 5 means good.

4.6.1 Graphite

Figure 4.30a shows the dispersibility of graphite just after adding, while b shows what it looked like just after 15 minutes of sonication, and c is after 24 hours.

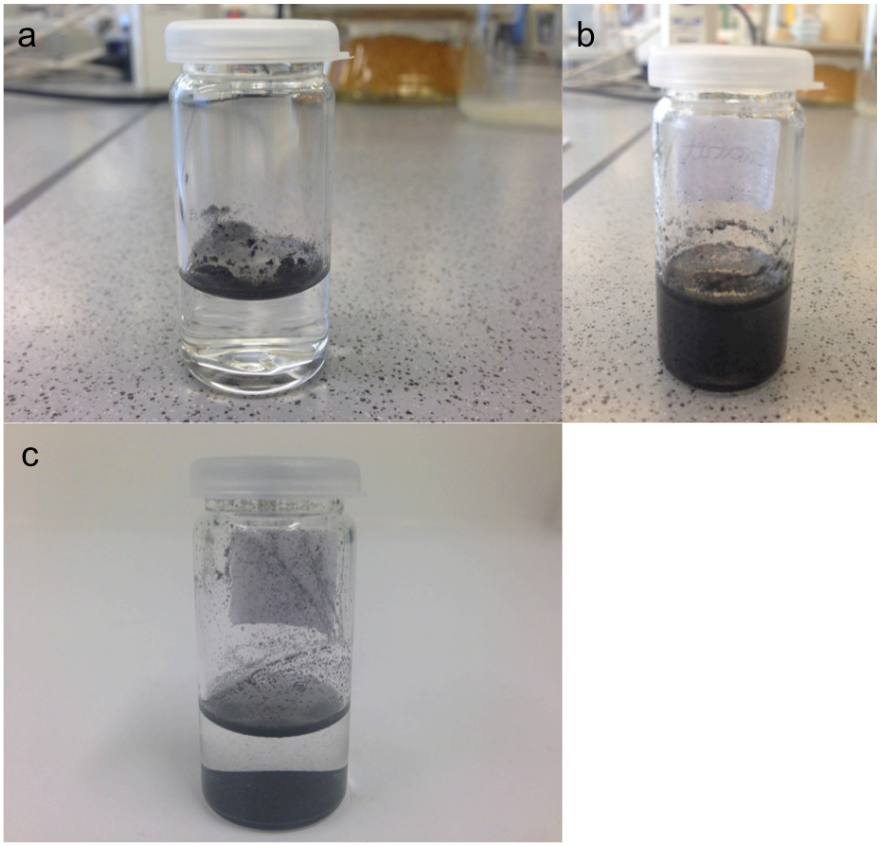

Figure 4.30: Dispersibility testing of graphite in deionized water, a) right after adding, b) right after 15 minutes of sonication, and c) 24 hours after sonication.

4.6.2 GO

Figure 4.31a, b and c, shows the dispersibility of GO3 right after adding it to water, just after 15 minutes of sonication, and 24 hours after the sonication, respectively.

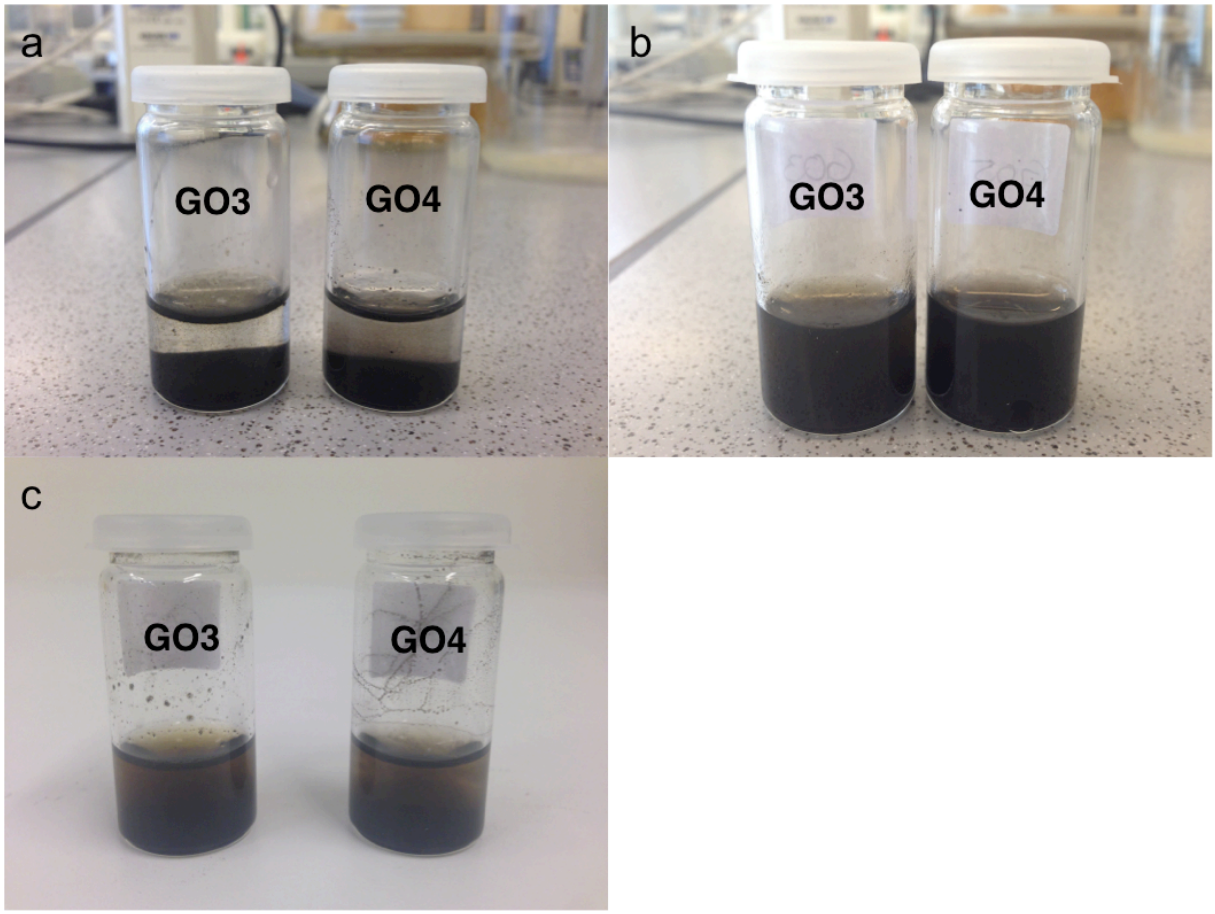

Figure 4.31: Dispersibility testing of GO3 and GO4 in deionized water, a) right after adding, b) after 15 minutes of ultrasonication, and c) 24 hours after ultrasonication. The beaker to the left contains GO3 and the one to the right GO4.

4.6.3 r-GO

Figure 4.31a, b and c, show the dispersibility of r-GO3 right after adding it to water, just after 15 minutes of sonication, and 24 hours after the sonication, respectively. Figure 4.32a, b, and c show the same for r-GO4 in 0.05 % calgon.

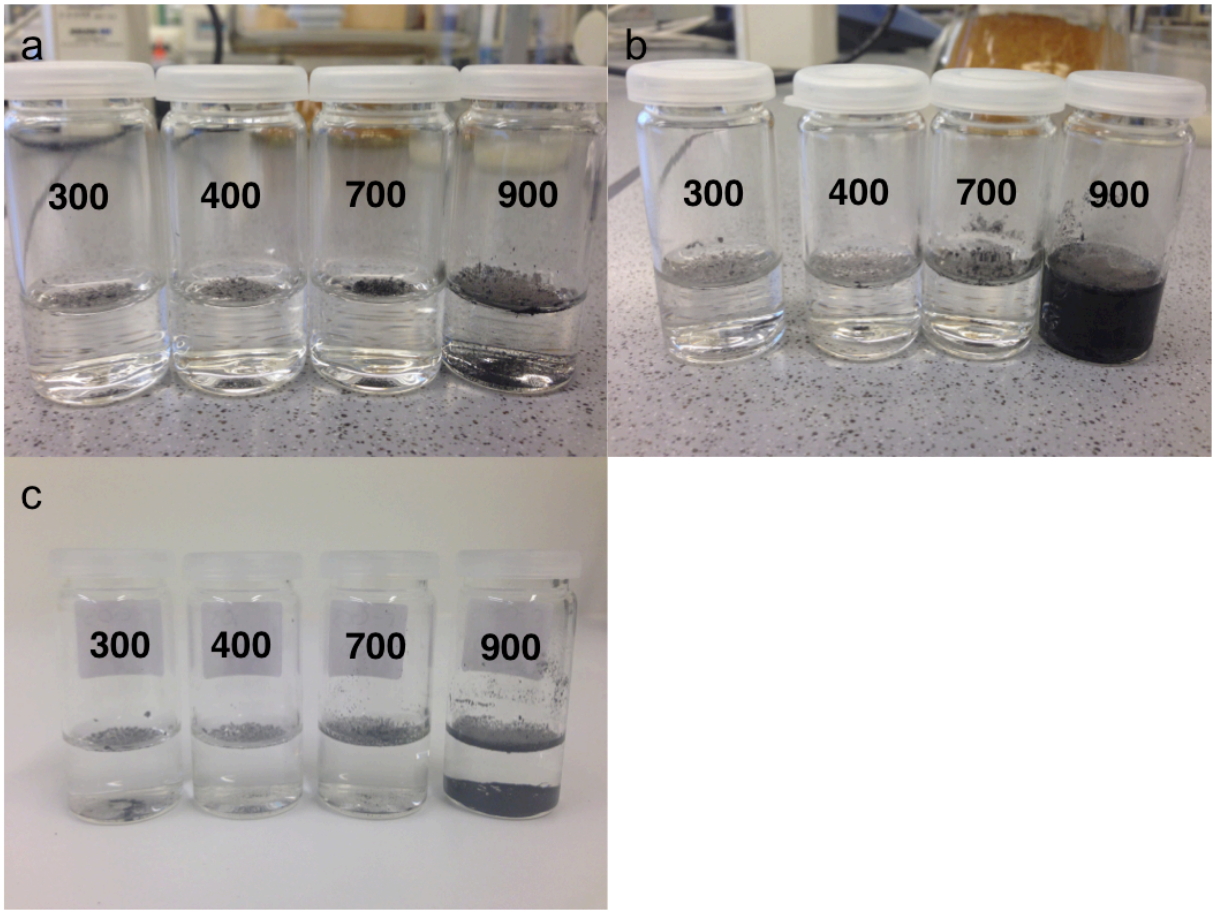

Figure 4.32: Dispersibility testing of r-GO3 in 0.05 % calgon, a) right after adding, b) after 15 minutes of ultrasonication, and c) 24 hours after ultrasonication. The beaker to the left contains r-GO3 300 °C, further 400 °C, 700 °C and 900 °C to the right.

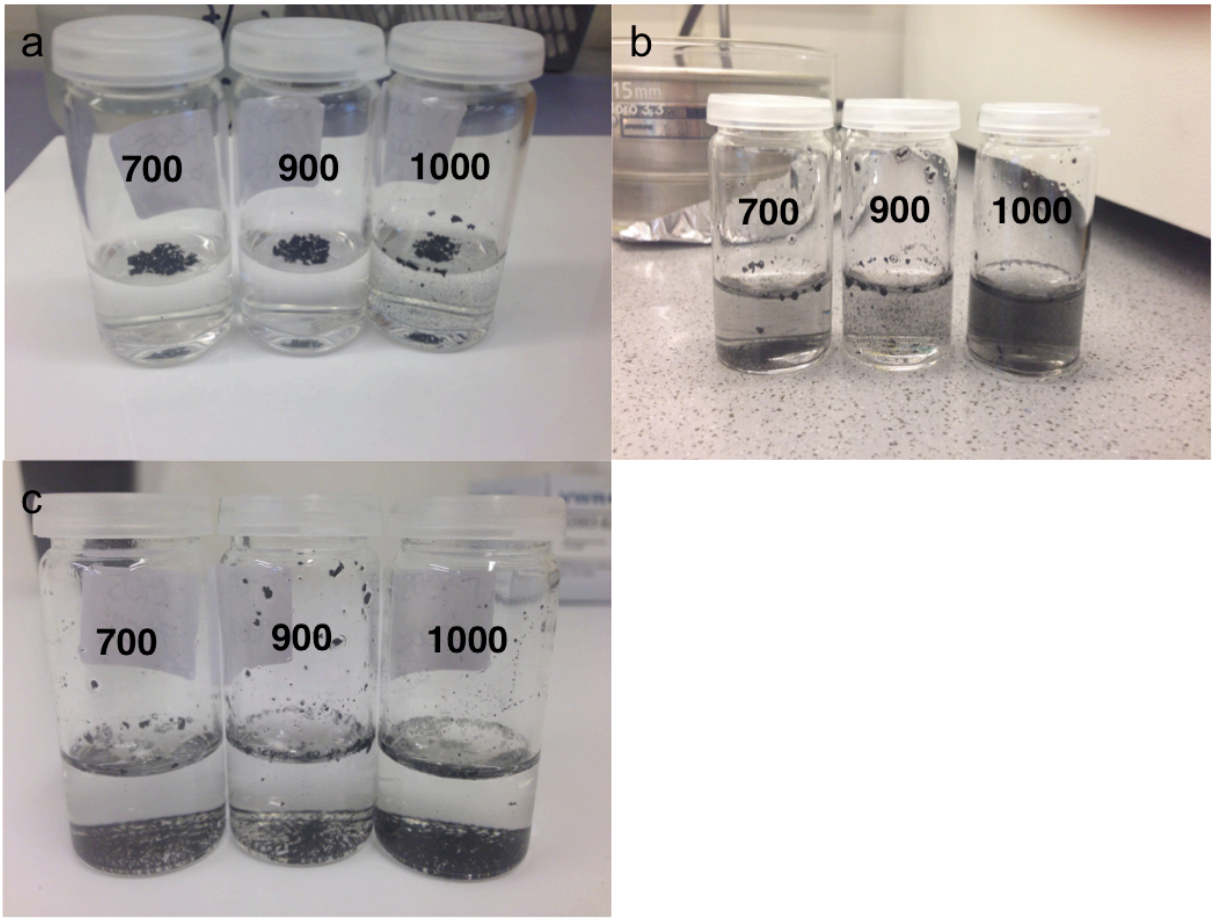

Figure 4.33: Dispersibility testing of r-GO4 in 0.05 % calgon a) right after adding, b) after 15 minutes of ultrasonication, and c) 24 hours after ultrasonication. Going from the left to the right, the beakers contains r-GO4 700 °C, r-GO4 900 °C and r-GO4 1000 °C, respectively.

Table 4.8: The dispersibility of graphite.

Sample	**Dispersibility right after adding**	**Dispersibility right after 15 min sonication**	**Dispersibility 24 hours after sonication**
Graphite	1	4	1

Table 4.9: The dispersibility of GO3 and r-GO3s.

Sample	**Dispersibility right after adding**	**Dispersibility right after 15 min sonication**	**Dispersibility 24 hours after sonication**
GO3	1	5	3
r-GO3 300	1	1	1
r-GO3 400	1	1	1
r-GO3 700	1	1	1
r-GO3 900	1	4	1

Table 4.10: The dispersibility of GO4 and r-GO4s.

Sample	**Dispersibility right after adding**	**Dispersibility right after 15 min sonication**	**Dispersibility 24 hours after sonication**
GO4	1	5	3
r-GO4 700	1	1	1
r-GO4 900	1	1	1
r-GO4 1000	1	2	1

5 Discussion

5.1 Observations during the syntheses

The first observation was the difference in the color change obtained after adding hydrogen peroxide. This addition should cause color change from dark brown to bright yellow. This did not happen for the syntheses produced by large particles (figure. 4.1), but when the particles were reduced to be less than 50 μm, the color change to bright yellow was easily observed (figure 4.2). As the color change is due to the hydrogen peroxide reducing the residual permanganate and manganese dioxide, which are produced during the oxidation of graphite, this indicates that the potassium permanganate has not fully oxidized the large graphite particles [5]. The more oxidized the solution is, the more permanganate and manganese dioxide are produced, which again result in a more bright yellow color. Obviously, the particle size of the starting material is of great importance when considering the oxidation of graphite. Even if the oxidation time was 10 days for GO3, this was not enough to fully oxidize the large graphite particles.

Furthermore, after washing with 1:10 HCl:water, figure 4.3 and 4.4 show that the color change caused by the addition of hydrogen peroxide was maintained for GO4, and that the dark color was maintained for GO1-3.

Moreover, after the agglomeration the pastes were washed with much water, using funnel and filter paper for vacuum filtration. The pH increased during the washing process. According to Chen et al. [27], the pH should increase to nearly 7. This did not happen, and no higher pH than 5 was achieved for all syntheses. This is due to the deionized water used in the washing process, which had a pH of 5.

However, the difference in color for GO1-3 and GO4 was also seen after the centrifugation, as shown in figure 4.5 and 4.6.

Finally, figure 4.7 and 4.8 show the alumina plates coated with graphene oxide before drying and after drying, and at this step all the synthesis showed the same behavior and same color. The consistency was like a liquid gel, and there was no problem to decant or to deposit the graphene oxide on the alumina plate. After drying, the water had been removed, and the dried graphene oxide that was left on the alumina plates was scraped off as GO flakes.

Thus, the color change was the biggest difference in the syntheses, emphasizing the importance of particle size and oxidation time.

5.2 Particle size and oxidation time

During the present work it is found that the particle size of the graphite powder is of great importance when the goal is to obtain fully oxidized GO, and many of the results emphasize this statement.

The first observation was the difference in the color change obtained after adding hydrogen peroxide, as discussed in section 5.1

Not only the color change indicates the importance of particle size, but also the XRD patterns. Figure 4.11 shows the XRD pattern of graphite powder, and it shows two characteristic peaks at 2θ values of 26.58° and 54.65°. By applying Bragg's law, the resulting *d*-spacing is 3.35 Å. Because of the oxygen containing functional groups introduced between the graphene layers, this distance is expected to increase during the oxidation.

As can be seen from the XRD patterns of GO produced by large particles in figure 4.12, all of them show a diffraction peak at a 2θ value around 11-12°, and this peak correspond to the 002 peak of GO. However, the graphite peaks at approximately 26 and 55° are still present, which means that some graphite from the starting material has not been oxidized. On the other hand, when the particle size was reduced, the graphite peaks disappeared, as shown in figure 4.13. All together, these results show that the particle size is crucial in obtaining fully oxidized GO. However, the diffraction peaks of GO1-3 correspond to *d*-spacings in the range 7.28-7.79, and GO4 has a *d*-spacing of 6.99 Å. This increase in distance indicates the presence of oxygen groups between the graphene layers.

It is also important to consider the oxidation time, as both GO2 and GO4 were oxidized for 5 days, but only the small particles in GO4 were fully oxidized. In other words, the larger particles, the longer oxidation time is needed. Note that an oxidation time of 10 days was used for GO3, but even this long time did not fully oxidize the large particles. This indicates that $KMnO_4$, which was used as the oxidizing agent, had problems with and oxidizing all the large particles.

These observations are in agreement with what McAllister et al. [31] found, and emphasizes that the oxidation happens faster when the particle size of the graphite is decreased, and that the particle size is important to control in order to obtain fully oxidized GO. It is found that an oxidation time of 5 days completely oxidize particles less than 50 μm.

Even if the particles are small enough to undergo fast oxidation, it is also important that the size distribution is not too broad, as it was for GO1, GO2 and GO3 (figure 4.3). A very broad size distribution will cause problems with controlling the oxidation, as the smaller particles will be oxidized much faster. In other words, the most important is to start the synthesis of GO with graphite powder consisting of small monodisperse particles, which means particles of approximately the same size.

5.3 Heating rate and reduction temperature

In addition to the particle size and oxidation time, the heating rate and reduction temperature turned out to be very important parameters to control.

The heating rate is crucial when considering thermal reduction of GO, as can be seen by comparing the XRD results of r-GO. After the slow reduction (1 °C/min up to 150 °C, then 5 °C/min), the samples were reduced back to a graphite-like carbon when the reduction temperature was 700 and 900 °C, having the same diffraction peaks as were shown for graphite in figure 4.11. These results are shown in figure 4.14-4.17. When the temperature was lower, 300 and 400 °C, an additional peak at a 2θ value at approximately 23° was also present. This peak shows a trend of moving to the right as the final temperature increases. This can be understood as a little peak remaining from the GO-peak, and that there are still some oxygen present when reducing at low temperatures. The reason why it moves towards higher 2θ values at higher temperature is that more of the oxygen is removed and hence the *d*-spacing gets smaller, which can be seen from tables 4.1, 4.2 and 4.3. At 700 and 900 °C, there is no oxygen left, and the *d*-spacing is the same as for graphite.

In addition, a peak broadening is observed for r-GO4 in figure 4.17 at approximately 26°, which indicates that the sample consists of crystallites of very small sizes, less than 100 nm. This is attributed to the fact that the periodic region in the atomic arrangements producing the same diffraction peak profile is limited [48]. This can also be understood from the "Scherrer's equation" (eq. 2.5):

$$t = \frac{0.9\lambda}{B_{1/2}cos\theta_B}$$

where t is the crystallite size, λ is the X-ray wavelength, $B_{1/2}$ is the width at half the maximum intensity and θ_B is the Bragg angle [48]. So, as t decreases, $B_{1/2}$ increases. However, that this peak broadening did only happen to r-GO4 and not r-GO3 indicates that it has to do with the small particle size and fully oxidation of GO4. Obviously, smaller particles that are completely oxidized find it more difficult to restore the interlayer distance of graphite when reduced at low heating rates.

When the heating rate was increased to 25 ˚C/min, the same tendencies were observed, as shown in figure 4.18.

However, when the heating rate was increased to 5 ˚C/s, which is remarkably faster than the other ones, the result was very different. Figure 4.19 shows these results. When GO4 was reduced at 700 °C, some small peaks were still present at 13.44° and 26.61°. These correspond to GO and graphite, respectively. In other words, a rapid heating treatment up to 700 °C did not work properly. The XRD patterns for the reduction up to 900 and 1000 °C are very similar to each other, and finally it seems like the reduction was successful. If the samples consist of pristine graphene, no peaks would be noticeable, as is shown by Lian et al. [47] and in figure 2.9. This indicates that the fast reduction of GO4 up to 900 and 1000 °C was the most successful reduction method. Table 4.6 shows the 2θ values and the corresponding *d*-spacings for GO4 and r-GO4 reduced by rapid heating rate in Ar/H_2-gas. However, more characterization methods are necessary in order to verify whether the product is pure graphene or not.

The reason why the heating rate is so important is that it affects the pressure build up in between the GO layers, and the pressure needs to overcome the van der Waals binding. The pressure needed to overcome the van der Waals binding is given by equation 2.1:

$$P = \frac{\partial G}{\partial l} = \frac{A_{Ham}}{6\pi l^3}$$

where G is the interaction free energy per unit area between two semi-infinite slabs, A_{Ham} is the Hamaker coefficient, and l is the interlayer distance [31]. Because the van der Waals binding force is inversely proportional to l^3 and the pressure generated from evolved gases is inversely proportional to l, once the exfoliation process in GO is initiated, the multilayer binding is ruptured at an accelerating pace [31].

McAllister et al. [31] evaluated the Hamaker constant numerically, and they estimated the pressure required to separate two GO sheets to be 2.5 MPa. This estimate is 1-2 orders of magnitude greater than the van der Waals forces binding the GO sheets together [31].
They did the calculations assuming that the gas cannot escape the inter-lamellar region of GO before the expansion occurs. What they also observed is that at heating rates of 1 °C/min or less, diffusion of the evolved gases is sufficient to avoid exfoliation, and hence the *d*-spacing for the slowly reduced GO samples reappears at a value very close to the native graphite. Relative to native graphite, the peak at $2\theta \approx 26°$ is now broad, presumably because of the corrugated structure of the GO sheets. So, the van der Waals forces are sufficient to maintain graphitic stacking if gas evolution, and expansion occur slowly enough that lateral diffusion can relieve the generated pressure [31].
The importance of the heating rate and the pressure created can aslo be seen from the SEM images in figure 4.28 and 4.29. When GO2 is reduced by slow reduction in Ar/H_2, the flakes are relatively large at low temperatures, and some scratches are obtained at high temperatures. However, for r-GO4 there are significant changes in the morphology when the reduction temperature exceeds 900 °C, and one clearly see that the pressure created during reduction was enough to overcome the wan der Waals forces, and that much smaller flakes were obtained. There are also seen changes at 700 °C, but not as much as for the higher temperatures. These observations are consistent with the XRD patterns, as the one reduced at 700 °C still has some GO and graphite present.
Apparently, 5 °C/min and 25 °C/min are too slow heating rates, as can be seen from the obtained XRD patterns. However, when the heating rate is increased to 5 °C/s, the diffusion is too slow and expansion can occur.
Even if the heating rate is high enough, it is important to notice that the samples also need to be heated to a certain temperature in order to be exfoliated. As shown in figure 4.19, a minimum temperature of 900 ˚C is necessary, and lower temperatures will not be able to remove all the oxygen groups.

5.4 FTIR

FTIR spectroscopy was used in order to examine the oxygen-containing functional groups in the graphene oxide, and also to determine which groups that were left and which that had disappeared after the reduction. The results are given in section 4.4.

5.4.1 Graphite

Figure 4.20 shows the absorption band of the graphite powder. As can be seen from the figure, the absorption band at 870 cm^{-1} corresponds to the C-C stretching vibration of the graphene sheets, and the band at around 1600 cm^{-1} is from the in-plane C=C bands and the skeletal vibration of the graphene sheets [52]. Moreover, the band at 2090 cm^{-1} is from the C-O stretching of CO gas [52, 56, 57]. In addition, the absorption bands at 2350 and 3700 cm^{-1} are originating from CO_2 and water, respectively [33, 58, 59]. The CO gas, CO_2 and water are most likely detected from the environment and not from the sample [59]. However, there is also a band at 1995 cm^{-1} (the circled area in the figure), but this band is very hard to identify because this is not a common area for absorption bands. As this is a band found in every sample, and it may be attributed to the instrument. This conclusion is realistic due to the appearance in every spectrum, both in GO and in the r-GOs. So, in the graphite sample there are only absorption bands that are characteristic for graphite present; C-C and C=C.

5.4.2 GO

Furthermore, when the graphite was oxidized, it was expected that the FTIR spectra should contain more absorption bands corresponding to the oxygen groups attached to the graphene sheets. Figure 4.21 show the FTIR spectra, and as can be seen from the figure, all of the graphene oxide samples have absorption bands at the same frequencies, as was expected since the synthesis route was the same for every sample. However, the strength of each band vary from sample to sample. The stronger a band is, the deeper is the valley. In addition, oxygen will usually give rise to strong bonds, and as the materials have been oxidized for different times, the oxygen concentration and the strength of the bands will vary from sample to sample [52]. Further, it is difficult to draw conclusion from the percentage of transmittance because this is highly affected by the amount of sample investigated, and was not well enough controlled.

The absorption bands at approximately 600 cm^{-1} are indicating the presence of the bending vibration of the CO_2 molecule, and the absorption band arising at 970 cm^{-1} corresponds to vibration in the graphene sheets [31, 52, 58, 60]. The next bands at around 1060 cm^{-1} and 1225 cm^{-1} imply that there are stretching vibrations of C-O from epoxides present [52]. Further, the absorption band and 1380 cm^{-1} is also related with C-O bending, but is usually

difficult to notice [48]. Moreover, at approximately 1550 and 1620 cm^{-1} there are bands attributed to in-plane C=C bands and the skeletal vibration of the graphene sheets [52, 59, 61-63]. Further, at 1714 cm^{-1} the C=O stretching vibration of carbonyl groups from ketones which are placed at the edges are detected [52, 59, 61, 62]. The sharp band at 2100 cm^{-1} corresponds to the absorption of CO gas, and this gas is most likely from the atmosphere around the sample [56, 57]. There are also bands arising at 2350 cm^{-1}, and these are associated with the stretching vibration of CO_2 [31, 58]. In addition the two smaller bands at 2900 cm^{-1} can be related to C-H stretching in aromatics compounds, which in this case are the benzene rings in the graphene structure [52]. The last and broad valleys at frequencies around 3200 and 3400 cm^{-1} shows that there are O-H stretching vibrations from carboxylic acids, hydroxyl groups and water present [52, 59]. Table 5.1 shows a clear overview of the wavenumbers and the corresponding functional groups present.
Overall, the spectra have changed from the spectrum of graphite, and this is indicating that all the samples have been oxidized to some extent.

Table 5.1: List of frequencies, bonds and functional groups.

Frequency (cm^{-1})	**Bond**	**Functional group**
600	C-O bend	CO_2
970	C-C stretch	Benzene rings
1060-1380	C-O stretch	Epoxides
1550-1620	C=C stretch	Benzene rings
1714	C=O stretch	Ketones
1995	Unknown	Unknown
2100	C-O	CO gas
2350	C-O stretch	CO_2
2900	C-H stretch	Aromatics
3200-3400	O-H stretch	Carboxylic acids, hydroxyls, water

5.4.3 r-GO

As the bonds present in graphite and graphene should be the same, the FTIR spectra of the r-GOs were expected to be like graphite. Figures 4.22-4.27 show the FTIR spectra of r-GO. The big tendency is that most of the oxygen containing functional groups have been removed

after reduction, and the spectra become similar to that of graphite. Therefore, since the spectra are similar, FTIR is not enough to evaluate if the sample is graphite or graphene.
However, as can be seen from figures 4.23-4.26, there are still some bumps in the 1300 cm^{-1} region, which indicates that there are still some epoxy groups (C-O) present after reduction. Even though some of these bumps are very hard no notice, they are still present to some extent.
Moreover, figure 4.27 shows the FTIR spectrum of the rapid reduced sample, epoxy groups were not detected when the temperature was 900 or 1000 ˚C. This imply that all of the oxygen containing functional groups are removed, and only the characteristic absorption bands, C-C and C=C are present. C-O from CO and CO_2-gas do most likely originate from the environment.
This is in agreement with what was found by Seresht and co-workers [62]. Different oxygen groups are removed at different temperatures, and reduction at 300 °C results in removing most of the carboxyl groups, heating at 500, 700 and 900 °C removed the residual carboxyl and partial hydroxyl groups, while heating at 900 °C also eliminates the residual hydroxyl groups and the epoxy group. In addition, heating at 1100 °C will lead to cracking of aromatic C=C bands. However, because the same bands are present in both graphite and graphene, it is difficult to distinguish whether the sample is graphite or successfully reduced graphene oxide. Therefore, it is of great importance to compare the FTIR with the XRD results. By doing this, one easily understand that GO4 and r-GO4 reduced by rapid reduction to 900 and 1000 °C are the most successful obtained samples.

5.5 Reduction atmosphere

Two different atmospheres have been investigated, pure Ar and Ar/H_2 consisting of 5% H_2. From the results it is hard to say which gas that was most appropriate. However, by comparing the FTIR results in figure 4.22-4.24 (slow reduction in Ar), with the results in figure 4.25 (slow reduction in Ar/H_2), one can see that the epoxides is still present after reduction at 900 °C in Ar, but these groups are almost not observed after reduction at 1000 °C in Ar/H_2. This may indicate that Ar/H_2 is better than pure Ar, but one cannot exclude that the increased temperature in Ar/H_2 may also have an impact.
However, Ar/H_2 is supposed to be better because the thermally dissociated hydrogen atoms from hydrogen molecules could transform the epoxies into hydroxyls, which further develop

into water molecules [28]. This is of importance because the outlet of oxygen in the form of CO or CO_2 through epoxies is related to the loss of carbon and implantation of oxygen. However, when the epoxies are transformed into hydroxyls, oxygen is released via H_2O, which does not introduce any oxygen into the carbon backbone.

5.6 Dispersibility

The dispersibility of the r-GO is essential if the product should be used for battery applications, and it is important that it is easily dispersed. The dispersibility results are given in section 4.6.

As expected, figure 4.30 shows that it was not possible to make a stable solution of graphite because of its hydrophobic nature. Moreover, figure 4.31 shows that the dispersibility was increased for the GOs, and figures 4.32 and 4.33 show that the dispersibility was reduced during the reduction of GO. However, the reason why the powder reduced at 900 °C in figure 4.32 and 1000 °C in figure 4.33 was the most well dispersed, is not very clear. These should be the ones with the fewest oxygen functionalities left, and hence be most hydrophobic. One cause can be that they consisted of smaller particles, as the pressure during the reduction did split the flakes in smaller pieces, and the samples were therefore more easily grounded into powder. When the particles get smaller, it may look like a more dispersed solution. Another cause can be that the smaller particles, the more surface area, and hence more graphene edges. As the present of edges increases, the percentage of dangling bonds does also increase, which can affect the dispersibility in a positive way.

Furthermore, no big differences were seen when considering dispersibility vs. degree of reduction. In other words, the r-GOs obtained at high reduction temperature are not more hydrophobic than the ones reduced at lower temperatures. The reason for this can be, as discussed in section 5.4.3, that most of the carboxylic groups are already removed at around 300 °C. When these groups are removed, the hydrophilicity decreases remarkably, and the r-GO becomes insoluble. Even if some other oxygen groups are present, it turned out that the carboxylic groups are the group contributing the most in order to increase the dispersibility. Since the r-GOs showed almost the same dispersibility, it may also indicate that the carboxylic acids constitute the largest amount of the functional groups attached to the graphene layers.

However, the tendency that GO was most soluble was expected, as the GO do have much more oxygen containing functional groups. These functional groups make the surface of the

flakes negatively charged when dispersed in water, and hence the GO induces electrostatic repulsion among the flakes and make them strongly hydrophilic [37, 38]. The negatively charged surface is apparently a result of ionization of the carboxylic acid and phenolic hydroxyl groups that are present on the GO sheets. However, when the GO was reduced by heat treatment, the polar functionalities on the surface of the sheets were removed, and the r-GOs showed the typical hydrophobic characteristic, leading to higher interfacial energy with water. Therefore, the r-GO experience higher van der Waals attractions enhancing flocculation tendency of r-GO [44, 64].

Nevertheless, there are ways to improve the dispersibility of graphene via functionalization. For example, some carboxylic groups, which have shown to increase the solubility, can be attached to the graphene sheets via Bingel reaction as described by Naebe et al. [55]. The only drawback is that this modification can affect other properties of graphene, as for example the electrical conductivity, which also is very important when considering graphene in battery applications.

6 Conclusions

A modified Hummers method was used for the synthesis of GO, which was further reduced to r-GO by thermal treatment.

Fully oxidized GO was obtained by using graphite powder consisting of particles smaller than 50 μm and an oxidation time of 5 days. Larger particles with an average diameter of ~200 μm were harder to oxidize, as an oxidation time of 10 days turned out to be too short and some graphite remained in the samples. The synthesis of well-oxidized graphite is characterized by a color change from dark brown to bright yellow during the addition of hydrogen peroxide. The functional groups introduced during oxidation were epoxy groups (C-O), ketones (C=O), carboxylic acids (O-H) and hydroxyls (O-H), which were identified by FTIR.

Successful reduction of GO was achieved by rapid heating (5 °C/s) to 900 and 1000 °C in a mixture of Ar/H_2-gas (5% H_2). The samples were held at this temperature for 30 minutes. At lower temperatures there were still oxygen containing functional groups attached to the graphene sheets. In addition, lower heating rates (5 °C/min and 25 °C/min) were not able to reduce GO because the pressure build up between the graphene sheets was not high enough to overcome the van der Waals forces and cause fully exfoliation. Moreover, the functional groups were removed at different temperatures. Carboxylic groups and ketones disappeared at temperatures below 700 °C, but temperatures above 900 °C is needed in order to get rid of the epoxy groups.

Furthermore, the FTIR results indicate that reduction in Ar/H_2 was better than in pure Ar, as the hydrogen atoms react with epoxy groups and release oxygen via H_2O, rather than CO or CO_2, which introduce oxygen into the graphene backbone.

GO showed much better dispersibility in water than r-GO did in 0.05% calgon, which is seen as an appropriate solvent for carbon samples. This poor dispersibility is due to the lack of oxygen containing functional groups, which are known to be beneficial for dispersion of carbons in polar solvents.

All together, the present work shows that the synthesis parameters have to be carefully controlled, and that the end result is highly affected by the parameters used in the production process.

7 Further work

In light of all presented results in this thesis, there are some definite recommendations for further work:

- Try to do the synthesis less time consuming by introducing shorter oxidation and reduction times, and even smaller graphite particles can also be investigated.
- Investigation of the dispersibility of r-GO after functionalization through Bingel reaction [36].
- Measure the electrical conductivity of the functionalized r-GO.
- Try to use the functionalized r-GO as conductive additive in an electrode in Li-ion battery.

There are also some more characterization methods that can be used in order to get more information about the produced r-GO:

- TEM, for investigation at the atomic level, and to verify whether the obtained product is graphene or not.
- Raman Spectroscopy, to obtain information about number and orientation of layers, the quality and type of edge, and the affects of perturbations, such as electric and magnetic fields, strain, doping, disorder and functional groups [65].
- BET, in order to measure the surface area [43].
- AFM, for measuring the thickness of the graphene sheets [66].

Bibliography

1. Bolotin, K. I., Sikes, K. J., Jiang, Z., Klima, M., Fudenberg, G., Hone, J., ... & Stormer, H. L. (2008). Ultrahigh electron mobility in suspended graphene. *Solid State Communications*, *146*(9), 351-355.

2. Morozov, S. V., Novoselov, K. S., Katsnelson, M. I., Schedin, F., Elias, D. C., Jaszczak, J. A., & Geim, A. K. (2008). Giant intrinsic carrier mobilities in graphene and its bilayer. *Physical Review Letters*, *100*(1), 016602.

3. Jiang, J. W., Wang, J. S., & Li, B. (2009). Young's modulus of graphene: a molecular dynamics study. *Physical Review B*, *80*(11), 113405.

4. Balandin, A. A., Ghosh, S., Bao, W., Calizo, I., Teweldebrhan, D., Miao, F., & Lau, C. N. (2008). Superior thermal conductivity of single-layer graphene. *Nano letters*, *8*(3), 902-907.

5. Hummers Jr, W. S., & Offeman, R. E. (1958). Preparation of graphitic oxide. *Journal of the American Chemical Society*, *80*(6), 1339-1339.

6. Bai, H., Li, C., & Shi, G. (2011). Functional composite materials based on chemically converted graphene. *Advanced Materials*, *23*(9), 1089-1115.

7. Dreyer, D. R., Ruoff, R. S., & Bielawski, C. W. (2010). From conception to realization: An historial account of graphene and some perspectives for its future. *Angewandte Chemie International Edition*, *49*(49), 9336-9344.

8. "Scientific Background on the Nobel Prize in Physics 2010", *The Royal Swedish Academy of Sciences*.

9. Geim, A. K., & Novoselov, K. S. (2007). The rise of graphene. *Nature materials*, *6*(3), 183-191.

10. De Andres, P. L., Ramírez, R., & Vergés, J. A. (2008). Strong covalent bonding between two graphene layers. *Physical Review B*, *77*(4), 045403.

11. Dreyer, D. R., Park, S., Bielawski, C. W., & Ruoff, R. S. (2010). The chemistry of graphene oxide. *Chemical Society Reviews*, *39*(1), 228-240.

12. He, H., Klinowski, J., Forster, M., & Lerf, A. (1998). A new structural model for graphite oxide. *Chemical physics letters*, *287*(1), 53-56.

13. Boehm, H. P., & Stumpp, E. (2007). Citation errors concerning the first report on exfoliated graphite. *Carbon*, *45*(7), 1381-1383.

14. Brodie, B. C. (1859). On the atomic weight of graphite. *Philosophical Transactions of the Royal Society of London*, *149*, 249-259.

15. Boehm, H. P., Clauss, A., Fischer, G., & Hofmann, U. (1962). Surface properties of extremely thin graphite lamellae. In *Proceedings of the fifth conference on carbon* (Vol. 1, pp. 73-80). Pergamon Press.

16. Shelton, J. C., Patil, H. R., & Blakely, J. M. (1974). Equilibrium segregation of carbon to a nickel (111) surface: A surface phase transition. *Surface Science*, *43*(2), 493-520.

17. IUPAC in *Compendium of Chemical Terminology* (Eds.: A. D. McNaught, A. Wilkinson), 2nd ed., Blackwell Scientific, Oxford, 1997

18. Novoselov, K. S., Geim, A. K., Morozov, S. V., Jiang, D., Zhang, Y., Dubonos, S. V., ... & Firsov, A. A. (2004). Electric field effect in atomically thin carbon films. *Science*, *306*(5696), 666-669.

19. Taghioskoui, M. (2009). Trends in graphene research. *Materials today*, *12*(10), 34-37.

20. Schedin, F., Geim, A. K., Morozov, S. V., Hill, E. W., Blake, P., Katsnelson, M. I., & Novoselov, K. S. (2007). Detection of individual gas molecules adsorbed on graphene. *Nature materials*, *6*(9), 652-655.

21. Stoller, M. D., Park, S., Zhu, Y., An, J., & Ruoff, R. S. (2008). Graphene-based ultracapacitors. *Nano letters*, *8*(10), 3498-3502.

22. Chang, H., & Wu, H. (2013). Graphene-based nanocomposites: preparation, functionalization, and energy and environmental applications. *Energy & Environmental Science*, *6*(12), 3483-3507.

23. Chen, J., Yao, B., Li, C., & Shi, G. (2013). An improved Hummers method for eco-friendly synthesis of graphene oxide. *Carbon*, *64*, 225-229.

24. Sorokina, N. E., Khaskov, M. A., Avdeev, V. V., & Nikol'skaya, I. V. (2005). Reaction of graphite with sulfuric acid in the presence of KMnO4. *Russian journal of general chemistry*, *75*(2), 162-168.

25. Koch, K. R., Krause, P. F., (1982). Oxidation by Mn_2O_7: An impressive demonstration of the powerful oxidizing property of dimanganeseheptoxide. *Journal of Chemical Education*, 59.11: 973.

26. Shih, C. J., Lin, S., Sharma, R., Strano, M. S., & Blankschtein, D. (2011). Understanding the pH-dependent behavior of graphene oxide aqueous solutions: a comparative experimental and molecular dynamics simulation study. *Langmuir*, *28*(1), 235-241.

27. Chen, T., Zeng, B., Liu, J. L., Dong, J. H., Liu, X. Q., Wu, Z., ... & Li, Z. M. (2009, September). High throughput exfoliation of graphene oxide from expanded graphite with assistance of strong oxidant in modified Hummers method. In *Journal of Physics: Conference Series* (Vol. 188, No. 1, p. 012051). IOP Publishing.

28. Mao, S., Pu, H., & Chen, J. (2012). Graphene oxide and its reduction: modeling and experimental progress. *RSC Advances*, *2*(7), 2643-2662.

29. Chen, W., Yan, L., & Bangal, P. R. (2010). Chemical reduction of graphene oxide to graphene by sulfur-containing compounds. *The Journal of Physical Chemistry C*, *114*(47), 19885-19890.

30. Schniepp, H. C., Li, J. L., McAllister, M. J., Sai, H., Herrera-Alonso, M., Adamson, D. H., ... & Aksay, I. A. (2006). Functionalized single graphene sheets derived from splitting graphite oxide. *The Journal of Physical Chemistry B*, *110*(17), 8535-8539.

31. McAllister, M. J., Li, J. L., Adamson, D. H., Schniepp, H. C., Abdala, A. A., Liu, J., ... & Aksay, I. A. (2007). Single sheet functionalized graphene by oxidation and thermal expansion of graphite. *Chemistry of Materials*, *19*(18), 4396-4404.

32. Yang, D., Velamakanni, A., Bozoklu, G., Park, S., Stoller, M., Piner, R. D., ... & Ruoff, R. S. (2009). Chemical analysis of graphene oxide films after heat and chemical treatments by X-ray photoelectron and Micro-Raman spectroscopy. *Carbon*, *47*(1), 145-152.

33. Jelea, A., Marinelli, F., Ferro, Y., Allouche, A., & Brosset, C. (2004). Quantum study of hydrogen–oxygen–graphite interactions. *Carbon*, *42*(15), 3189-3198.

34. Stankovich, S., Dikin, D. A., Piner, R. D., Kohlhaas, K. A., Kleinhammes, A., Jia, Y., ... & Ruoff, R. S. (2007). Synthesis of graphene-based nanosheets via chemical reduction of exfoliated graphite oxide. *Carbon*, *45*(7), 1558-1565.

35. Dai, L. (2012). Functionalization of graphene for efficient energy conversion and storage. *Accounts of chemical research*, *46*(1), 31-42.

36. Naebe, M., Wang, J., Amini, A., Khayyam, H., Hameed, N., Li, L. H., ... & Fox, B. (2014). Mechanical Property and Structure of Covalent Functionalised Graphene/Epoxy Nanocomposites. *Scientific reports*, *4*.

37. Park, S., & Ruoff, R. S. (2009). Chemical methods for the production of graphenes. *Nature nanotechnology*, *4*(4), 217-224.

38. Li, D., Müller, M. B., Gilje, S., Kaner, R. B., & Wallace, G. G. (2008). Processable aqueous dispersions of graphene nanosheets. *Nature nanotechnology*, *3*(2), 101-105.

39. Pumera, M. (2011). Graphene-based nanomaterials for energy storage. *Energy & Environmental Science*, *4*(3), 668-674.

40. Tarascon, J. M., & Armand, M. (2001). Issues and challenges facing rechargeable lithium batteries. *Nature*, *414*(6861), 359-367.

41. Liu, R., Duay, J., & Lee, S. B. (2011). Heterogeneous nanostructured electrode materials for electrochemical energy storage. *Chemical Communications*, *47*(5), 1384-1404.

42. Wang, G., Shen, X., Yao, J., & Park, J. (2009). Graphene nanosheets for enhanced lithium storage in lithium ion batteries. *Carbon*, *47*(8), 2049-2053.

43. Abu-Lebdeh, Y., Davidson, I., "Nanotechnology for Lithium-Ion Batteries", Springer, 2013, ISBN: 9781461446040

44. Matsumura, Y., Wang, S., & Mondori, J. (1995). Mechanism leading to irreversible capacity loss in Li ion rechargeable batteries. *Journal of The Electrochemical Society*, *142*(9), 2914-2918.

45. Laser diffraction, website visited May 25th, 2014 http://www.malvern.com/en/products/technology/laser-diffraction/

46. Callister, W. D., Rethwisch, D. G., "Materials Science and Engineering: An Introduction" 7th edition, Wiley, 2007

47. Lian, P., Zhu, X., Liang, S., Li, Z., Yang, W., & Wang, H. (2010). Large reversible capacity of high quality graphene sheets as an anode material for lithium-ion batteries. *Electrochimica Acta*, *55*(12), 3909-3914.

48. Yoshio Waseda, Eiichiro Matsubara, Kozo Shinoda, "X-Ray Diffraction Crystallography: Introduction, Examples and Solved Problems", Springer, 2011, ISBN: 9783642166358

49. Quirk, M., Serda, J., "Semiconductor manufacturing technology", NJ Prentice Hall. 2001

50. Scanning Electron Microscope, website visited May 25th, 2014 http://www.purdue.edu/rem/rs/sem.htm#2

51. Loryuenyong, V., Totepvimarn, K., Eimburanapravat, P., Boonchompoo, W., & Buasri, A. (2013). Preparation and Characterization of Reduced Graphene Oxide Sheets via Water-Based Exfoliation and Reduction Methods. *Advances in Materials Science and Engineering*, *2013*.

52. Günzler, H., Gremlich, H-U., "IR spectroscopy: an introduction", Wiley, 2002, ISBN: 3-527-28896

53. Pavia, D. L., Lampman, G. M., Kriz, G. S, "Introduction to spectroscopy" 3rd edition, Thomson Learning, 2001, ISBN: 0-03-031961-7

54. "Introduction to Fourier Transform Infrared Spectroscopy", *Thermo Nicolet Corporation,* 2001.

55. Mitsui, T., & Takada, S. (1969). On factors influencing dispersibility and wettability of powder in water. *Journal of the Society of Cosmetic Chemists*, *20*(6), 335-351.

56. Esler, M. B., Griffith, D. W., Wilson, S. R., & Steele, L. P. (2000). Precision trace gas analysis by FT-IR spectroscopy. 1. Simultaneous analysis of CO2, CH4, N2O, and CO in air. *Analytical Chemistry*, *72*(1), 206-215.

57. Zecchina, A., Bordiga, S., Spoto, G., Marchese, L., Petrini, G., Leofanti, G., & Padovan, M. (1992). Silicalite characterization. 2. IR spectroscopy of the interaction of carbon monoxide with internal and external hydroxyl groups. *The Journal of Physical Chemistry*, *96*(12), 4991-4997.

58. Barnes, J. A., & Gough, T. E. (1987). Fourier transform infrared spectroscopy of molecular clusters: The structure and internal mobility of clustered carbon dioxide. *The Journal of chemical physics*, *86*(11), 6012-6017.

59. Guo, H. L., Wang, X. F., Qian, Q. Y., Wang, F. B., & Xia, X. H. (2009). A green approach to the synthesis of graphene nanosheets. *ACS nano*, *3*(9), 2653-2659.

60. Gerakines, P. A., Schutte, W. A., Greenberg, J. M., & van Dishoeck, E. F. (1994). The infrared band strengths of H2O, CO and CO2 in laboratory simulations of astrophysical ice mixtures. *arXiv preprint astro-ph/9409076*.

61. Wojtoniszak, M., & Mijowska, E. (2012). Controlled oxidation of graphite to graphene oxide with novel oxidants in a bulk scale. *Journal of Nanoparticle Research*, *14*(11), 1-7.

62. Seresht, R. J., Jahanshahi, M., Rashidi, A. M., and Ghoreyshi, A. A. (2013). Synthesis and Characterization of Thermally-Reduced Graphene. *Iranica Journal of Energy & Environment*, 4(1), 53-56

63. Acik, M., Lee, G., Mattevi, C., Pirkle, A., Wallace, R. M., Chhowalla, M., ... & Chabal, Y. (2011). The role of oxygen during thermal reduction of graphene oxide studied by infrared absorption spectroscopy. *The Journal of Physical Chemistry C*, *115*(40), 19761-19781.

64. Stankovich, S., Dikin, D. A., Piner, R. D., Kohlhaas, K. A., Kleinhammes, A., Jia, Y., ... & Ruoff, R. S. (2007). Synthesis of graphene-based nanosheets via chemical reduction of exfoliated graphite oxide. *Carbon*, *45*(7), 1558-1565.

65. Ferrari, A. C., & Basko, D. M. (2013). Raman spectroscopy as a versatile tool for studying the properties of graphene. *Nature nanotechnology*, *8*(4), 235-246.

66. Nemes-Incze, P., Osváth, Z., Kamarás, K., & Biró, L. P. (2008). Anomalies in thickness measurements of graphene and few layer graphite crystals by tapping mode atomic force microscopy. *Carbon*, *46*(11), 1435-1442.

Appendices

A – Things that did not work properly

When working with research and development, there will always be some situations where things do not work properly, and there will be room for improvements. Regarding further work, these situations are as useful as the ones that are successful, as we will not do the same mistake one more time.

Reduction in CVD

When the CVD was used in the reduction process, it turned out that the graphene oxide flakes that should be reduced had to be big enough so that they were not moving around by the gas flow. The picture in figure A.1 is taken after too small graphene oxide flakes of GO4 were reduced in CVD. It was impossible to collect the "dust" produced, and no characterization could be done. The next time, larger flakes were used, and the reduction process was successful.

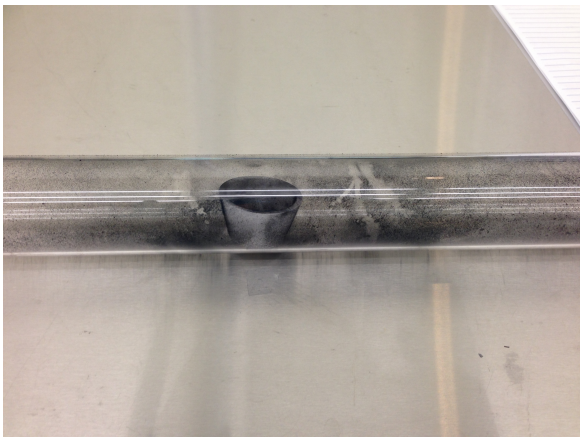

Figure A.1: Graphene "dust" produced after reduction of too small graphene oxide flakes in CVD.

Too small amount GO produced for further reduction

In addition to the syntheses discussed in this master's thesis, another synthesis was done with particle size smaller than 50 μm. However, some of the GO was lost during the washing processes, and there was not produced enough GO for further characterization and reduction. However, the amount was just enough to undergo XRD, and the result is given in figure A.2.

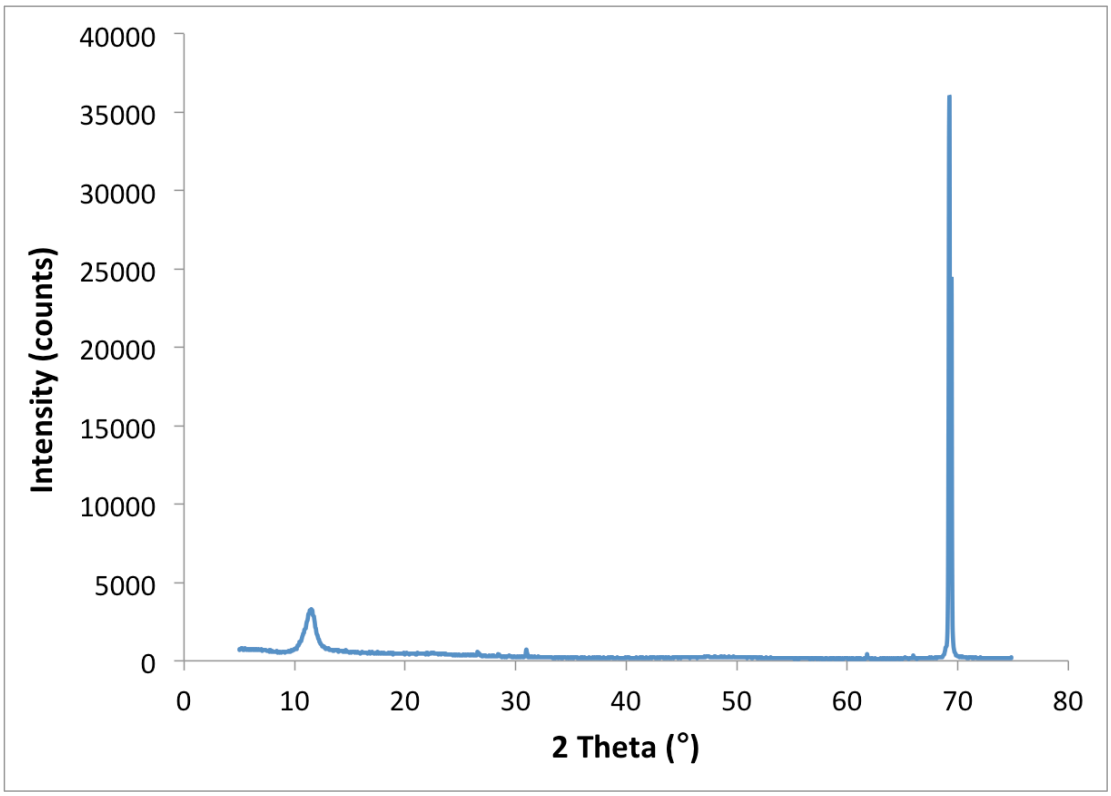

Figure A.2: XRD pattern of GO from an additional synthesis.

As can be seen from the figure, the diffraction peaks from graphite has disappeared, and the new peak observed at 11.51° corresponds to GO with a *d*-spacing of 7.68 Å and GO. The intense peak around 68° originate from Si. The reason why there are only one peak from Si is that a monocrystalline Si wafer that was grounded into powder was used instead of Si powder. The wafer was obviously not grounded to as small particles as the Si powder, and hence only the preferred orientation was shown in the XRD pattern.

However, the XRD result shows again that decreasing the particle size make it possible to control the oxidation and obtain fully oxidized GO without any graphite left. The oxidation time for this sample was 5 days, the same as for the successful GO4 that is discussed earlier. In other words, the synthesis of GO4 is reproducible.